

Stable Isotope studies of Atmospheric Water Vapour and Clouds

A THESIS

submitted for the Award of Ph. D. degree of

MOHANLAL SUKHADIA UNIVERSITY

in the

Faculty of Science

by

Rohit Srivastava



Under the Supervision of

R. Ramesh, Senior Professor,
Physical Research Laboratory, Ahmedabad, INDIA

DEPARTMENT OF PHYSICS

FACULTY OF SCIENCE

MOHANLAL SUKHADIA UNIVERSITY

UDAIPUR

2009

CERTIFICATE

*I feel great pleasure in certifying that the thesis entitled “**Stable Isotope studies of Atmospheric Water Vapour and Clouds**” embodies a record of the results of investigation carried out by Rohit Srivastava under my guidance. I am satisfied with the analysis of data, interpretation of results and conclusions drawn.*

He has completed the residential requirement as per the rules.

I recommend the submission of thesis.

Date:

Prof. R. Ramesh

Geosciences Division

Physical Research Laboratory

Navrangpura, Ahmedabad- 380 009

India.

DECLARATION

*I hereby declare that the work incorporated in the present thesis entitled “**Stable Isotope studies of Atmospheric Water Vapour and Clouds**” is my own work and is original. This work (in part or in full) has not been submitted to any University for the award of a Degree or a Diploma.*

Date:

Rohit Srivastava

(Author)

“सत्यस्य वचनं श्रेयः, सत्यस्य ज्ञानं तु दुष्करम् ।
यद् भूतहितमत्यन्तम्, एतत् सत्यं ब्रवीम्यहम् ॥”

सबसे बढ़कर कल्याण करने वाला सत्य का कथन है, परन्तु सत्य का ज्ञान तो बहुत ही कठिन है । इसलिये सुगम रूप से उसी को मैं सत्य कहता हूँ, जो प्राणियों के लिये अधिकांशतः हितकर हो ।

- महाभारत शान्तिपर्व २६३ . १९

**To my
Family and Gurus**

Abstract

With the advent of Global Warming it has become very important to understand hydrological cycle as it has shown several changes in the recent years. Models predict even more drastic changes in the coming years. Measurements of changing atmospheric water vapor and understanding its causes may help in modelling the frequency of rain events in monsoon regions. This thesis work tries to understand several hitherto unexplored features of the hydrological cycle using stable water isotopes as tracers.

Stable isotopes of water have proved efficient tracers to study various hydrological processes. Isotopes store information of hydrological processes by means of isotopic fractionation during phase change. Recently, a few isotope based models have become available which incorporate the full hydrological cycle. Accuracy of these models depend on the *a priori* information of source parameters (such as in initial isotopic composition of a reservoir), fractionation factor, type of fractionation and various processes which may change isotopic composition at different stages of evolution. Only a few studies are available to characterize them and most of these are laboratory experiments or model generated results. So the aim of the present work is to understand isotopic equilibrium/disequilibrium conditions during phase change over land and ocean and demonstrate the potential of stable isotopes as powerful tracers to capture microphysical processes associated with rain formation.

Cruises were made to understand surface water and atmospheric water vapor properties over the Southern Ocean and the Indian Ocean. To understand various ocean surface water processes in the northern and southern hemispheres and surface water isotopic variability, for the first time a large transect (13°N to 68°S) was explored. This study shows a very clear signature of the domination of evaporation-precipitation process near the equator whereas precipitation dominated zone was located between two evaporation dominated zones south of the equator. For the first time signature of the Agulhas Front and the Subtropical Front in the surface waters were identified at 41°S and 44°S in February. During the return jour-

ney (March) these two fronts had merged and were located at 41°S. Our study demonstrates that the region between 41°S and 45°S is a transition zone between evaporation/precipitation processes dominated zone (north of this zone) and melting/freezing processes dominated zone (south of this zone up to Antarctica). We also found that the Southern Ocean evaporates under the isotopic non-equilibrium. For the first time a simultaneous collection of atmospheric water vapor and ocean surface water was done to understand isotopic equilibrium/disequilibrium conditions over the Bay of Bengal. It is a general understanding that ocean properties are homogeneous. Our results are the first to show small scale stable isotopic heterogeneity for atmospheric water vapor ($\sim 2.8\%$ for $\delta^{18}O$, $\sim 20\%$ for δD) in a small region ($1^\circ \times 2^\circ$). Vapor was mostly not in the isotopic equilibrium with surface water. Effect of kinetic fractionation was seen all the time and it increases towards north. Our results show that the deviation in the fractionation factors from their equilibrium value can be explained by kinetic fractionation over ocean surface.

High time resolution stable isotopic study of rain water can be an effective tool to get micro-physical information of rain formation processes as isotopic fractionation is very sensitive to phase change. This thesis demonstrates the potential of stable isotopes as powerful tracers to understand microphysical processes associated with rain formation. For the first time a high time resolution stable isotopic study of rain water along with radar and disdrometer data show that a single rain parcel can change from stratiform to convective nature in the same day.

Efforts are also made to understand annual atmospheric water vapor cycle, rain water - vapor isotopic equilibrium, source characterization of vapor and effect of rain on local atmospheric water vapor. This study shows a large impact of rain water on the local water vapor during the monsoon, when rain water and atmospheric water vapor were in the isotopic equilibrium mostly. This is not true for the non-monsoon period. Stable isotopes of vapor are also able to trace short term effects such as western disturbances in the month of February.

Acknowledgments

I am greatly indebted to Prof. R. Ramesh for his guidance, advice, criticism and for providing all possible facilities required for this work. He always explained and encouraged to learn science in a very simple and realistic way. He always says “Great scientific discoveries are always simple”. Not only in the professional life but also in the personal life, he provided encouragement to remain optimistic for ever.

I thank Dr. Rajesh Pandey (MLSU, Udaipur) for his help during my synopsis presentation and Ph.D. registration.

I appreciate fruitful collaboration with Dr. T. N. Rao (NARL, Gadanki). He provided me an opportunity to use MST radar and Disdrometer which led us to make new findings about the rain formation system. I learnt many things about rain formation and cloud dynamics from him. I must thank Radhakrishna and Mohan for their help in collecting rain water samples.

I must thank Dr. M. Sudhakar and Dr. N. Anil Kumar (NCAOR, Goa) for providing valuable opportunities to participate in the cruises. Special thanks are due to Dr. M. M. Subbu of NCAOR for arranging liquid nitrogen whenever required. Their continuous support, help and guidance helped me to obtain new insight in the ocean sciences. I also thank Dr. Shailesh Pednekar for his kind support during the Southern Ocean (ABP-35) cruise.

I am indebted to the faculty members of Planetary and Geosciences Division at PRL for their comments and suggestions which helped me to improve this work. I specially thank Profs. J. N. Goswami, S. Krishnaswami, M. M. Sarin, S. K. Bhattacharya, A. K Singhvi, S. V. S. Murty, Utpal Sarkar, Drs. P. K. Panigrahi, S. K. Gupta, J. S. Ray, Sunil Kumar Singh, S. Ramachandran, Dilip Angom, D. Benargee, V. K. Rai and K. K. Marhas for their guidance.

I also thank Dr. M .S. Sheshshayee of GKVK Bangalore for providing significant help during my Bangalore visit.

Special thanks are due to Jani ji for his help in mass spectrometric measurements and laboratory work. Pranav Bhai, Manan and Lakhan Singh helped me a lot in maintaining the electronics units. I also thank Jayanti bhai and Bankim for their help and support

I greatly acknowledge Drs. M. G. Yadava, Ravi Bhushan, Navin Juyal, R. D. Deshpande, R. Rengarajan, Som Kumar Sharma, Rao ji, Padia ji, Shukla ji, Deepak panda, Mr. T. A. Rajesh, Neeraj bhai, Venkat, Dipu da, Vaghela bhai, Bhavsar Bhai and late Shri. M. H. Patel, for their time to time help.

I can never forget my batch mates Ritesh, Nabi, Rajesh, Salman, Santosh, Akhilesh and Ramkrishna for their kind support and help starting from the course work. We always had nice discussions on all aspects of life with fruitful results.

I am thankful to all my lab members Drs. Sanjeev Kumar, Manish Tiwari, Satya, Shreyas, and Naveen, Arvind, Amzad for providing me lot of help and support. I also thank Dr. D. Jagadheesha for teaching me Grads software.

I must thank Bhavesh and Madhav bhai for introducing me to Matlab. It helped me a lot for my research work.

I thank my seniors Drs. Rajnish, Harish bhai, Prashanta, Jayesh, Lokesh, Anirban , Santosh bhai, Morthekai, Neeraj Rastogi, Gowda, Dilip, Amit, Antra, Vandna, Sasadhar, Uma, Sanat, Subimal, Shilpi, Ashutosh, Nagar, Ramya, Latha and Maurya Ji for their encouragement and guidance.

I also thank all PRL students specially Gyana, Alok, Jitendra, Brajesh, Sumita, Sumanta, Shuchita, Manan, Harinder, Kirpa, Waliur, Ashwini, Timmi, Lokesh, Vishal, Bhavik, Anil, Sanjeev, Ram, Vivek, Jayati, Rabiul, Satinder, Vineet, Naveen Chauhan, Sreekanth, Srinivas, Suratna, Shinde, Neeraj, Arvind Saxana, Ashish, Tapas, Bhaswar, Soumya, Praveen, patra, Sandeep, Ashok, Vimal, Pankaj, Suman, Arvinder and Rahul Shah for their helpful nature. It is a rare environment at PRL which never makes you feel away from the home. I thank my NARL friends, N.Venkateswara Rao, Uma, Padma, Debashis, Mohan, basha, Niranjana and Shravan for providing me a loving atmosphere.

I also acknowledge help and support provided by the members in Administration, Purchase, Accounts, Computer Centre, Library and Services, specially, Mr. Y. M. Trivedi, Pauline madam, Parul ben, Priti ben, Jayshree ben, Gandhi bhai, Pradeep bhai, Mr. Senthil, Gupta ji, Mr. Deekshitulu, Mr. G. P. Ubale, Mr. Hitesh Vaghela, Mr. Ranganathan, Vishnu bhai, Rajesh bhai, Nandini madam, Mr. Rajiv, Mr. Sunil, Mr. P. K. Gopi, Ghanshyam bhai, Mr. G. G. Dholakia, Jigar bhai, Hitendra Mishra, Alok Shrivastava, Tejas, Nishtha madam, Uma madam.

These colleagues made things much easier.

Lot of help and support was provided by my namesake, Rohit, of Space and Atmospheric Sciences Division. Specially whatever I know today in linux is due to him. He was always with me like my younger brother. Rather than giving thanks I wish him a bright and successful carrier for his life.

I am highly obliged to several other colleagues, too numerous to list individually, who helped me in different ways.

I can never forget great affections of my sisters Shalini and Pallavi, which has been a continuous source of inspiration. Finally, I express my deep sense of gratitude to my parents and my Gurus without their blessings, love and support I am nowhere.

Contents

Abstract	i
Acknowledgments	iii
List of Figures	ix
List of Tables	xi
1 Introduction	1
1.1 Earth's hydrological cycle	1
1.1.1 Oceans: An important source of moisture	2
1.1.2 Cloud formation and its importance	4
1.1.3 Atmospheric Water vapor	9
1.2 Isotopes	10
1.2.1 Isotopic fractionation	11
1.2.2 Meteoric Water Line (MWL):	16
1.2.3 d-excess:	16
1.3 Aim of This work	17
1.4 Scientific questions addressed	18
1.5 Organization of the Thesis	19
2 Experimental Techniques	25
2.1 Instruments and sampling	26
2.1.1 Vapor Collection Line	26
2.1.2 Rain water collection	28
2.1.3 Ocean water collection	29

2.1.4	Disdrometer	30
2.1.5	MST Radar	32
2.2	Mass Spectrometry	33
2.2.1	Mathematical basis of isotope separation:	37
2.2.2	Delta notation	38
2.2.3	Water equilibration System (WES):	39
2.2.4	$\delta^{18}O$ measurements:	41
2.2.5	δD Measurements:	42
2.3	Calibration tables	43
2.3.1	IAEA Inter laboratory comparison exercise for $\delta^{18}O$ and δD analysis of water samples	43
2.3.2	Laboratory standard (Narmada water) reproducibility	44
3	Ocean Studies	52
3.1	Stable isotopic study of the Southern Ocean surface water:	52
3.1.1	Cruise Track and sampling locations:	55
3.1.2	Salinity and Oxygen isotopic study	56
3.1.3	Hydrogen isotopic study	61
3.1.4	Sea water line over the Southern Ocean	62
3.1.5	Zone demarcation for the Southern Ocean	63
3.2	Effect of the Global warming over oceans	64
3.3	Stable isotopic study of Ocean surface water and Atmospheric water vapor over the Bay of Bengal	69
3.3.1	Cruise track and sampling locations	69
4	Land studies	80
4.1	Microphysical studies of rain formation processes over the tropical region	80
4.1.1	Sampling Location	82
4.1.2	Short term variations in the raining cloud parcel	83
4.2	Characterization of Atmospheric Water Vapor and Rain over the tropical region (Ahmedabad)	94
4.2.1	Vapor sources over Ahmedabad	95

4.2.2	Annual water vapor cycle	96
4.2.3	Modifications in AWV due to monsoonal rain	98
4.2.4	Stable isotopic equilibrium between vapor and rain	100
5	Summary and Scope for Future Work	104
5.1	Ocean Studies	105
5.1.1	Stable isotopic study of the Southern Ocean surface water .	105
5.1.2	Stable isotopic study of ocean surface water (OSW) and at- mospheric water vapor (AWV) over the Bay of Bengal (BOB)	105
5.2	Land Studies	107
5.2.1	Simultaneous study of rain drop size distribution (DSD) and stable isotopic composition of rain water	107
5.2.2	Stable isotopic study of rain water and atmospheric water vapor (AWV) at Ahmedabad	108
5.3	The future scope of the present work	110
	List of Publications	113

List of Figures

1.1	Earth's radiation budget (source: IPCC, AR4)	5
1.2	Rain formation processes: Bergeron-Findeisen and collision-coalescence	6
1.3	Schematic diagram of fractionation processes	13
1.4	Rayleigh isotopic fractionation	15
2.1	Vapor Collection Line	27
2.2	Author with rain collector.	28
2.3	Niskin bottles attached to a CTD rosette	29
2.4	(a) Disdrometer and (b) Schematic diagram of Disdrometer.	31
2.5	MST radar At Gadanki.	33
2.6	Author with stable isotope ratio Mass Spectrometer at PRL.	34
2.7	Schematic diagram of a mass spectrometer.	35
2.8	Schematic diagram of faraday cup.	36
2.9	Schematic diagram of Water Equilibration System.	40
2.10	Schematic diagram of Gilson needle	40
3.1	Cruise track for Southern Ocean Expedition, 2006	55
3.2	Latitudinal variation of (a) salinity (b) $\delta^{18}O$ and (c) SST of surface waters	57
3.3	Surface water freezing observed during the Southern Ocean cruise.	59
3.4	$\delta^{18}O$ – salinity relationship for the Indian Ocean, 2006.	59
3.5	Latitudinal variation of δD	61
3.6	Plot of $\delta^{18}O$ vs. δD of surface sea water from the Indian Ocean	62
3.7	Schematic diagram showing different zones in the Southern Indian Ocean depending on domination of different hydrological processes.	64

3.8	Sampling locations for Duplessy, Kallel, Archambeau and this data	65
3.9	Comparison among (a) Duplessy (1969), (b) Kallel (1984), (c) Archambeau (1993) and (d) This work for latitudinal variation of $\delta^{18}O$ (\bullet) and salinity (\circ).	67
3.10	Comparison among (a) Duplessy (1969), (b) Kallel (1984), (c) Archambeau (1993) and (d) This work for salinity- $\delta^{18}O$ relation.	68
3.11	Cruise track for the Bay of Bengal study.	70
3.12	Oxygen isotopic variation of vapor and surface water over BOB	71
3.13	Hydrogen isotopic variation of vapor and surface water over BOB	72
3.14	Plot of $\delta^{18}O$ vs. δD for atmospheric water vapor over the BOB.	73
3.15	Variation of fractionation factor for (a) oxygen and (b) hydrogen over the BOB.	74
4.1	Sampling location (NARL, Gadanki).	82
4.2	Satellite pictures of five major rain events.	83
4.3	Temporal variation of rain integral parameters	84
4.4	Plot of $\delta^{18}O$ variation with time for (a) 12 September, (b) 14 September, (c) 5 October, (d) 17 October and (e) 26 October 2006.	85
4.5	Schematic diagram of $\delta^{18}O$ variation of (a) type 1 and (b) type 2.	86
4.6	Time-height contours of profiler spectral moments at vertical incidence	88
4.7	Temporal and vertical variation of rain DSD.	89
4.8	Scatter plot between $\delta^{18}O$ and mass weighted mean diameter of rain drops	90
4.9	Plot of $\delta^{18}O$ vs. δD .	92
4.10	Variation of $\delta^{18}O$ and δD of rain water with d-excess	92
4.11	Possible water vapor sources over Ahmedabad	95
4.12	Stable oxygen isotopic composition of atmospheric water vapor with relative humidity over Ahmedabad from April 2007 –April 2008	96
4.13	Back trajectory analysis on 8 Feb 08 to trace western disturbances.	98
4.14	Stable oxygen isotopic composition of rain water, atmospheric water vapor, and rainfall during monsoon, 2007	99

List of Tables

2.1	Results from water samples provided by IAEA for $\delta^{18}O$ measurement (with respect to VSMOW).	44
2.2	Results from water samples provided by IAEA for δD measurement (with respect to VSMOW).	44
2.3	$\delta^{18}O$ values (with respect to VSMOW) of Narmada water standard measured at PRL.	45
2.4	$\delta^{18}O$ values (with respect to VSMOW) of new Narmada water standard measured at PRL.	48
2.5	δD values (with respect to VSMOW) of Narmada water standard measured at PRL.	49
4.1	Simultaneous rain and vapor collection	101

Chapter 1

Introduction

1.1 Earth's hydrological cycle

The hydrological cycle on the planet earth is driven by the unequal solar energy distribution on the surface. It mainly comprises of evaporation from oceans and land water bodies, rain from clouds and water discharge from rivers. There are several potential factors such as global warming and pollution which may affect hydrological balance by influencing the heat budget. In the present day scenario continuously increasing surface temperatures and pollution may have serious effects on the hydrological cycle. Collectively they may change ocean and cloud properties drastically. Increase in the specific humidity due to global warming in the lower atmosphere is likely to have important implications for extreme precipitation events and tropical cyclones [Willett et al., 2007]. So it is very important to understand the hydrological cycle in the changing global scenario for better predictions.

Stable isotopes of water deuterium (D) and oxygen (^{18}O) are important tracers of the natural hydrological processes [Friedman et al., 1964; Craig and Gordon, 1965; Clark and Fritz, 1997] because they fractionate during phase change (1.2.1). This isotopic fractionation is very sensitive to the changes in the atmospheric parameters (e.g. temperature, humidity). Their usefulness in studying atmospheric water vapor transport [Smith et al., 2006], cloud physics [Jouzel and Merlivat,

1984; Scholl et al., 2007], paleoclimatology [Duplessy, 1993; Ramesh, 2001; Gupta et al., 2003] and oceanography [Archambeau et al., 1998; Delaygue et al., 2001] has been amply demonstrated. In the present study stable isotopes of water are used as tracers to decipher some aspects of the hydrological cycle.

1.1.1 Oceans: An important source of moisture

In the ocean-atmosphere energy exchange process, ocean loses energy to the atmosphere in the form of vapor. Being the largest water body on the earth it is a major source of moisture. Evaporation of ocean surface waters not only depends on the local climatic conditions (e.g. sea surface temperature, air temperature, wind speed and salinity) but also on the global climatic conditions (e.g. atmospheric circulations, global warming and ocean currents). For example sea surface temperature (SST) plays an important role in deciding the nature of the clouds i.e. if SST is higher then the cloud system formed is more turbulent. There is a threshold of about 28°C of SST above which the tendency of convection is high [Gadgil, 1984]. Likewise other parameters too have important effects on evaporation. Thus the source parameters decide the nature of cloud. This necessitates the study of water vapor over oceans for the proper understanding of ocean-atmospheric energy exchange and cloud formation. Unlike the land based studies, direct measurements of vapor properties over oceans are sparse due to its vastness and the experimental difficulties.

It is very important to understand isotopic variability of ocean surface waters (OSW) as it is an important parameter for isotope based models and decides isotopic composition of atmospheric water vapor. Isotopic variability of OSW depends upon the physical processes affecting the ocean surface such as evaporation/precipitation, melting/freezing, upwelling/advection and continental runoff. For a proper understanding of these processes and isotopic variability of OSW, large spatial and temporal data coverage is needed. The Southern Ocean has been

proved an important ocean affecting tropical monsoon system but such datasets are limited [e.g. Schmidt et al., 1999] for this region. This makes the Southern Ocean an important region to study.

Evaporation, the first step in the hydrological cycle, plays a key role in determining relation between δD and $\delta^{18}O$ (δ refers to the deviation of the isotopic ratio (e.g. $^{18}O/^{16}O$) of the sample from that of the standard in parts permil, for details see 2.2.2) in the global precipitation. The Craig-Gordon model [Craig and Gordon, 1965] describes the initial isotopic compositions in the water vapor (δ_{vo}) as a function of the isotopic compositions of the evaporating water (δ_E), relative humidity (h), and sea surface temperature (SST). However, the value of δ_{vo} is difficult to estimate as it is difficult to estimate or observe the δ_E . Making a global-scale closure assumption ($\delta_{vo} = \delta_E$) [Merlivat and Jouzel, 1979], the model can be written as

$$1 + \delta_{vo} = \frac{1}{\alpha} \frac{(1 - k)}{(1 - kh)} (1 + \delta_{ocean}) \quad (1.1)$$

where k is a kinetic fractionation factor, α is an equilibrium fractionation factor, and δ_{ocean} is an ocean isotopic composition. But this global-scale closure assumption ($\delta_{vo} = \delta_E$) causes a systematic bias [Jouzel and Koster, 1996]. So, for the accuracy of isotope based models, fractionation between OSW and atmospheric water vapor needs to be tested under various climatic conditions.

Also a few models (isotope based) are available to understand the rain formation process [Jouzel, 1986; Ciais and Jouzel, 1994]. They require stable isotopic composition of OSW as an input parameter and based on the prior information about amount and type of fractionation (i.e. equilibrium or kinetic fractionation), which occurs during the phase changes at various steps, they predict the isotopic composition of rain. Models use indirect way of calculating isotopic compositions of water vapor i.e. they calculate isotopic composition of vapor using isotopic composition of ocean surface water with the assumption of vapor-OSW isotopic equilibrium with surface water. So precise data on the isotopic compositions of

water vapor over ocean surface are very critical. In most models it is assumed that vapor is in isotopic equilibrium with ocean surface water which need not to be necessarily true. Kinetic fractionation (for details see 1.2.1) plays an important role for the open water bodies like ocean and causes deviation from the equilibrium. Very few systematic experimental studies are available to date for the characterization of fractionation over oceans [Lawrence, 2003; Lawrence et al., 2004; Uemura et al., 2008] but they are limited to small regions. No observations have been made for the stable isotopic composition of the atmospheric water vapor over the Bay of Bengal and the Arabian Sea prior to this work.

This gives strong motivation for stable isotopic study of ocean surface water and atmospheric water vapor to understand ocean-atmosphere interaction and isotopic fractionation over ocean surface. This will help to understand the first phase of the hydrological cycle.

1.1.2 Cloud formation and its importance

Clouds play a very important role in the atmosphere. They influence the energy budget of the atmosphere through two main ways (1) latent heat is released on condensation and liquid water is removed from the atmosphere by precipitation; (2) by scattering, absorption and emission of solar and terrestrial radiation clouds strongly influence the atmosphere's radiation budget. Figure (1.1) shows the recent radiation budget of the atmosphere estimated by Inter governmental panel on climate change, assessment report *IV* (IPCC, AR4). It demonstrates strong influence of clouds in the earth's energy budget.

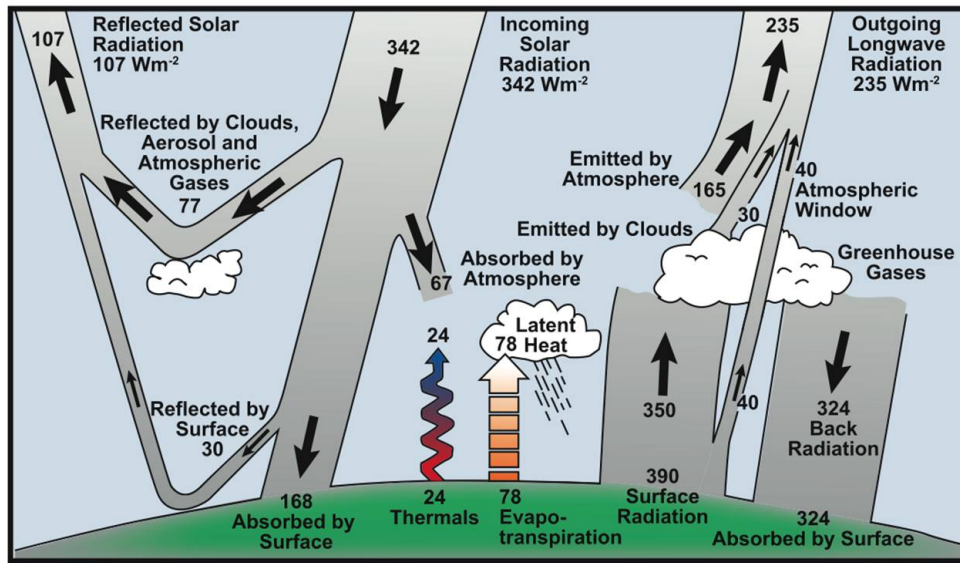


Figure 1.1: Earth's radiation budget (source: IPCC, AR4)

Most of the quantitative information on clouds and precipitation, and the processes which are involved in producing them, has been obtained since 1940 though the first classification of clouds was done in 18th century by Lamarck [Lamarck, 1802]. Since then this field has been making remarkable progress as can be easily seen by increasing number of publications. But still due to lack of *in-situ* observations and sample collection from clouds, many aspects (specially the microphysical processes related to cloud and rain formation) are not well understood. This leads us to poor weather predictions in spite of having good computational power and frequent satellite observations.

Very recently it has been realized that poor weather predictions may be due to insufficient understanding of cloud microphysical processes such as condensation, collision and coalescence. Though these processes operate on a smaller scale in comparison to the other processes such as evaporation from ocean and cloud parcel dynamics, their collective strength becomes very strong and decides the fate of the cloud parcel. So far only radars provide ground based observations of the cloud parcel but they are limited to the large scale dynamics only. Stable isotopes may

act as a good tracer to study cloud microphysical processes, as they are very sensitive to these processes.

Cloud formation takes place by the adiabatic cooling of ascending moist air. This cooling super saturates the air parcel and nucleation begins with the help of cloud condensation nuclei (CCN). This process is called condensation. If cloud temperatures are very low ($\sim -20^\circ\text{C}$) then nucleation is triggered by the ice nuclei (Bergeron-Findeisen process, after T. Bergeron and W. Findeisen) (Fig. 1.2a).

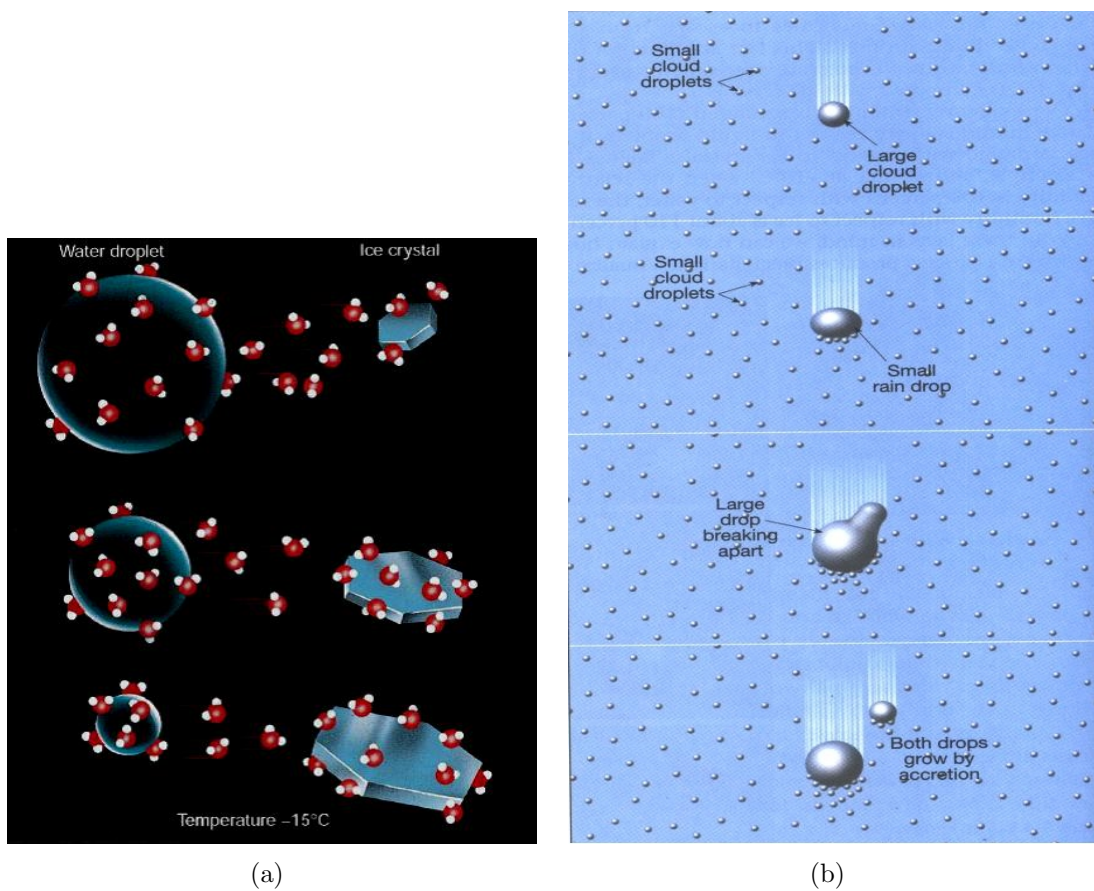


Figure 1.2: (a) Rain formation through Bergeron-Findeisen process and (b) Rain formation through collision-coalescence process. (source:(a) www.cbs3springfield.com and (b) Lutgens and Tarbuck, 1998)

Collision and coalescence process converts these *tinny* cloud drops ($\sim 10\ \mu\text{m}$) to rain drops ($\sim 1000\ \mu\text{m}$) (Fig. 1.2b). On the basis of the strength of these

microphysical processes and turbulence, cloud systems can be classified into two:

- **Convective (or Cumulus) clouds:** These clouds are generally associated with high turbulence. Their vertical extent is much higher than the horizontal one (tower or cauliflower like structure). They generally form due to the strong heating of the surface. These clouds ascend very fast and in a very short time (order of minutes) they become supersaturated and start condensing. Due to the high vertical extent of these clouds, cloud drop which forms in the top-most part in the cloud has to travel more distance inside the cloud to come out from the cloud base. During the downward motion this small cloud drop collects other smaller drops by collision-coalescence and converts into a rain drop. Due to high turbulence and high vertical dimension of these clouds, condensational growth of the cloud drops is less prominent than the growth through collision and coalescence process. Cumulus clouds form and become mature in a very short time with lots of thundering and lightening. They produce heavy rains and die fast.
- **Stratiform clouds:** In contrast to convective clouds, stratiform clouds have higher horizontal extent than the vertical. They generally form during monsoon period and cover large area. Due to the large cloud coverage land surface cools faster which makes these clouds less turbulent. Their life time is more (of order of days) than the convective clouds (of the order of minutes to hours). Due to less turbulence and high horizontal dimension, cloud drops have sufficient time to grow through condensational process. So the stratiform clouds can be characterized by less prominent collision-coalescence process and more prominent condensation process.

Stable isotopic analysis of rain water is a promising way of getting microphysical information of rain formation processes, because the isotopic fractionation of rain water depends, primarily, on phase changes of hydrometeors and evaporation. Temporal changes in the isotopic content of rain water, thus, provide clues to the

microphysical processes occurring within the cloud and precipitation below the cloud base. Condensation of vapor, as an air parcel cools progressively, lowers the isotope ratio of the remaining vapor and the condensate that forms from it. Because most condensation results from moist adiabatic ascent, the stable isotopic ratios of vapor and precipitation both decrease with altitude [Dansgaard, 1964]. Using these isotopes it is possible to study various processes in the hydrological cycle. Large scale variations, both in temporal as well as spatial, of stable isotopic abundances are widely reported [Rozanski et al., 1993] but shorter term variations are yet to be studied extensively [Celle-Jeanton et al., 2004].

In-cloud processes may involve fast advective transport of moist air from below, phase changes during the formation of rain and/or snow, isotope exchange between liquid and gaseous phases in the cloud and during rain-out. Rain drops on their way down to the surface undergo partial evaporation in the unsaturated atmosphere below the cloud base. As the stable isotopic ratio of the drops depends on the condensational growth, higher growth would lead to higher isotopic enrichment in the rain drop. Due to the small size of cloud drops, collision and coalescence would not affect the isotopic composition much and this can be treated as mixing of small reservoirs (smaller drops). Dependence of isotopic fractionation on temperature can be neglected to a first order because in tropical environments, its temperature dependence is small.

Variations in drop size distribution (DSD) with space and time have been widely reported, which show that cloud processes are very sensitive to the climatic conditions (local as well as global). In addition, they show large variations from storm to storm within a season and also within a storm from one rain regime to the other [Tokay and Short, 1996; Atlas et al., 1999; Rao et al., 2001]. It is well known that the rain DSD depends on rain intensity. However, Tokay and Short (1996) have shown that the DSD in convection differs from that in stratiform precipitation, even at the same rainfall rate, indicating that the DSD varies with rain type as well. Such differences do exist and are attributed mainly to the

different microphysical processes, a proper understanding of which is essential for better weather prediction [Baker, 1997]. Thus stable Isotopes can be a sensitive tool to study such microphysical processes. So simultaneous measurements of rain DSD and stable isotopic analysis of rain water has been performed in the present thesis work to get better insight on cloud precipitation-evaporation processes in the tropical monsoon environment, which is the second step of the hydrological cycle.

1.1.3 Atmospheric Water vapor

Water vapor plays an important role in the global warming [Hartmann, 2002] and is a good tracer for atmospheric transport due to its long atmospheric residence time [Webster and Heymsfield, 2003]. Lower tropospheric water vapor reservoir is very dynamic, quickly responding to ambient changes. The amount of atmospheric water vapor (AWV) depends on evaporation from open water bodies, soil and plants. Evaporation of rain drops is also a significant source of water vapor, contributing to humidity, typically 20% in the lower troposphere and up to 50% near the convective clouds [Worden et al., 2007]. Increase of water vapor in the lower troposphere induces precipitation (rain) by providing saturation to the unsaturated cloud systems, especially in convective zones. Measurements of changing AWV, and understanding its causes, are useful in modelling the frequency of rain events in the monsoon regions.

Several studies have reported the isotopic composition of rain water [e. g. Rindsberger et al., 1990; Rozanski et al., 1993; Celle-Jeanton et al., 2004]. However, measurements of the isotopic composition of AWV and clouds [He and Smith, 1999; Scholl et al., 2007; Angert et al., 2008; Wen et al., 2008] are relatively recent. Some studies are limited to either only cyclonic events or to very few rain events [Lee et al., 2006; Fudeyasu et al., 2008]. Very recently a few satellite based observations for the hydrogen isotopic composition of AWV are also documented [Worden et al.,

2007; Brown et al., 2008] but these satellite observations have a large uncertainty ($\sim 10\%$ in the tropics and $\sim 24\%$ at the poles). Ground-based observations of the isotopic compositions of AWV provide an opportunity to validate satellite data and could help to verify their accuracy. Thus the stable isotopic study of the AWV and rain help to understand the important aspects of the hydrological cycle i.e. secondary evaporation of rain drops, local recycling of moisture, rain-vapor isotopic equilibrium and the annual vapor cycle.

1.2 Isotopes

Atoms having same atomic number but different atomic masses are known as isotopes (Greek *isos* = equal, *topes* = place). Isotopes can be either unstable (known as radioactive) or stable. Radioactive isotopes have a certain probability of decay whereas stable isotopes do not spontaneously disintegrate by any known mode of decay. So far 270 stable nuclides and over 1700 radionuclides have been identified [Clark and Fritz, 1997].

There are two stable isotopes of hydrogen (^1H and ^2H) and three of oxygen (^{16}O , ^{17}O , ^{18}O) present in the nature. Among all isotopes of oxygen and hydrogen ^1H and ^{16}O are the most abundant. Their natural abundances as a percent are given below [Mook, 2006]:

Hydrogen	$^1\text{H}=99.985 \%$
	$^2\text{H}=0.015 \%$
Oxygen	$^{16}\text{O}=99.760 \%$
	$^{17}\text{O}=0.035 \%$
	$^{18}\text{O}=0.205 \%$

Among the three stable isotopes of oxygen, ^{17}O is the least abundant. So in the present study only ^{16}O and ^{18}O are used. The first precise measurements of the isotope abundance ratios were done by Alfred Nier in 1939 using a mass spectrometer. Since then several advancements have been made in mass spectrometers

to improve the detection limit, precision and to make them fully automatic. The present day mass spectrometers have given more power to isotopes by providing high precision and ability to measure a very small amounts of samples.

1.2.1 Isotopic fractionation

The heavier isotopologue of water (HDO or H₂¹⁸O) have lower vapor pressure than the lighter ones (i.e. H₂¹⁶O) and, therefore, are relatively enriched in liquid or solid phases and correspondingly depleted in the vapor phase [Gat, 1996] as explained by Rayleigh rain out process [Ciais and Jouzel, 1994]. Isotopic fractionation highly depends on the changes in atmospheric parameters (e.g. temperature, humidity). This occurs in any thermodynamic reaction due to differences in the reaction rate for different molecular species. The result is disproportionate concentration of one isotope over the other on one side of the reaction. It is expressed by the fractionation factor (α) which is the ratio of the isotope ratios for the reactant and product.

$$\alpha = \frac{R_{Product}}{R_{Reactant}} \quad (1.2)$$

$$e.g. \quad \alpha^{18}O_{vapor-water} = \frac{(^{18}O/^{16}O)_{vapor}}{(^{18}O/^{16}O)_{water}} \quad (1.3)$$

Mathematical formulation of fractionation factor: For a isotopic exchange reaction



where asterisk indicates the presence of heavier isotope. We can define the equilibrium constant for this reaction as:

$$K = \frac{[A^*][B]}{[A][B^*]} = \frac{[A^*]/[A]}{[B^*]/[B]} \quad (1.5)$$

where square brackets denote the activity. The concentration of the isotope on either side of the exchange reaction is determined by its partition function (Q). If

Q is the total partition function ($Q = Q_{\text{translation}} * Q_{\text{vibrational}} * Q_{\text{rotational}}$) defined as:

$$Q = \sigma^{-1} m^{2/3} \sum e^{-E/kT} \quad (1.6)$$

where σ = symmetry number

m = mass

E = integrated energy states from zero point energy to dissociated state of molecule

k = Boltzmann constant ($1.38 \times 10^{-23} \text{ JK}^{-1}$)

T = absolute temperature (in K)

Then the equilibrium constant for the reaction (1.4) can be written as:

$$K = \frac{(Q_A^*/Q_A)}{(Q_B^*/Q_B)} = \frac{R_A}{R_B} = \alpha_{A-B} \quad (1.7)$$

As for the isotopic species translational and rotational frequencies are nearly identical so the vibrational frequency is effectively responsible for the isotopic fractionation. α also depends on temperature:

$$\alpha = Ae^{B/T} \quad (1.8a)$$

where the coefficients A and B do not depend on temperature, but contain all temperature independent quantities (such as atomic and molecular masses of the isotopes and molecules involved). The natural logarithm of the fractionation factor can be approximated by the power series:

$$\ln \alpha = c_1 + \frac{c_2}{T} + \frac{c_3}{T^2} \quad (1.8b)$$

$$10^3 \ln \alpha^{18}O_{w-v} = 1.137 \left(\frac{10^6}{T^2} \right) - 0.4156 \left(\frac{10^3}{T} \right) - 2.0667 \quad (1.8c)$$

$$10^3 \ln \alpha^2H_{w-v} = 24.844 \left(\frac{10^6}{T^2} \right) - 76.248 \left(\frac{10^3}{T} \right) - 52.612 \quad (1.8d)$$

Values of coefficients (c_1 , c_2 , c_3) for ^{18}O and ^2H for water-vapor are shown in equations (1.8c) and (1.8d) [Majoube, 1971].

Isotopic fractionation can take place during a physical or chemical process. On the basis of forward and backward reaction rates, isotopic fractionation can be divided into three categories (Fig. 1.3):

1. Kinetic Fractionation
2. Equilibrium Fractionation
3. Non-equilibrium Fractionation

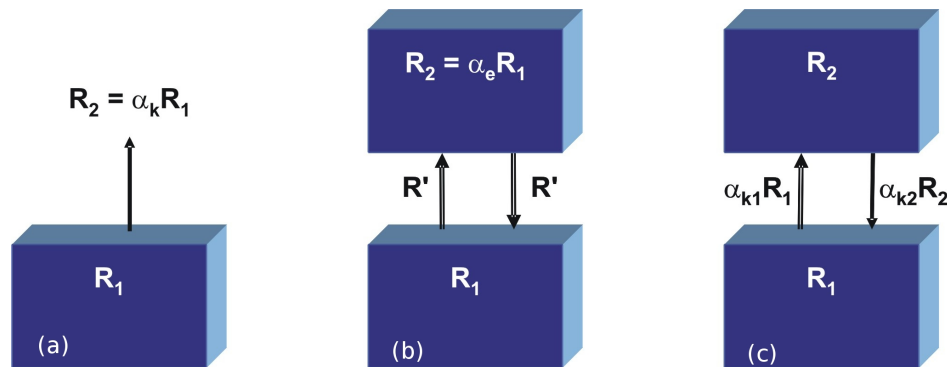


Figure 1.3: Schematic diagram of (a) kinetic (b) equilibrium and (c) non-equilibrium fractionation processes (where α : fractionation factor and R : isotopic ratio)(source: Mook, 2006).

Kinetic fractionation results from one-way physical or chemical processes i.e. there is a one-way mass transport. For example combustion of organic matter or the evaporation of water with immediate removal of the water vapor without any further contact with the evaporating water body.

Equilibrium fractionation is essentially the isotope effect involved in a reversible equilibrium reaction, where the total as well as isotope mass transport is equal in both directions (forward and backward)[example: the equilibrium between water and water vapor in the closed volume].

In nature, isotopic fraction processes are often neither purely kinetic, nor purely equilibrium processes. These are referred as a non- equilibrium fractionation [example: evaporation of vapor from ocean as there is a net evaporation].

Equilibrium fractionation process can be well explained by the Rayleigh fractionation model [Dansgaard, 1964]. The Rayleigh equation (1.9) provides information about how the isotopic ratio of parent reservoir changes with fraction remaining of the original reservoir.

$$R = R_o f^{\alpha-1} \quad (1.9)$$

where R_o = Initial isotopic ratio of parent reservoir

f = Fraction of the parent reservoir remaining

α = Fractionation factor

R = Isotopic ratio of parent reservoir at time when fraction left is f

The Rayleigh equation is based on four assumptions:

1. Temperature of the system should remain constant. If this is not valid, different values of α must be used.
2. The abundance of heavier isotope should much smaller than the lighter isotope. ($^{18}\text{O} \ll ^{16}\text{O}$).
3. The parent reservoir homogenizes itself all the time. There should not be any isotopic gradient in the parent reservoir.
4. Product should be in the isotopic equilibrium with the reservoir before it gets removed.

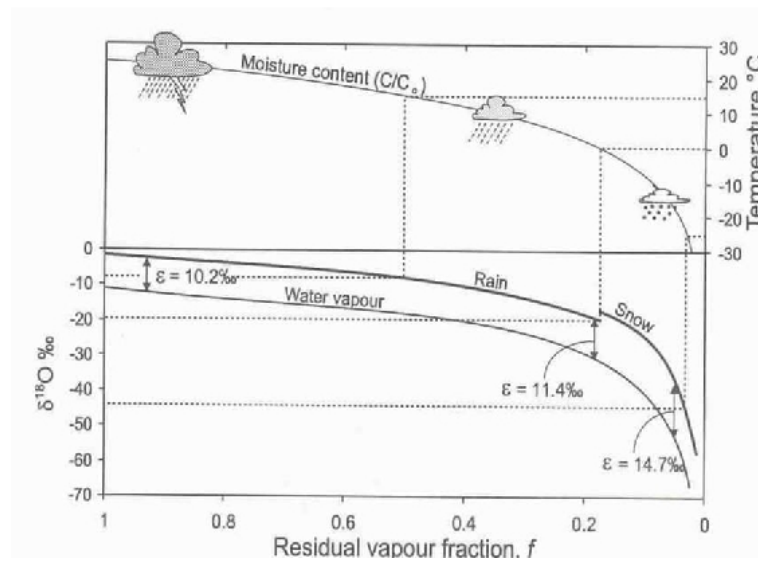
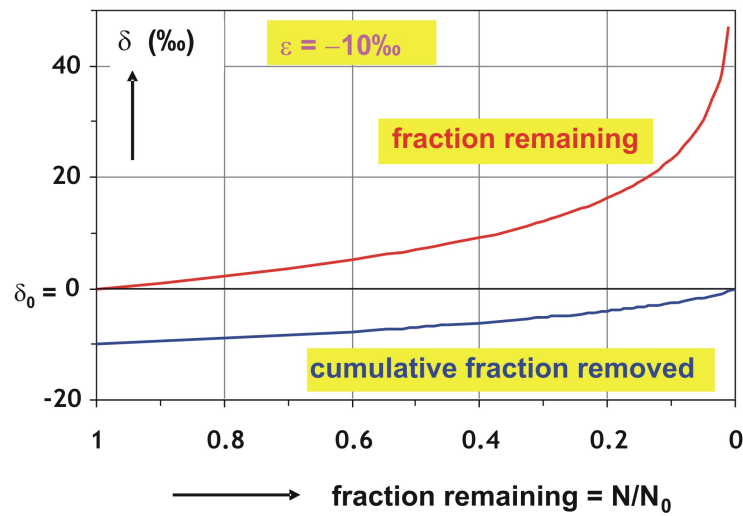


Figure 1.4: Rayleigh isotopic fractionation during (a) evaporation from a confined water body and (b) rain-out process (source: (a) Mook, 2006 and (b) Clark and Fritz, 1997).

Figure 1.4(a) shows the change in the isotopic composition of an evaporating confined water body as time progresses. As water evaporates, the parent water body enriches in the heavy isotopes while the vapor gets depleted. When all water gets evaporated, the isotopic composition of vapor becomes same as the initial iso-

topic composition of water body. In the same way clouds will continuously deplete in the heavier isotopes as rain progresses because heavy isotopes preferentially go to the liquid phase (rain) (Fig. 1.4(b)). The upper part of the figure 1.4(b) shows the progressive cooling of cloud parcel which provides saturation for the rain.

1.2.2 Meteoric Water Line (MWL):

On the global and annual scale ^{18}O and ^2H in the fresh water follow a linear relation which is known as “global meteoric water line (GMWL) ” [Craig, 1961] defined as:

$$\delta D = 8 \delta^{18}\text{O} + 10 \quad (1.10)$$

Here the slope is due to the equilibrium fractionation effect (because $10^3 \ln^2 \alpha / 10^3 \ln^{18} \alpha = 72.8/9.2 \approx 8$, for equilibrium fractionation at 25°C) whereas intercept is due to the kinetic fractionation effects. Slope of MWL changes with changing humidity conditions over oceans (decreases with low humidity conditions). Slope 8 of MWL can be achieved only when humidity approaches to 90% [Gat, 1971]. Local meteoric water line can be different than GMWL as it is highly governed by the local atmospheric conditions such as temperature and humidity. Subsequent monitoring of the stable isotopic composition of precipitation world wide (IAEA Global Network for Isotopes in Precipitation - GNIP) has refined this relationship [Rozanski et al., 1992] .

$$\delta D = (8.13 \pm 0.07) \delta^{18}\text{O} + (11.27 \pm 0.65) \quad (1.11)$$

1.2.3 d-excess:

The combined use of hydrogen and oxygen isotopes in the rain water provides an additional parameter, deuterium excess (the d-excess, Dansgaard, 1964)

$$d = \delta D - 8 \delta^{18}\text{O} \quad (1.12)$$

The d-excess parameter provides information of local moisture recycling. Kinetic fractionation occurs during the evaporation of water bodies under low relative humidity conditions (significantly <100%). Under evaporative conditions, a water body will become enriched in ^{18}O and D, generating values on slope < 8 with a d-excess less than the initial value. Considering conservation of mass, the resultant vapor and precipitation will have a d-excess value greater than the source value. As a water body goes through successive evaporation and precipitation cycles, the d-excess will consequently increase [Lachniet and Patterson, 2002]. Thus, water that is evaporated back into the atmosphere is effectively labeled and can be traced through the water cycle.

1.3 Aim of This work

The aim of the present work is to understand isotopic equilibrium/disequilibrium conditions during phase change over land and ocean and demonstrate potential of stable isotopes as powerful tracers to understand the microphysical processes associated with rain formation.

The specific aims of the present study are:

- To understand stable isotopic heterogeneity of the atmospheric water vapor over the Indian Ocean. Only a few direct observations are available for the stable isotopic compositions of the vapor over the Indian Ocean. Generally it is assumed that vapor over oceans is highly homogeneous for the isotopes but this needs experimental verifications over several parts of the world oceans.
- To understand stable isotopic heterogeneity of the ocean surface water, as isotope based models require this as an input. Still isotopic studies of ocean surface waters are sparse especially in the Indian Ocean and the Southern Ocean.
- To understand isotopic equilibrium/disequilibrium between ocean surface wa-

ters and atmospheric water vapor. Also to study the dependency of the isotopic equilibrium on the different atmospheric parameters such as relative humidity, sea surface temperature and winds.

- To trace changes in the isotopic composition of atmospheric water vapor and precipitation over Ahmedabad (23°N, 72.5°E) during pre-monsoon (April and May), monsoon (June, July, August, and September), and post-monsoon seasons (October, November, and December).
- Investigate from the above data whether the rainfall is in isotopic equilibrium with the atmospheric water vapor. Investigate whether the Rayleigh isotopic fractionation model is obeyed.
- Investigate whether the overall isotopic variability in rain, vapor and clouds has any patterns that could help to understand the monsoon better.
- To test whether rain isotopic ratios have some relation with the rain drop size distribution. This will help to gain insight into the rain formation process.
- High resolution sampling of rain water for isotopic study along with MST radar operation at Gadanki (13.5°N, 79.2°E) to understand microphysical processes associated with rain formation.

1.4 Scientific questions addressed

The present study has attempted to address following important scientific questions:

- What is the extent of isotopic heterogeneity in the ocean surface and atmospheric water vapor?
- Are water and its vapor in isotopic equilibrium over the Indian Ocean?
- How does water-vapor equilibrium vary in space and time?

- Is there any significant contribution of kinetic fractionation over the Indian Ocean?
- Is rain over land/ocean in isotopic equilibrium with atmospheric water vapor?
- What is the contribution of secondary evaporation of rain over the land?
- Is there a pattern in the isotopic variability of rain and vapor that can be useful to understand the monsoon better?
- What is the role of local moisture during the monsoon and non-monsoon days?
- Does high time-resolution study of rain water help to understand microphysical processes associated with rain formation?
- How do microphysical processes associated with rain formation vary in different types of clouds?
- Is there any relationship between the rain drop size distribution and its isotopic composition?

In short, the main aim of the present study is to understand the hydrological cycle by analyzing its important component i.e. ocean surface water, vapor and rain and fill the gaps related to equilibrium/disequilibrium conditions during phase change over land and ocean. Also to explore the usefulness of stable isotopes as a tracer to understand microphysical processes associated with rain formation.

1.5 Organization of the Thesis

This thesis has been divided into five chapters. Their contents are as follows: **Chapter 2** discusses details about the instruments used for the present study along with the international protocols followed.

Chapter 3 discusses important findings from the ocean studies from ocean surface

water, water vapor and rain water samples. For this cruises were undertaken to the Southern Ocean as it is a less explored region and the Indian Ocean.

Chapter 4 deals with the important results obtained from the land based studies performed at Ahmedabad and Gadanki. This includes results from the simultaneous study of rain using MST Radar, Disdrometer and isotopic composition of rain water over Gadanki. This chapter also includes atmospheric water vapor and rain water studies over Ahmedabad.

Chapter 5 This chapter summarizes the results obtained from the present study and discusses their importance in the global scenario. This chapter also provide a future direction to develop better understanding of earth's hydrological system.

References:

- Angert, A., J. E. Lee and D. Yakir (2008), Seasonal variations in the isotopic composition of near-surface water vapor in the eastern Mediterranean, *Tellus*, 60B, 674-684.
- Archambeau, A. S., C. Pierre, A. Poisson and B. Schauer (1998), Distribution of oxygen and carbon stable isotopes and CFC-12 in the water masses of the southern ocean at 30°E from South Africa to Antarctica: results of CIVA1 cruise, *Journal of Marine System*, 17, 25-38.
- Atlas, D., C. W. Ulbrich, F. D. Marks Jr., E. Amitai and C. R. Williams (1999), Systematic variation of drop size and radar-rainfall relations, *J. Geophys. Res.*, 104, 6155-6169.
- Baker, M. B. (1997), *Cloud Microphysics and Climate*, Science, 276, 1072-1078.
- Brown, D., J. Worden and D. Noone (2008), Comparison of atmospheric hydrology over convective continental regions using water vapor isotope measurements from space, *J. Geophys. Res.*, doi:10.1029/2007JD009676.
- Celle-Jeanton, H., R. Gonfiantini, Y. Travi and B. Sol (2004), Oxygen-18 variations of rainwater during precipitation: application of the Rayleigh model to selected rainfalls in Southern France, *J. Hydrol.*, 289, 165-177.
- Ciais, P. and J. Jouzel (1994), Deuterium and oxygen 18 in precipitation: Isotopic model, including mixed cloud processes, *J. Geophys. Res.*, 99, 16,793-716,803.

Clark, I. D. and P. Fritz. (1997), *Environmental Isotopes in Hydrology*, CRC Press, Boca Raton, Fla, USA.

Craig, H. (1961), Isotopic Variations in Meteoric Waters, *Science*, 133 (3465), 1702-1703.

Craig, H. and L. I. Gordon (1965), Deuterium and oxygen 18 variations in the ocean and the marine atmosphere, in *Stable Isotopes in Oceanographic Studies and Paleotemperatures*, edited by E. Tongiorgi, Lab. Geol. Nucl., Pisa, Italy, 9-130.

Dansgaard, W. (1964), Stable isotopes in precipitation, *Tellus*, 16, 436-468.

Delaygue, G., E. Bard and C. Rollion (2001), Oxygen isotope/salinity relationship in the north Indian Ocean, *J. Geophys. Res.*, 106 (C3), 4565-4574.

Duplessy, J. C. (1993), Century-scale events in monsoonal climate over the past 20000 years, *Nature*, 364, 322-324.

Friedman, I., A. C. Redfield, B. Schoen and J. Harris (1964), The variation of deuterium content of natural waters in the hydrological cycle, *Rev. Geophys.*, 2, 177-224.

Fudeyasu, H., K. Ichiyanagi, A. Sugimoto, K. Yoshimura, A. Ueta, M. D. Yamanaka and K. Ozawa (2008), Isotope Ratios of Precipitation and Water Vapor observed in Typhoon Shanshan, *J. Geophys. Res.*, 113, D12113, doi:12110.11029/12007JD009313.

Gadgil, S., P. V. Joseph and N. V. Joshi (1984), Ocean-Atmospheric coupling over monsoonal regions, *Nature*, 312, 141-143.

Gat, J. R. (1971), Comments on the stable isotope method in regional ground-water investigation, *Wat. Resour. Res.*, 7, 980-993.

Gat, J. R. (1996), Oxygen and Hydrogen isotope in Hydrologic cycle, *Annu. Rev. Earth Planet Sci.*, 24, 225-262.

Gupta, A. K., D. M. Anderson and J. T. Overpeck (2003), Abrupt Changes in the Holocene Asian Southwest Monsoon and Their Links to the North Atlantic, *Nature*, 421, 354-357.

Hartmann, D. L. (2002), *CLIMATE CHANGE: Tropical Surprises*, *Science*, 295

(5556), 811-812.

He, H. and R. B. Smith (1999), Stable isotope composition of water vapor in the atmospheric boundary layer above the forests on New England, *J. Geophys. Res.*, 104 (D9), 11,657-611,673.

Jouzel, J. (1986), Isotopes in cloud physics: Multiphase and multistage condensation process, *Handbook of environmental isotope geochemistry*, Elsevier Sci., New York, 2, 61-112.

Jouzel, J. and R. D. Koster (1996), A reconsideration of the initial conditions used for stable water isotope models, *J. Geophys. Res.*, 101 (D17), 22,933-922,938, doi:910.1029/1096JD02362.

Jouzel, J. and L. Merlivat (1984), Deuterium and oxygen 18 in precipitation, Modeling of the isotopic effects during snow formation, *J. Geophys. Res.*, 89, 11,749-711,757.

Lachniet, M. S. and W. P. Patterson (2002), Stable isotope values of Costa Rican surface waters, *Journal of Hydrology*, 260, 135-150.

Lamark, J. B. (1802), Sur la forme des nuages, *Annuaire Meterologique pour l'An XI de la Republique Francaise*, 3, 149-64, Paris.

Lawrence, J. R. (2003), Tropical ice core isotopes: Do they reflect changes in storm activity?, *Geophys. Res. Lett.*, 30 (2), 1072, doi:1010.1029/2002GL015906.

Lawrence, J. R., S. D. Gedzelman, D. Dexheimer, H.-K. Cho, G. D. Carrie, R. Gasparini, C. R. Anderson et al. (2004), Stable isotopic composition of water vapor in the tropics, *J. Geophys. Res.*, 109, D06115, doi:06110.01029/02003JD004046.

Lee, X., R. Smith and J. Williams (2006), Water vapour $^{18}\text{O}/^{16}\text{O}$ isotope ratio in surface air in New England, USA, *Tellus*, 58B, 293-304.

Luntgens, F. K. and E. J. Tarbuck (1998), *The atmosphere: An Introduction to Meteorology*, Prentice hall college Div.

Majoube, M. (1971), Fractionnement en oxygen-18 et en deuterium entre l'eau et sa vapeur., *J. Chem. Phys*, 68, 1423-1436.

Merlivat, L. and J. Jouzel (1979), Global climatic interpretation of deuterium-oxygen 18 relationship for precipitation, *J. Geophys. Res.*, 84, 5029-5033.

- Mook, W. G. (2006), *Introduction to Isotope Hydrology: Stable and Radioactive Isotopes of Hydrogen, Oxygen and Carbon.*, Taylor and Francis.
- Ramesh, R. (2001), High resolution Holocene monsoon records from different proxies: An assessment of their consistency, *Curr. Sci.*, 81, 1432-1436.
- Rao, T. N., D. N. Rao, K. Mohan and S. Raghavan (2001), Classification of tropical precipitating systems and associated Z-R relationships, *J. Geophys. Res.*, 106, 17699-17711.
- Rindsberger, M., S. Jaffe, S. Rahamim and J. R. Gat (1990), Patterns of the isotopic composition of precipitation in time and space: data from the Israeli storm water collection program, *Tellus*, 42B, 263-271.
- Rozanski, K., L. Araguas-Araguas and R. Gonfiantini (1992), Relation Between Long-Term Trends of Oxygen-18 Isotope Composition of Precipitation and Climate, *Science*, 258 (5084), 981-985.
- Rozanski, K., L. Araguas-Araguas and R. Gonfiantini (1993), Isotopic patterns in modern global precipitation, in *Climate Change in Continental Isotopic Records*, *Geophys. monogr. Ser.*, vol 78, edited by P. K. Swart et al., pp 1-36, AGU, Washington, D. C.
- Schmidt, G. A., G. R. Bigg and E. J. Rohling (1999), Global Seawater Oxygen-18 Database, <http://data.giss.nasa.gov/o18data/>, NASA Goddard Inst. of Space Sci., New York, N. Y.
- Scholl, M. A., T. W. Giambelluca, S. B. Gingerich, M. A. Nullet and L. L. Loope (2007), Cloud water in windward and leeward mountain forests: The stable isotope signature of orographic cloud water, *Water Resour. Res.*, 43, W12411.
- Smith, J. A., A. S. Ackerman, E. J. Jensen and O. B. Toon (2006), Role of deep convection in establishing the isotopic composition of water vapor in the tropical transition layer, *J. Geophys. Res.*, 33, L06812, doi: 06810.01029/02005GL024078.
- Tokay, A. and D. A. Short (1996), Evidence from tropical raindrop spectra of the origin of rain from stratiform versus convective clouds, *J. Appl. Meteorol.*, 35, 355-371.
- Uemura, R., Y. Matsui, K. Yoshimura, H. Motoyama and N. Yoshida (2008), Evidence of deuterium excess in water vapor as an indicator of ocean surface conditions, *J. Geophys. Res.*, 113, D19114, doi:19110.11029/12008JD010209.

Webster, C. R. and A. J. Heymsfield (2003), Water Isotope Ratios D/H, $^{18}\text{O}/^{16}\text{O}$, $^{17}\text{O}/^{16}\text{O}$ in and out of Clouds Map Dehydration Pathways, *Science*, 302 (5651), 1742-1745.

Wen, X. F., X. M. Sun, S. C. Zhang, G. R. Yu, S. D. Sargent and X. Lee (2008), Continuous measurement of water vapor D/H and $^{18}\text{O}/^{16}\text{O}$ isotope ratios in the atmosphere, *Journal of Hydrology*, 349, 489-500.

Willett, K. M., N. P. Gillett, P. D. Jones and P. W. Thorne (2007), Attribution of observed surface humidity changes to human influence, *Nature*, 449 (7163), 710-712.

Worden, J., D. Noone, K. Bowman and the Tropospheric Emission Spectrometer science team and data contributors contributors (2007), Importance of rain evaporation and continental convection in the tropical water cycle, *Nature*, 445, 528-532.

Chapter 2

Experimental Techniques

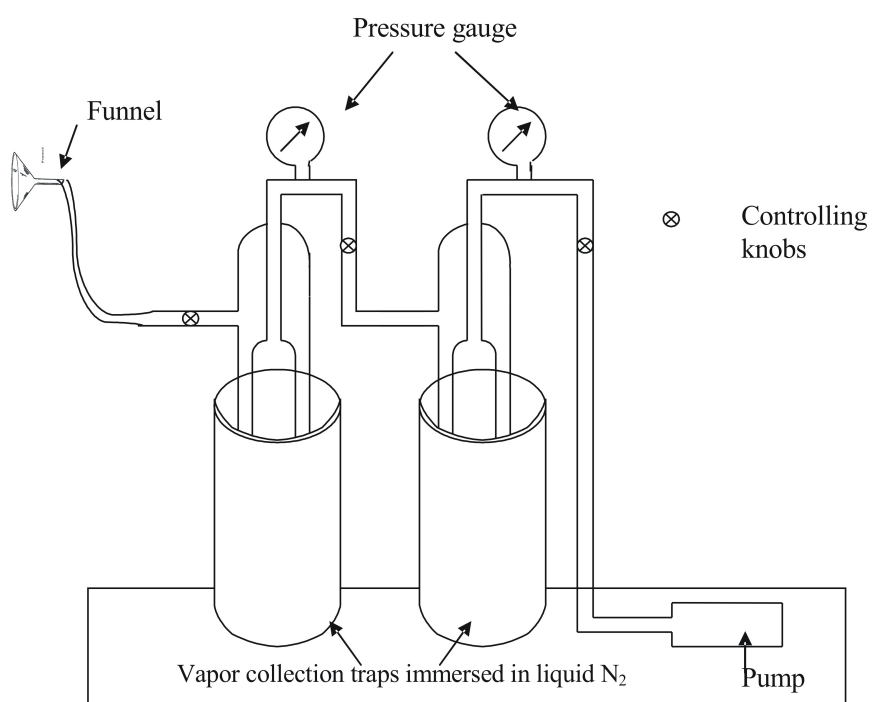
This chapter discusses the instruments used in the present study and the international protocols followed. Atmospheric water vapor, rain water and ocean water samples were collected to understand various processes related to the hydrological cycle such as atmosphere-ocean interaction and rain formation processes. A glass line was designed to collect atmospheric water vapor (2.1.1) whereas rain water collection was done using a rain collector (2.1.2). Ocean water samples were collected with the help of Niskin bottles attached to a CTD rosette (2.1.3). Sometimes a clean plastic bucket with a plastic rope was also used to collect the ocean surface water (plastic was used to avoid any metallic contamination). Disdrometer (2.1.4) and MST Radar (2.1.5) were used for the drop size distribution and cloud structure studies. Water samples were analyzed for stable isotopic studies ($\delta^{18}O$ and δD) using a stable isotope ratio mass spectrometer (2.2). Calibration and reproducibility of the lab standards are discussed in 2.3.

2.1 Instruments and sampling

2.1.1 Vapor Collection Line

Atmospheric water vapor (AWV) samples were collected at the Physical Research Laboratory, Ahmedabad (23.03°N, 72.55°E) at a height of ~ 8 m above the ground level. There are no open water bodies nearby for ~ 2 km. These samples were collected daily from 1000 Hrs -1200 Hrs IST (IST = Universal Time + 5:30). Weekly cleaning and maintenance of the vapor sampling line was carried out on sundays, when samples were not collected.

Water vapor was collected cryogenically using liquid nitrogen (-196°C) and an extraction line composed of U-shaped glass traps (Fig. 2.1) [e.g. Fudeyasu et al., 2008]. Three U-shaped vapor traps were used to ensure efficient trapping of vapor, as partial trapping may cause fractionation. In the schematic diagram of vapor collection only two traps are shown for simplicity of figure. Ambient air was sampled using a rotary vacuum pump through a system consisting of a funnel, polyethylene tube, and an extraction line. The funnel was connected to the extraction line through the polyethylene tube. Proper arrangements were made to ensure that the rain water did not enter into the extraction unit. The flow rate of air was about 2 Lmin^{-1} for the water vapor collection (to obtain at least 2 ml of vapor sample). Generally, vapor samples were collected for a period of 2 h from 1000 Hrs - 1200 Hrs IST (except in April 2007 when low humidity values necessitated the collection for 4 h, from 1100 Hrs - 1500 Hrs to ensure sufficient amount of vapor sample). Trapped atmospheric CO_2 was removed by pumping out the extraction line at the end of the vapor collection by replacing the liquid nitrogen with ethanol slush (maintained at -90°C). Thus, CO_2 free water vapor was collected and immediately transferred to good quality double cap sample bottles for subsequent isotopic analysis.



(a)



(b)

Figure 2.1: (a) Schematic diagram of Vapor Collection and (b) Author with Atmospheric water vapor collection unit on ship.

2.1.2 Rain water collection

Rain water collection was done using a rain collector (Fig. 2.2). This collector contains a carboy and a funnel on its mouth. The mouth of the funnel was kept very narrow with the help of one another cap and a thin wire. This thin wire creates a narrow way for the rain water to go inside the carboy. This whole arrangement was made to prevent re-evaporation of rain water after its collection in the carboy. A special metallic stand was designed to hold the carboy vertical and to prevent it from moving by winds. Finally the collected rain water was transferred to double capped plastic bottles and taped on the neck. Bottles were filled up to the brim to prevent any re-evaporation.



Figure 2.2: Author with rain collector.

2.1.3 Ocean water collection

Most of the time ocean water collection was done using Niskin bottles attached to a CTD rosette (Fig. 2.3). These bottles were kept open when CTD goes down. Once it reaches to the required depth, bottles were triggered to close before bringing it up. Occasionally when CTD did not work, a cleaned plastic bucket with plastic rope was used for ocean surface water collection; these ocean water samples were transferred in 100 ml plastic bottles with tight-fitting double cap to prevent any further evaporation after collection. The bottles were filled to the brim and taped at the neck as a further precaution.

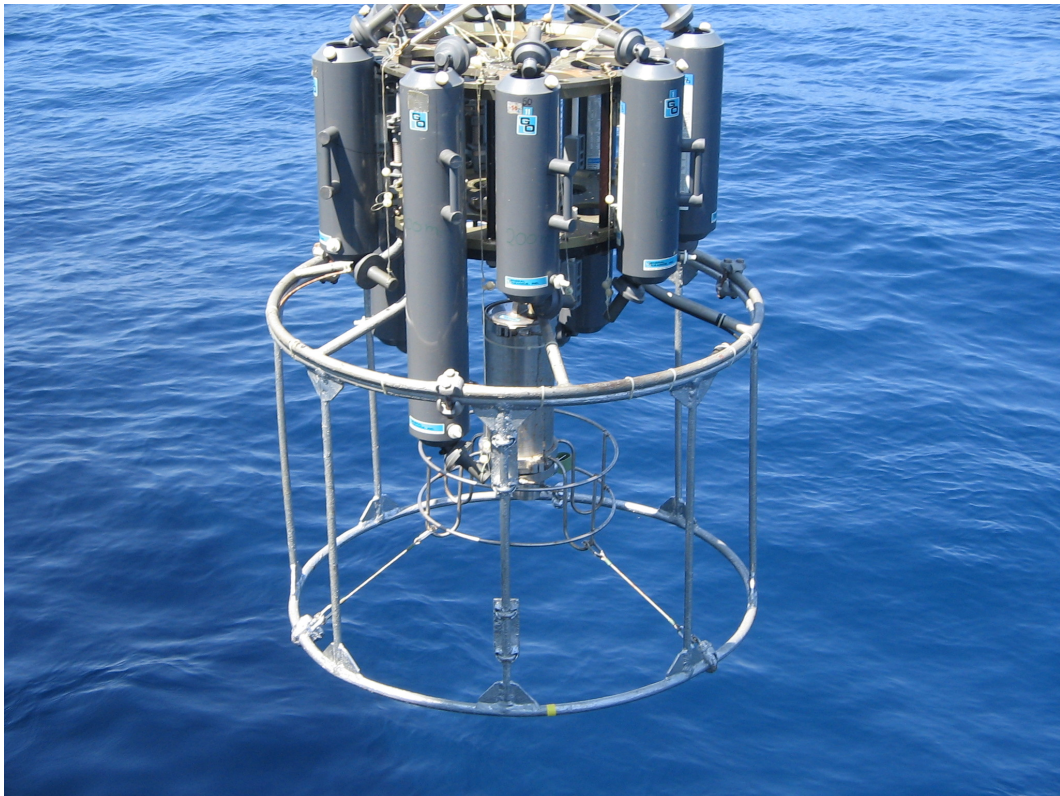


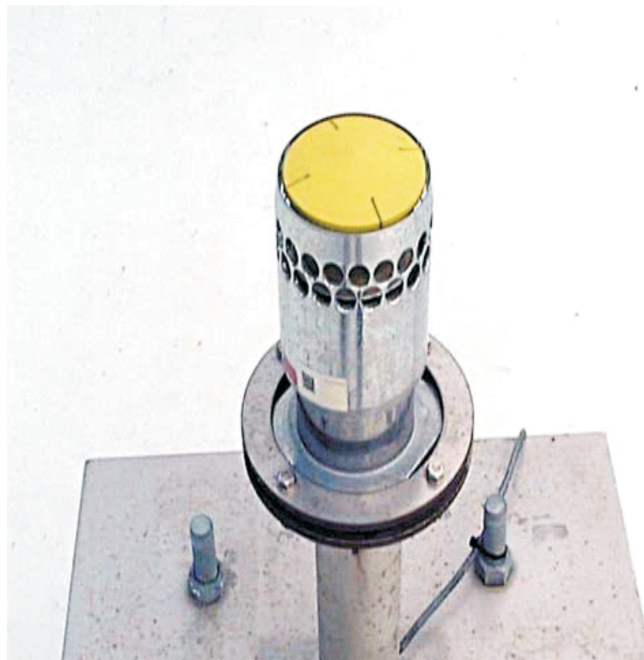
Figure 2.3: Niskin bottles attached to a CTD rosette used to collect sea-water samples from surface and different depths.

2.1.4 Disdrometer

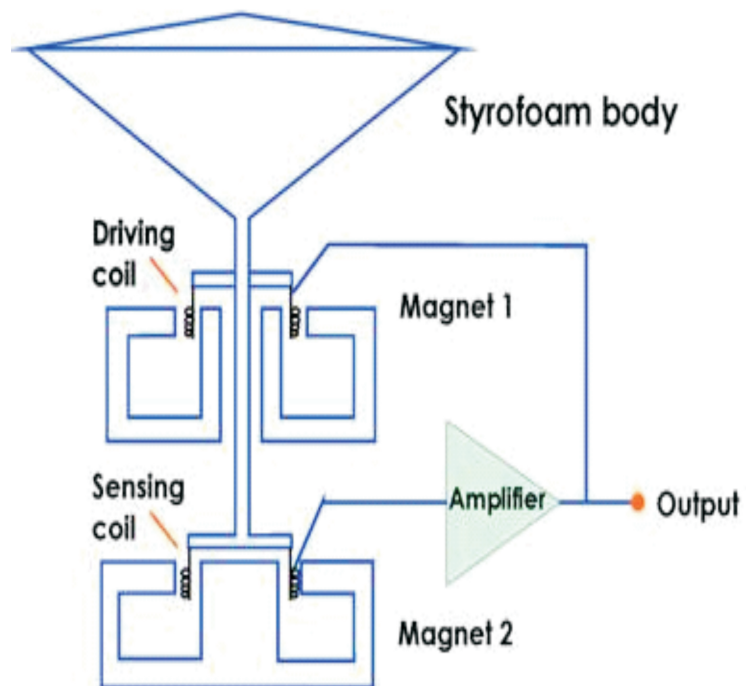
A simultaneous study of drop size distribution (DSD) and stable isotopic composition of rain water was done to understand the microphysical processes related to the rain formation. For this study rain water collection and DSD measurements were done at National Atmospheric Research Laboratory (NARL), Gadanki (13.5°N, 79.2°E). The rain DSD at the ground was measured with a RD-69 Joss-Waldvogel (JW) disdrometer, located ~ 5 m away from rain collection spot. This was used to measure rain drop size distributions continuously and automatically at every minute. It records number and size of raindrops hitting the 50 cm² sensor head. This allows estimating rain rate, liquid water content, and the median volume diameter. The range of drop diameters that can be measured spans from 0.3 mm to 5 mm in 20 drop-size classes. The instrument consists of a sensor and a processor connected to a computer. The sensor consists of styrofoam body, driving coil and magnet, and an amplifier in a common housing (Fig. 2.4 (a) and (b)).

When a rain drop falls over the styrofoam surface, the two moving coils attached with it move downwards and a voltage is induced in the sensing coil. This voltage is amplified by an amplifier and also applied to the driving coil so that a force counteracting the movement is produced which brings the system to its original position within a short duration. The amplitude of the pulse so produced by the electromechanical transducer is a function of drop diameter [Suresh et al., 2004]. The instrument transforms the vertical momentum of an impacting rain drop into an electric pulse whose amplitude is a function of the drop diameter. A conventional pulse height analysis yields the size distribution of the raindrops.

To ascertain quality of disdrometer measurements, the disdrometer estimated rainfall rates were compared with those obtained with a co-located Optical Rain Gauge (ORG-815). Very good agreement has been found between these measurements (with a linear correlation coefficient, r , of 0.99).



(a)



(b)

Figure 2.4: (a) Disdrometer and (b) Schematic diagram of Disdrometer.

2.1.5 MST Radar

The Indian Mesosphere–Stratosphere–Troposphere (MST) radar located at, NARL, Gadanki is a powerful very high frequency (VHF) Doppler radar, which not only provides 3D wind and turbulence information but also useful to study the precipitation [Rao et al., 1999] (Fig. 2.5). Vertically pointing Doppler radars operating at VHF and ultra high frequency (UHF) can provide information about ambient air motion and the structure of hydrometeors, respectively, in the precipitating clouds that are present overhead. As a result, one can directly determine the fall velocity spectrum of hydrometeors by using accepted empirical relations. The DSD can be estimated accurately from its fall velocity spectrum. The Indian MST radar operates at a frequency of 53 MHz and with a peak power of 2.5 MW. The antenna array consisting of 1024 crossed yagi antennas and generates a radiation pattern with a half power beam width of 3°. During the campaign period, the radar was kept on alert and operated in a special mode, whenever rain occurred over Gadanki. The important parameters of the radar for this experiment were as follows: pulse width - 1 μ s, inter pulse period - 250 μ s, coherent integrations - 128, incoherent integrations - 4, FFT (Fast Fourier Transform) points - 512, number of radar beams - 3 (zenith and 10° off-zenith towards west and south), temporal resolution - 4 min, and range resolution - 150 m. Echoes due to refractive index fluctuations and hydrometeors were identified in the spectral domain and were separated [Rao et al., 1999].

There are two approaches to get DSD from radar: (1) parameterization method and (2) deconvolution method. The parameterization method first assumes a functional form for DSD, either an exponential [Wakasugi et al., 1986; Sato et al., 1990] or a gamma [Currier et al., 1992; Rajopadhyaya et al., 1998; Cifelli et al., 2000] and then convolutes with the known clear-air spectrum. This model spectrum is then fitted, using nonlinear least squares fitting, to the observed precipitation spectrum to retrieve DSD parameters. The deconvolution method

obtains the true precipitation spectrum from the observed precipitation (UHF) spectrum by deconvolving it with the clear-air (VHF) spectrum [Kobayashi and Adachi, 2005; Kirankumar et al., 2007]. Schafer et al. [2002] compared these two approaches for dual-frequency retrievals and found that the deconvolution method generally performed better for a broader range of median diameters. So the direct deconvolution method has been employed to retrieve rain DSD. The JW disdrometer is used for absolute calibration of the radar power. Modeling and experimental studies have shown that DSD retrieval with VHF radars may not, always be able to resolve drops smaller than 1 mm [Rajopadhyaya et al., 1993].



Figure 2.5: MST radar At Gadanki.

2.2 Mass Spectrometer (Stable Isotope Ratio Mass Spectrometer)

Mass spectrometry is a technique to separate ions according to their mass to charge (m/q) ratios. In the mass spectrometer, gas is ionized using high energetic electrons emitted by a thoriated tungsten filament. These ionized gas particles get acceler-

ated by an accelerating potential and enter into the magnetic field which splits it into beams of ions of different masses. These separated ion beams get collected in Faraday cups and isotope ratios are calculated according to their fluxes. Stable isotopic study of the collected water samples was done using a dual inlet Stable Isotope Ratio Mass spectrometer (PDZ-Europa Geo 20-20). This mass spectrometer was manufactured by Europa Scientific, UK and became operational since 1998 at the Physical Research Laboratory, Ahmedabad (Fig. 2.6). It is a triple collector mass spectrometer and contains a separate collector for H_2 measurements. It has two separate spurs for the measurement of H_2 and CO_2 isotopic ratios.



Figure 2.6: Author with stable isotope ratio Mass Spectrometer at PRL.

Dual inlet mass spectrometer contains two separate inlets for reference and sample gas. Gas sample goes into the source chamber through a metallic capillary

(length $\sim 1\text{m}$ and diameter $\sim 10^{-4}\text{m}$). This not only provides a steady mass flow due to high pressure gradient but also prevents the back diffusion of gas sample. Change from sample gas to standard gas is done by changeover valve. So once measurement for reference gas is done it allows the sample gas to flow inside. Like this it keeps on changing and helps rapid and repeated comparison of the sample with reference.

Mass spectrometer mainly consists of three units (Fig. 2.7).

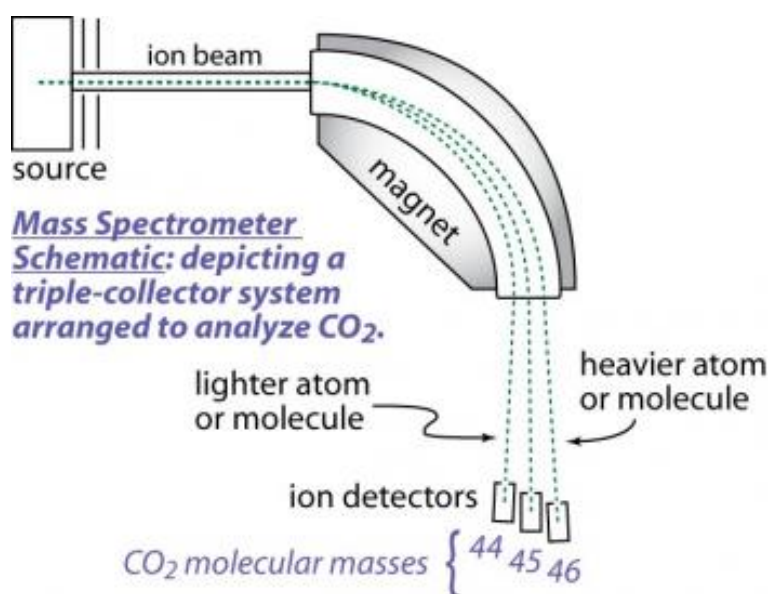


Figure 2.7: Schematic diagram of a mass spectrometer.

1. **Source:** This part of the mass spectrometer converts purged gas into positively ionized gas molecules. High energetic electrons ($\sim 70\text{ eV}$) are emitted by a thoriated tungsten filament by the thermionic emission. This energy is sufficient for single ionization of gas molecules. A low magnetic field makes these electrons path spiral, so that they travel a longer distance within the source. This provides more interaction of electrons with gas molecules and increases the ionization rate. These electrons strike gas molecules, leaving molecules positively charged. Ionized gas molecules are then accelerated by the high voltage (0-5kV) and focused into a narrow beam (beam

diameter < 1 mm) with the help of collimating plates and electronic lenses. These accelerated positively charged gas molecules then enter the magnetic field.

2. **Analyzer:** Main function of analyzer is to split the ionized beam according to m/q ratio. A stable magnetic field is generated (3.8 k Gauss for CO_2 and 1 k Gauss for H_2) around the flight tube from which ionized gas molecules travel and get deflected according to their m/q ratio and enter the collector.
3. **Collector:** Collector is made of Faraday cups, resistances ($\sim 10^9 \Omega$) and counters. A Faraday cup (Fig. 2.8) is a metal cup designed to catch charged particles in vacuum. These cups are positioned in such a way that ionized deflected gas molecules enter into the cups and get neutralized. The resulting current is measured and used to determine the number of ionized gas molecules entering in the cups.

Faraday cups are connected with a glass encapsulated high resistance ($\sim 10^9 \Omega$). Resultant voltage is measured and converted to the frequency using voltage to frequency converter (VFC) which is then converted to the digital form.

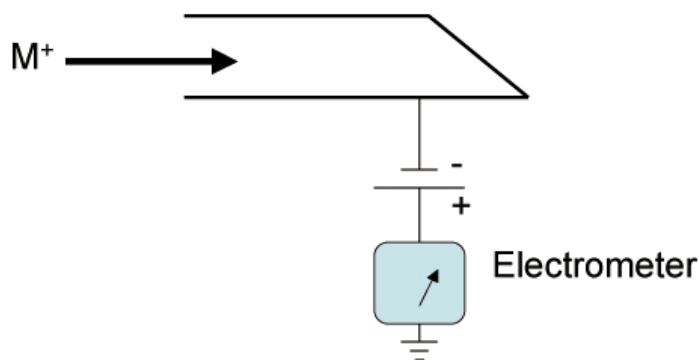


Figure 2.8: Schematic diagram of faraday cup.

In the faraday cup when a beam or packet of ions hits the metal it gains a small net charge while the ions get neutralized. The metal can then be discharged

to measure a small current equivalent to the number of impinging ions. By measuring the electrical current (the number of electrons flowing through the circuit per second) in the metal part of the circuit the number of charges being carried by the ions in the vacuum part of the circuit can be determined. For a continuous ion beam (each with a single charge)

$$q = It = Ne \quad (2.1)$$

$$\frac{N}{t} = \frac{I}{e} \quad (2.2)$$

where 'N' is the number of ions observed in a time 't' (in seconds), 'I' is the measured current (in amperes) and 'e' is the elementary charge. Separated ion beams of different masses are electronically counted and compared in this part of mass spectrometer.

2.2.1 Mathematical basis of isotope separation:

Energy gained by an ion of charge 'q' in an accelerating voltage 'V' is given by 'qV'. This energy is transferred to the molecule as kinetic energy. So

$$qV = \frac{1}{2}mv^2 \implies v = \sqrt{\left(\frac{2qV}{m}\right)} \quad (2.3)$$

If the molecule enters in a magnetic field, it experiences a force (Lorentz force) of magnitude $q(\mathbf{v} \times \mathbf{B})$ which imparts a centripetal force (mv^2/r) of equal magnitude.

$$q(\mathbf{v} \times \mathbf{B}) = \frac{mv^2}{r}\hat{\eta} \quad (2.4)$$

Since magnetic field is perpendicular to the velocity vectors, $\theta = 90^\circ$.

Using equation(2.3), equation (2.4)can be written as

$$r = \sqrt{\frac{2Vm}{B^2q}} \quad (2.5)$$

So for a constant V, B and q, radius of curvature will be proportional to the square root of mass. Hence ions of different masses follow different radial paths and get deflected by the magnetic field.

2.2.2 Delta notation

Isotope ratios such as

$${}^2R = \frac{{}^2H}{{}^1H} \quad {}^{13}R = \frac{{}^{13}C}{{}^{12}C} \quad {}^{18}R = \frac{{}^{18}O}{{}^{16}O}$$

are generally not reported as absolute ratios because of necessity for international comparison which requires the use of standards to which the sample has to be related. Also absolute ratios are less relevant than the changes in the ratios occurring during certain processes.

Therefore, isotopic abundance is generally reported as a deviation of the isotope ratio of a sample 'A' relative to that of a reference sample or standard 'r':

$$\delta_{A/r} = \left(\frac{R_A}{R_r} - 1 \right) \times 10^3 \quad (2.6)$$

For example oxygen isotopic composition will be written as [Coplen, 1996]

$$\delta^{18}O = \left\{ \frac{({}^{18}O/{}^{16}O)_{sample}}{({}^{18}O/{}^{16}O)_{standard}} - 1 \right\} \times 10^3 \quad \text{in permil} \quad (2.7)$$

In the present study VSMOW (Vienna Standard Mean Ocean Water) has been used as a standard. This standard is provided by International Atomic Energy Agency (IAEA).

2.2.3 Water equilibration System (WES):

Water sample equilibration was done with the help of a separate preparation unit attached to the mass spectrometer known as water equilibration system (WES) (Fig. 2.9). It is an automatic system controlled by computer. WES contains a constant temperature bath with a sample tray having capacity of keeping 59 samples at a time, Gilson needle (for injection and taking out the gas from sample vials), metallic line (to insert gas into the mass spectrometer), a rotary pump (to create vacuum in the line), a vapor trap (to remove vapor from the equilibrated gas), valves (to control gas flow) and electronic circuits.

1 ml of each water sample was first loaded in a 6.8 ml glass bottle and then covered using a cap with neoprene septum (provided by LABCO, UK). Good quality caps and septum are very important to prevent any leak from the sample bottles. After loading water sample in sample bottle air was flushed by CO₂ gas (or by H₂ gas for δD) using Gilson needle (Fig. 2.10) at a little higher pressure than the atmospheric pressure. Each sample was flushed for about 30 seconds and left with pressurized CO₂ gas in the bottle for equilibration.

Equilibrated gas was taken out by Gilson needle and purged to the mass spectrometer through a spiral line (trap) for the isotopic analysis. This trap was kept at -70°C using a cryocool to remove any moisture that might be present along with CO₂ gas.

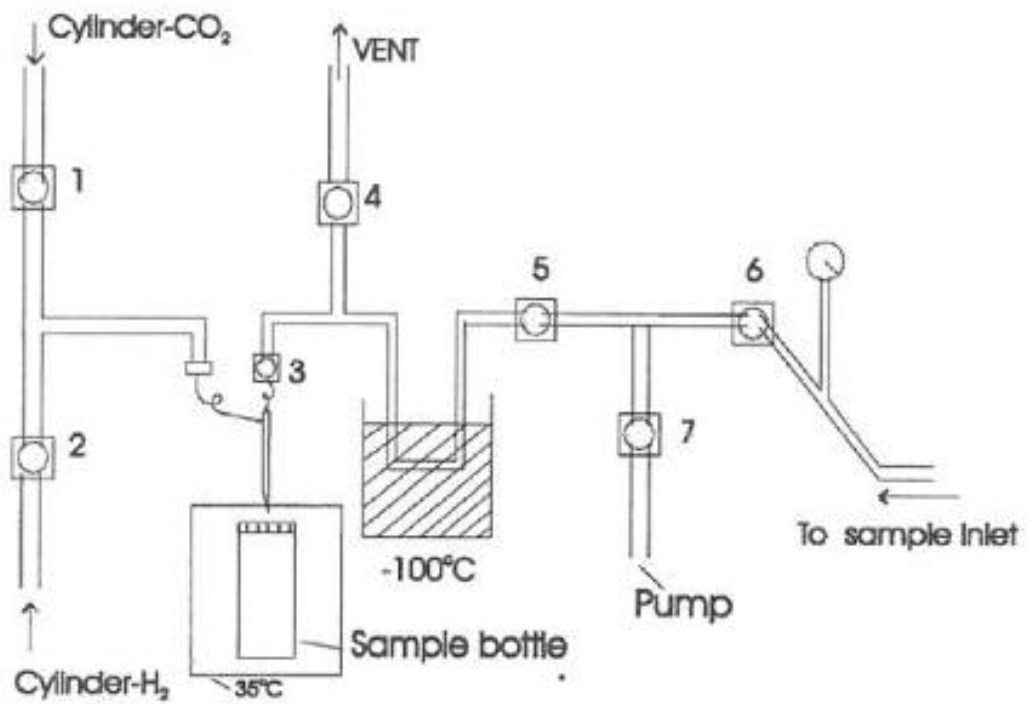


Figure 2.9: Schematic diagram of Water Equilibration System.

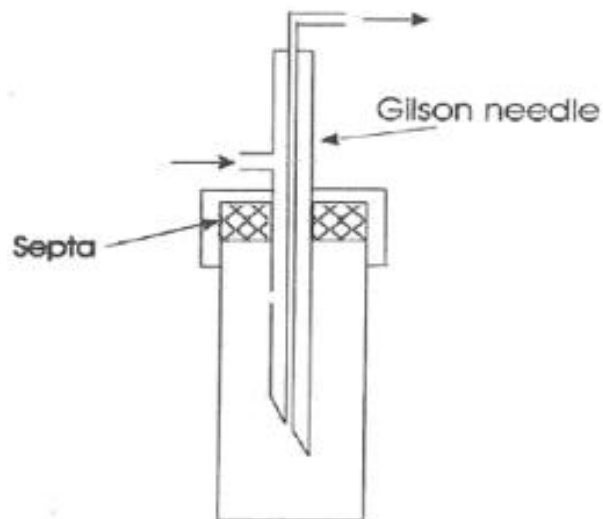


Figure 2.10: Schematic diagram of Gilson needle in a sample bottle.

2.2.4 $\delta^{18}O$ measurements:

Water samples were first isotopically equilibrated with CO_2 gas (Provided by Vadilal Company, 99.9% pure) [Gonfiantini, 1981]. Equilibration takes minimum 8 hours at $35^\circ C$. Equilibrated CO_2 is 41.2‰ [Clark and Fritz, 1997] enriched relative to the water in ^{18}O . ^{18}O preferentially goes to CO_2 as heavier atoms prefer stronger bonding ((H-OH) = 492 kJ mol⁻¹, (O=CO) = 531 kJ mol⁻¹) [Atkins and Paula, 2002]. This equilibrated CO_2 gas is purged into mass spectrometer for stable isotopic analysis. Mass spectrometer is capable of measuring even a very small amount of CO_2 ($\sim 5 \mu mole$) with the precision of 0.1‰. Measurement of stable isotope ratios of CO_2 involves preparation of calibrated working standard. This working standard gas (Vadilal CO_2 gas with $\delta^{18}O_{VSMOW} = 17.4\text{‰}$) was used regularly in mass spectrometer as a reference gas.

The measurement of $\delta^{18}O$ and $\delta^{13}C$ is done simultaneously at the same focusing condition in this mass spectrometer. The ion beams corresponding to the different species (i.e. 44, 45 and 46 which correspond to the species $^{12}C^{16}O^{16}O$, $^{13}C^{16}O^{16}O + ^{12}C^{17}O^{18}O$ and $^{12}C^{16}O^{18}O + ^{13}C^{16}O^{17}O + ^{12}C^{17}O^{17}O$, respectively) are collected separately in the different collectors. Major ion current corresponds to the mass 44 as it is most abundant in the nature than the other CO_2 forming species. First δ_{45} and δ_{46} were calculated according to the number density ratios using electronic circuit. As these were the molecular ratios so to convert these molecular ratios to atomic ratios Craig corrections [Craig, 1957] were applied:

$$\delta^{13}C = 1.0676 \delta_{45} - 0.0338 \delta^{18}O \quad (2.8)$$

$$\delta^{18}O = 1.0010 \delta_{46} - 0.0021 \delta^{13}C \quad (2.9)$$

This gives the $\delta^{18}O$ value with respect to the working gas (δ_{wg}^s). For all measurements, after every 8 water samples a secondary lab standard (Narmada river water calibrated with VSMOW) was kept to monitor the performance of mass spectrom-

eter. This standard also goes through the same procedure as other water samples. Isotope ratios of the samples were corrected according to deviation in value of the Narmada standard. Such deviations were small ($<0.1\%$ for $\delta^{18}O$).

δ_{wg}^s is used to calculate delta value with respect to the Narmada standard (δ_{Narm}^s) by applying a simple algebraic equation (derived using definition of delta value).

$$\delta_C^A = \delta_B^A + \delta_C^B + \delta_B^A \delta_C^B \times 10^{-3} \quad (2.10)$$

Here δ_C^A represents isotopic composition of A with respect to C. This can be rewritten for our case as:

$$\delta_{Narm}^s = \delta_{wg}^s + \delta_{Narm}^{wg} + \delta_{wg}^s \delta_{Narm}^{wg} \times 10^{-3} \quad (2.11)$$

Where s: sample, Narm: Narmada standard water, wg: working gas. Using equation (2.10) δ_{Narm}^s again is converted to the delta value with respect to the international standard, which is VSMOW.

$$\delta_{Vsmow}^s = \delta_{Narm}^s + \delta_{Vsmow}^{Narm} + \delta_{Narm}^s \delta_{Vsmow}^{Narm} \times 10^{-3} \quad (2.12)$$

δ_{Vsmow}^{Narm} is determined by analysing the water standard provided by IAEA.

2.2.5 δD Measurements:

Water samples were equilibrated with H_2 gas (H_2 gas purchased from Vadilal, 99.9% pure) for hydrogen isotopic (δD) analysis [Gonfiantini, 1981]. As H_2 is a lighter gas relative to CO_2 , it requires more time for the equilibration. To reduce the equilibration time, platinum coated beads (known as Hokko Beads) were used as catalyst. This catalyst reduces the equilibration time up to two hours. After loading water samples, 3 beads were added for each sample. Then bottles were closed and flushed with H_2 gas for 40 seconds. Water samples were left for equilibration for 2 hours at $35^\circ C$ in the WES. This equilibrated H_2 gas was purified

through spiral trap (maintained at -70°C) and taken to mass spectrometer. The hydrogen gas was ionized to H_2^+ and HD^+ ions due to the impact of high energetic electron in the mass spectrometer and the ratio of mass -3 to mass -2 i.e. HD^+/H_2^+ was calculated. For δD analysis again Narmada river water was used as a secondary lab standard whereas H_2 gas calibrated with respect to VSMOW was used as the reference gas. In the same way as for $\delta^{18}\text{O}$ measurements, after eight water samples one Narmada water standard was kept to continuously monitor the performance of mass spectrometer. Mass spectrometer gives δD value of the sample with respect to the working gas (H_2). This value is then converted relative to the international standard (VSMOW) using equation (2.10).

During ionization process H_3^+ ion is also being produced by the following reaction



which has the same mass as HD^+ . To get the correct isotopic ratio, a correction is applied (known as H_3 correction) [Gonfiantini, 1981]. Formation of H_3^+ is directly proportional to the major ion current. So by calculating $((\text{HD}^+ + \text{H}_3^+)/\text{H}_2^+)$ for different values of major ion currents, actual $((\text{HD}^+)/\text{H}_2^+)$ can be calculated. This correction is estimated by the GEO 20-20 using a linearity routine which is run (before every batch of samples) at different concentrations of the major beam (H_2^+) using the reference H_2 gas. The correction is then applied to all the HD analysis. Contribution from H_3^+ ions is around 4.2%.

2.3 Calibration tables

2.3.1 IAEA Inter laboratory comparison exercise for $\delta^{18}\text{O}$ and δD analysis of water samples

Inter comparison exercise was organized by IAEA in 2002 (WICO-2002). More than 85 laboratories participated in this work. Results from our laboratory and

provided by IAEA (consensus value) are shown in Table (2.1) and (2.2)

Table 2.1: Results from water samples provided by IAEA for $\delta^{18}O$ measurement (with respect to VSMOW).

Sample code	PRL values (‰)	Consensus values (‰)
OH-5	-0.29	-0.20
OH-6	-4.16	-4.17
OH-7	-10.69	-10.65
OH-8	-16.21	-16.20

Table 2.2: Results from water samples provided by IAEA for δD measurement (with respect to VSMOW).

Sample code	PRL values (‰)	Consensus values (‰)
OH-5	-2.5	-1.7
OH-6	-38.2	-38.7
OH-7	-77.3	-77.8
OH-8	-121.1	-121.8

2.3.2 Laboratory standard (Narmada water) reproducibility

(A) For $\delta^{18}O$ Measurements:

Values for the different runs of Narmada water standard are given in Table (2.3). Mean of all runs of the standard is $-4.51 \pm 0.09\text{‰}$ which is same as calibrated value of Narmada water relative to the VSMOW (-4.51‰). Old Narmada standard got finished after May 08. So a new Narmada standard was used with $\delta^{18}O = -4.57\text{‰}$ (with respect to VSMOW) (Table 2.4).

Table 2.3: $\delta^{18}O$ values (with respect to VSMOW) of Narmada water standard measured at PRL.

Date	$\delta^{18}O$ (‰)
10/05/06	-4.45
	-4.47
	-4.48
	-4.54
	-4.59
	-4.56
	-4.50
	-4.51
	-4.51
12/05/06	-4.37
	-4.42
	-4.45
	-4.52
	-4.62
	-4.60
	-4.55
	-4.56
14/05/06	-4.36
	-4.47
	-4.54
	-4.46
	-4.57
16/05/06	-4.49
	-4.50
	-4.51
	-4.54
	-4.51
18/05/06	-4.36
	-4.46
	-4.45
	-4.56
	-4.64
	-4.57
	-4.54
01/05/07	-4.34
	-4.56
	-4.30
	-4.37

Date	$\delta^{18}O$ (‰)
	-4.63
	-4.52
	-4.55
	-4.80
22/06/07	-4.35
	-4.53
	-4.54
	-4.61
	-4.56
	-4.53
	-4.44
26/06/07	-4.42
	-4.45
	-4.46
	-4.51
	-4.53
	-4.52
	-4.51
	-4.57
	-4.60
28/06/07	-4.51
	-4.50
	-4.50
	-4.59
	-4.55
	-4.50
	-4.43
	-4.51
	-4.53
30/06/07	-4.51
	-4.50
	-4.46
	-4.51
	-4.55
	-4.53
	-4.50
	-4.48

09/07/07	-4.55
	-4.59
	-4.45
	-4.55
	-4.50
	-4.54
	-4.49
	-4.45
	-4.46
20/09/07	-4.4
	-4.26
	-4.52
	-4.62
	-4.63
	-4.48
	-4.67
24/09/07	-4.47
	-4.41
	-4.50
	-4.55
	-4.57
	-4.51
	-4.60
	-4.50
28/09/07	-4.64
	-4.60
	-4.46
	-4.52
	-4.58
	-4.39
	-4.37
	-4.49
01/10/07	-4.62
	-4.58
	-4.34
03/10/07	-4.52
	-4.47
	-4.54
	-4.57

	-4.33
	-4.60
	-4.53
	-4.53
05/10/07	-4.48
	-4.54
09/12/07	-4.43
	-4.45
	-4.43
	-4.62
	-4.63
12/12/07	-4.37
	-4.37
	-4.56
	-4.68
	-4.55
10/04/08	-4.45
	-4.46
	-4.54
	-4.76
	-4.69
	-4.63
	-4.77
	-4.82
12/04/08	-4.53
	-4.42
	-4.50
	-4.58
	-4.57
	-4.57
	-4.49
	-4.46
14/04/08	-4.46
	-4.48
	-4.52
	-4.56
	-4.52
	-4.57
	-4.44

16/04/08	-4.27
	-4.41
	-4.52
	-4.62
	-4.55
	-4.59
	-4.60
18/04/08	-4.45
	-4.56
	-4.51
22/04/08	-4.43
	-4.44
	-4.43
	-4.47
	-4.64
	-4.55
	-4.51
	-4.56
	-4.58
24/04/08	-4.23
	-4.28
	-4.43
	-4.58
	-4.59
	-4.64
	-4.67
	-4.68
25/04/08	-4.35
	-4.41
	-4.46
	-4.55
	-4.57
	-4.55
	-4.60
	-4.62
27/04/08	-4.38
	-4.43
	-4.36
	-4.48
	-4.64
	-4.65
	-4.65

02/05/08	-4.39
	-4.39
	-4.49
	-4.55
	-4.60
	-4.62
	-4.52
12/05/08	-4.44
	-4.50
	-4.57
	-4.55
14/05/08	-4.37
	-4.44
	-4.54
	-4.59
	-4.55
	-4.57
15/05/08	-4.38
	-4.38
	-4.45
	-4.58
	-4.56
	-4.58
	-4.56
	-4.6
17/05/08	-4.49
	-4.54
	-4.48
	-4.54
	-4.49
20/05/08	-4.43
	-4.48
	-4.61
	-4.54
22/05/08	-4.46
	-4.48
	-4.54
	-4.43
	-4.59

Mean $\delta^{18}O = -4.51 \pm 0.09\text{‰}$ (n=233); where n is number of times standard measured.

Table 2.4: $\delta^{18}O$ values (with respect to VSMOW) of new Narmada water standard measured at PRL.

Date	$\delta^{18}O$ (‰)
24/05/08	-4.57
	-4.58
	-4.56
	-4.64
	-4.61
27/05/08	-4.53
	-4.52
	-4.65
	-4.60
	-4.65
	-4.54
	-4.67
	-4.52
29/05/08	-4.54
	-4.55
	-4.62
	-4.68
	-4.61
	-4.54
	-4.61
	-4.56
03/06/08	-4.50
	-4.53
	-4.69

Mean $\delta^{18}O = -4.59 \pm 0.06\text{‰}$ (n=24); where n is number of times standard measured.

(B) For δD Measurements:

Values of the different runs of Narmada water standard is given in Table 2.5. Mean of all runs of the standard is $-35.78 \pm 0.81\text{‰}$ which is same as the calibrated value of Narmada water relative to the VSMOW (-35.78‰).

Table 2.5: δD values (with respect to VSMOW) of Narmada water standard measured at PRL.

Date	δD (‰)	Date	δD (‰)
27/05/06	-35.07	25/07/07	-36.15
	-36.16		-35.41
	-34.47	27/07/07	-35.19
	-36.37		-36.10
	-36.83		-36.23
28/05/06	-35.21		-35.60
	-36.27	28/07/07	-36.94
	-36.00		-36.41
	-34.28		-36.37
	-36.35		-35.51
	-36.57		-34.66
29/05/06	-36.37		-34.79
	-35.95	30/07/07	-34.31
	-34.48		-37.37
	-35.83		-35.66
	-36.27	01/08/07	-36.24
30/05/06	-35.87		-35.56
	-33.76		-36.06
	-34.90		-35.25
	-35.52	02/08/07	-35.99
	-36.21		-36.20
	-38.51		-35.32
	-35.69		-35.61
03/06/06	-36.67	05/08/07	-36.25
	-36.10		-36.77
	-35.61		-36.01
	-34.74		-34.74
04/06/06	-35.62		-35.41
	-35.94		-35.49
09/06/06	-36.54		
	-35.16		
	-34.82		
	-36.74		
	-35.64		

Mean $\delta D = -35.78 \pm 0.81\text{‰}$ (n=62); where n is number of times standard measured.

References:

- Atkins, P. and J. D. Paula. (2002), *Physical Chemistry*, Oxford University Press. UK.
- Cifelli, R., C. R. Williams, D. K. Rajopadhyaya, S. K. Avery, K. S. Gage and P. T. May (2000), Drop-size distribution characteristics in tropical mesoscale convective systems, *J. Appl. Meteor.*, 39, 760-777.
- Clark, I. D. and P. Fritz. (1997), *Environmental Isotopes in Hydrology*, CRC Press, Boca Raton, Fla, USA.
- Coplen, T. B. (1996), Editorial: More uncertainty than necessary, *Paleoceanography*, 11 (4), 369-370.
- Craig, H. (1957), Isotopic standards for carbon and oxygen and correction factors for mass-spectrometric analysis of carbon dioxide, *Geochimica et Cosmochimica Acta*, 12, 133-149.
- Currier, P. E., S. K. Avery, B. B. Balsley, K. S. Gage and W. L. Ecklund (1992), Combined use of 50 MHz and 915 MHz wind profilers in the estimation of raindrop size distributions, *Geophys. Res. Lett.*, 19, 1017-1020.
- Fudeyasu, H., K. Ichiyanagi, A. Sugimoto, K. Yoshimura, A. Ueta, M. D. Yamanaka and K. Ozawa (2008), Isotope Ratios of Precipitation and Water Vapor observed in Typhoon Shanshan, *J. Geophys. Res.*, 113, D12113, doi:10.1029/2007JD009313.
- Gonfiantini, R. (1981), In *Stable Isotope Hydrology: Deuterium and Oxygen-18 in the Water Cycle*. Technical Report Series No.210 (eds. Gat J R and Gonfiantini R.), IAEA, Vienna, 103-142.
- Kirankumar, N. V. P., T. N. Rao, B. Radhakrishna and D. N. Rao (2007), Statistical characteristics of raindrop size distribution in southwest monsoon season, *Journal of Applied Meteorology and Climatology*, 47, 576-590.
- Kobayashi, T. and A. Adachi (2005), Retrieval of arbitrarily shaped raindrop size distributions from wind profiler measurements, *J. Atmos. Oceanic Technol.*, 22, 433-442.
- Rajopadhyaya, D. K., P. T. May, R. Cifelli, S. K. Avery, C. R. Williams, W. L. Ecklund and K. S. Gage (1998), The effect of vertical air motions on rain rates and median volume diameter determined from combined UHF and VHF wind profiler

measurements and comparisons with rain gauge measurements, *J. Atmos. Oceanic Technol.*, 15, 1306-1319.

Rajopadhyaya, D. K., P. T. May and R. A. Vincent (1993), A general approach to the retrieval of raindrop size distributions from wind profiler Doppler spectra: Modeling results, *J. Atmos. Oceanic Technol.*, 10, 710-717.

Rao, T. N., D. N. Rao and S. Raghavan (1999), Tropical precipitating systems observed with Indian MST radar, *Radio Sci.*, 34, 1125-1139.

Sato, T., D. Hiroshi, H. Iwai, I. Kimura, S. Fukao and M. Yamamoto (1990), Computer processing for deriving drop-size distributions and vertical air velocities from VHF Doppler radar spectra, *Radio Sci.*, 25, 961-973.

Schafer, R., S. Avery, P. May, D. Rajopadhyaya and C. Williams (2002), Estimation of rainfall drop size distributions from dual frequency wind profiler spectra using deconvolution and a nonlinear least squares fitting technique, *J. Atmos. Oceanic Technol.*, 19, 864-874.

Suresh, R., J. P. Gupta, P. R. Rao and A. K. Bhatnagar (2004), Time evolution of rain drop spectra over Coddalore in coastal Tamilnadu, *Mausam*, 55, 441-456.

Wakasugi, K., A. Mizutani, M. Matsuo, S. Fukao and S. Kato (1986), A direct method for deriving drop-size distribution and vertical air velocities from VHF Doppler radar spectra, *J. Atmos. Oceanic Technol.*, 3, 623-629.

Chapter 3

Ocean surface water and water vapor studies

3.1 Stable isotopic study of the Southern Ocean surface water:

The Southern Ocean, defined as the region between the south of 60°S and Antarctica [International Hydrographic Organization, 2000], is an important region that affects the climate of the earth. The main bottom and intermediate water masses of the world ocean originate here. The Antarctic zone of the Southern Ocean refers to the vast area between the polar front and the Antarctic continent. The surface water in this zone, characterized by a commonly observed summer minimum surface temperature, is the Antarctic Surface Water (AASW) [Park et al., 1998]. The thermohaline structure of this water mass is determined by seasonally changing air-sea interaction (air-sea fluxes of momentum, heat and fresh water), advection and formation/melting of sea ice [Gordon and Huber, 1984]. Despite its close relationship with changing atmospheric conditions, the vertical and horizontal structures of AASW of the Indian sector of the Southern Ocean, as a whole, have not been studied to any extent, although some detailed studies exist for limited locations.

Several expeditions have been made earlier to explore the Indian Ocean as well as the Southern Ocean [Duplessy, 1970; Kallel, 1985; Archambeau et al., 1998; Delaygue et al., 2001]. But due to high spatial and temporal variability this region needs more studies to characterize its physical (such as temperature and salinity), chemical and isotopic properties adequately. Some studies have shown that due to global warming, parts of Antarctic ice sheet are melting and the Southern Ocean is getting more and more melt water [Banks and Bindoff, 2002; Aoki et al., 2003; Aoki et al., 2005; Barnett et al., 2005]. This makes the isotopic study of the Southern Ocean all the more urgent.

The stable isotopic composition ($\delta^{18}O$ and δD) of ocean waters provides specific information on several aspects of the water cycle, and is useful to elucidate the mechanism and estimate the magnitude of the fluxes between the ocean and atmospheric reservoirs. The spatial distribution of $\delta^{18}O$ (and δD) is useful to understand the mechanism responsible for the internal variability of water masses in their source region and allows one to follow their circulation far away from their origin. The isotopic compositions at various stages of the hydrological cycle help constrain different water masses as well as their movement. The variation in the isotopic composition of deep-sea water is relatively smaller than that in freshwater and mainly determined by freshwater input and mixing between water masses [Paul et al., 1999].

A simultaneous study of $\delta^{18}O$ and salinity provides specific information about sea surface processes such as (1) evaporation/precipitation (2) melting/freezing (3) upwelling/advection (4) continental runoff and also helps to understand reasons for the isotopic heterogeneity of the surface waters. In the case of the Southern Ocean, changes due to continental run off are very small. Salinity and $\delta^{18}O$ co-vary in the case of evaporation/precipitation because both parameters decrease due to precipitation whereas evaporation increases both. Salinity and $\delta^{18}O$ exhibit a linear relationship and its slope depends on regional climate, but in the case of melting/freezing, $\delta^{18}O$ does not change much while salinity changes significantly. δD

co-varies with $\delta^{18}O$ generally. Being lighter than oxygen, fractionation factor is higher for hydrogen. δD not only helps to confirm processes detected by $\delta^{18}O$ but also provide information about the humidity conditions at the time of evaporation and extent of kinetic fractionation through the deuterium excess. Proper understanding of these surface processes is very important over the Southern Ocean as it influences monsoon. So a combined study of stable hydrogen (δD) and oxygen ($\delta^{18}O$) isotopes and salinity is ideal to monitor various oceanic processes.

The Southern Ocean is characterized by the presence of several fronts; fronts are defined as water masses with marked changes in the properties [Park et al., 1998]. The Indian sector of the Southern Ocean is characterized by the presence of two such major fronts: the Agulhas Front (AF) and the Subtropical Front (STF) (Fig. 3.1) [Rintoul and England, 2002; Belkin and Gordon, 1996; Michael et al., 1996; Rintoul and Bullister, 1999]. The former is the connecting link between the generically similar Southern Atlantic and Southern Indian Ocean Currents [Deacon, 1937]. It is a major source of water exchange between the Atlantic and the Indian Oceans [Peterson and Stramma, 1991; Read and Pollard, 1993; Lutjeharms, 2006]. It is characterized by the temperature gradient between 15.7°C to 21°C at 200 m depth [Gordon et al., 1978]. AF can merge with the STF or form a separate front to the north of STF between 39°S to 40°S [Lutjeharms and Valentine, 1984]. STF makes an interface between Subtropical Surface Waters and Subantarctic Surface Water [Deacon, 1937]. It is characterized by the horizontal surface temperature and salinity transitions of 10°C to 14°C and 34.6 to 35.1, respectively with the mean location of 42°S [Whitworth and Nowlin, 1987]. While these criteria may be useful to recognize the positions of AF and STF at depths, but we found in the surface they are traceable using $\delta^{18}O$ (and δD) as well, as we show here. Thus, to understand the characteristics of the Southern Ocean (fronts and ocean surface processes) a special expedition was undertaken.

3.1.1 Cruise Track and sampling locations:

Surface seawater samples were collected during the second expedition to the Southern Ocean and Larsemann Hills, Antarctica on board *R/V “Akademik Boris Petrov”* during January to March, 2006. We reached the Prydz Bay area, Antarctica, on 25th February, a time when freezing started in the Antarctic Zone. This cruise covered a large area (from 13°N to 68°S and 71°E to 77°E). 97 ocean surface water samples were collected at one degree latitude intervals.

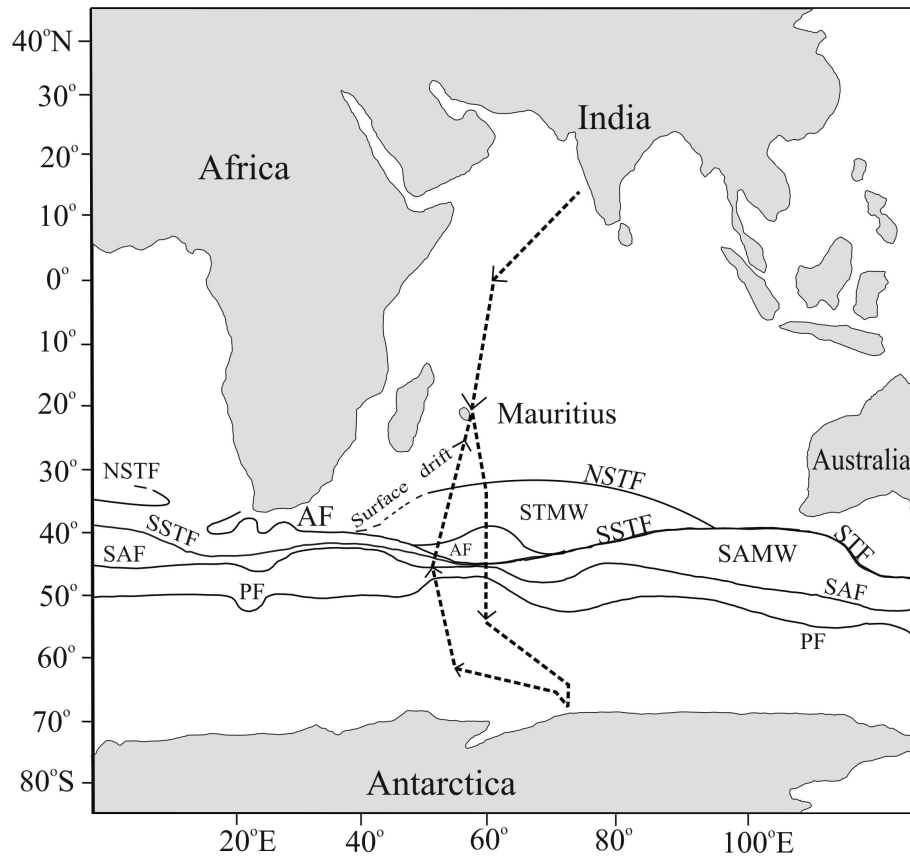


Figure 3.1: Cruise track along which sampling was done. Approximate locations of the various fronts are marked (after Belkin and Gordon, 1996): AF: Agulhas Front; NSTF & SSTF: North and South Sub-Tropical Fronts; PF: Polar front; SAF: Sub-Antarctic Front; SAMW & STMW: Sub -Antarctic and Sub -Tropic Mode Waters. Onward and return journeys are shown by arrows.

The cruise track is shown in figure 3.1. Using a Niskin bottles or clean

plastic bucket, sea surface water samples were collected. Salinity was measured on board using a salinometer (Autosal) with a reproducibility of 0.001. The accuracy was checked by using IAPSO standard sea water of salinity 34.995, conductivity 1.997435, conductivity ratio (K15) 0.99987. An isotope ratio mass spectrometer (PDZ-Europa, Geo 20-20) was used for isotopic analysis.

3.1.2 Salinity and Oxygen isotopic study

The observed latitudinal variations of $\delta^{18}O$, salinity and Sea Surface Temperature (SST) are shown in figure 3.2 (a), (b) and (c) respectively. From 5°N to 45°S salinity follows the $\delta^{18}O$ pattern. North of 4.5°S lies a high salinity and high $\delta^{18}O$ region, indicating a positive E–P (i.e. evaporation dominates). Between 4.5°S to 20°S lies a low salinity and low $\delta^{18}O$ region, with a negative E–P (i.e. precipitation dominates). Moving further south of 20°S, the salinity and $\delta^{18}O$ values again start increasing. This indicates again the domination of evaporation. Due to solar heating, water around the equator (from 13°N to 4.5°S) evaporates and rains south of 4.5°S upto 20°S in the austral summer, when the ITCZ (Inter Tropical Convergence Zone) is located south of the equator.

AF and STF have been reported earlier to be at subsurface; but during our poleward journey (February) we could observe their signature at the very surface. At 41°S there is a change in salinity by 0.69 while $\delta^{18}O$ changes by 0.35‰, showing the presence of AF. Again at 44°S sharp changes in the salinity and oxygen isotopic composition occur. Between 44°S and 45°S, salinity changes by 1.02 and $\delta^{18}O$ by 0.49‰, indicating the position of STF. SST too decreases by 2°C (from 18°C to 16°C) at AF whereas a decrease of 4.5°C (from 15°C to 10.5°C) at STF is seen figure 3.2 (c). During the return journey (March) a sharp increase in $\delta^{18}O$ by 0.95‰ is noticed at 41°S. This indicates that both fronts (AF and STF) have merged at least at the surface; SST too decreased sharply by 9°C at 41°S [Fig. 3.2(c)].

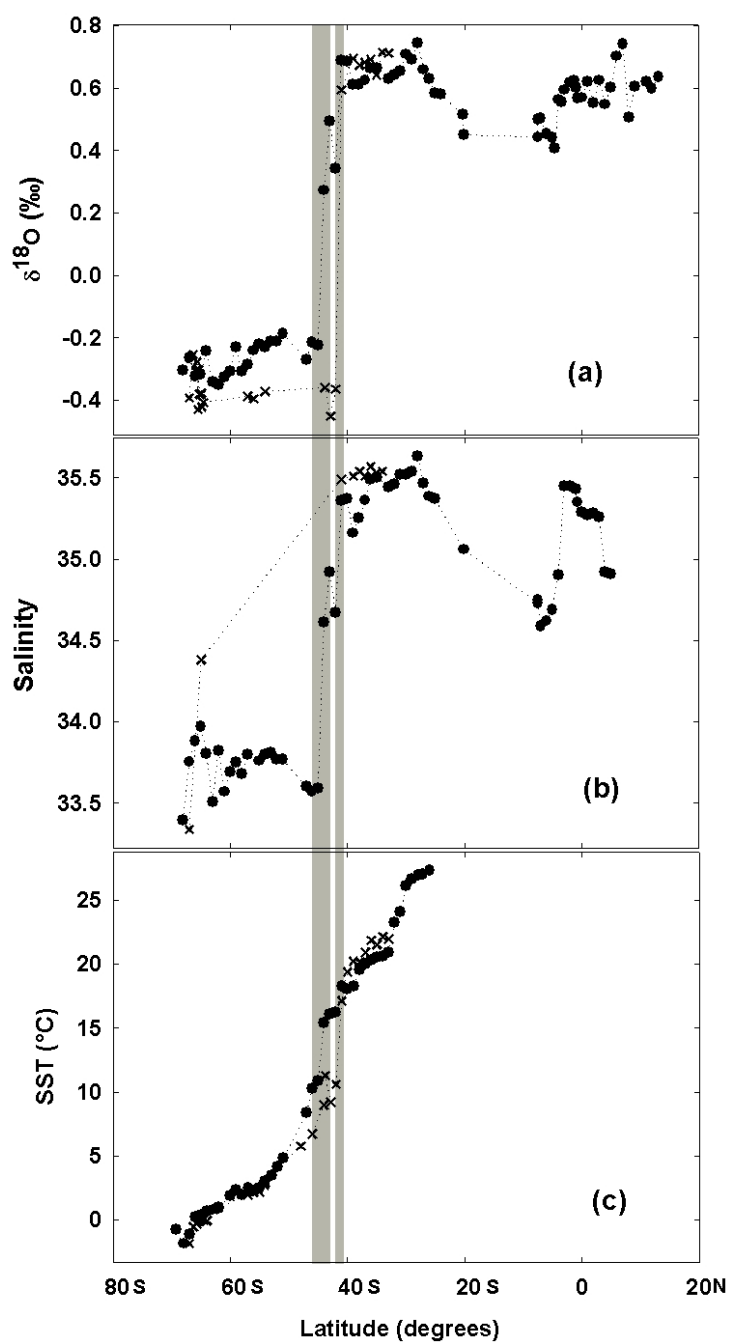


Figure 3.2: Latitudinal variation of (a) salinity (b) $\delta^{18}\text{O}$ and (c) SST of surface waters. The two vertical bands refer to positions of the fronts: STF (left) and AF (right). The filled circles and crosses refer to data collected during onward and return journeys, respectively.

In the case of freezing/melting of an *in situ* ice, sea water $\delta^{18}O$ does not change much whereas the salinity varies significantly. Since the fractionation factor for water to ice transition is very small, freezing does not change the $\delta^{18}O$ of the remaining water or ice significantly. But salinity changes as during freezing ice discards salt; the salt content in the remaining water increases; during melting salinity decreases due to fresh water input from ice. The case of continental ice melt is different. The ice forms by precipitation which is highly depleted in the heavier isotope. So mixing of continental melt water decreases salinity as well as $\delta^{18}O$ of the ocean surface water [e.g. Archambeau et al., 1998]. The region from 45°S to 68°S shows much less variation in $\delta^{18}O$ (between -0.2‰ and -0.4‰) than salinity. From 45°S to 61°S salinity follows the same trend as $\delta^{18}O$ except for some minor variations. From 47°S to 51°S increase of 0.17 in salinity and 0.08‰ in $\delta^{18}O$ are observed. This is a cyclonic area. Winds are very strong (about 10 m/s to 14 m/s) in this region. Due to strong winds evaporation is also high and thus salinity and $\delta^{18}O$ increase. From 51°S (58.8°E) to 62°S (67°E) salinity and $\delta^{18}O$ co-vary, indicating minor effect of precipitation/evaporation. The region between 63°S to 67°S exhibits high salinity (increase in salinity by 0.25 for first region and 0.49 for second region) while $\delta^{18}O$ remains constant. This region is affected by ocean water freezing; we observed freezing during the cruise south of 63°S (Fig. 3.3). From 67°S onwards both $\delta^{18}O$ and salinity start decreasing possibly due to mixing of continental melt ice to the coastal ocean water. During the return journey (March) we have only one sample for salinity up to 41°S (48°E) at 65°S. This high value of salinity (34.38) is due to a strong freezing effect, as visually observed. This is also the beginning of the austral fall. $\delta^{18}O$ shows a constant value from 68°S to 42°S but for small variations between -0.25‰ to -0.45‰ during the return journey. From 41°S to 33°S salinity and $\delta^{18}O$ are both constant except for small variations.



Figure 3.3: Surface water freezing observed during the Southern Ocean cruise.

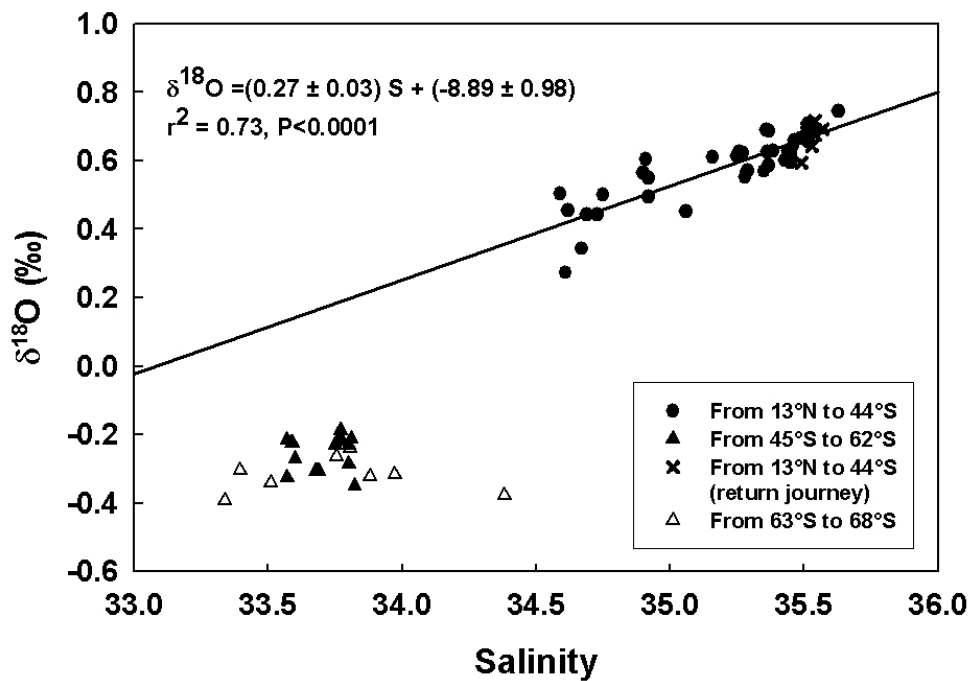


Figure 3.4: $\delta^{18}\text{O}$ – salinity relationship for the Indian Ocean, 2006.

Figure 3.4 shows the relationship between $\delta^{18}O$ and salinity. All points plotted as circles and crosses are from north of 44°S (13°N to 44°S). In the graph, best fit line has a slope of 0.27 ± 0.03 (best fit line: $\delta^{18}O = (0.27 \pm 0.03)S - (8.89 \pm 0.98)$, $r^2 = 0.73$, $P \ll 0$), indicating that this region is governed by local evaporation and precipitation. On the other hand, points plotted as triangles from 45°S to 68°S, lie in a line of negligible slope (best fit line: $\delta^{18}O = -(0.01 \pm 0.06)S + (0.04 \pm 2.10)$, $r^2 = 0.0011$, $P = 0.88$). The data points are further distinguished as filled (upto 62°S) and open triangles (south of 63°S). While the freezing effect is clearly seen for the latter, some evaporation effect can not be ruled out for the former. LeGrande and Schmidt [2006] presented global gridded data set of sea water $\delta^{18}O$ values, with variable number of observations for different oceanic regions. They reported $\delta^{18}O$ -salinity relationships for different oceanic regions, whose definition was somewhat arbitrary, according to them. They cautioned that their data set was too sparse to capture consistently seasonal or longer variability except in localized regions. Our $\delta^{18}O$ data fall in a similar range reported by them. Our results are consistent with their general observations that (i) the $\delta^{18}O$ -salinity slope is greatest at mid-latitudes and shallowest at low latitudes and the Southern Ocean, and (ii) in areas of sea ice formation and melting, the slopes tend to be shallow. They reported slopes of 0.24 and 0.16 respectively for the Southern Ocean and the Indian Ocean. A direct comparison of the slopes obtained by us is difficult because (i) our data are seasonal and theirs pertain to long term means, and (ii) our data pertain only to the Indian sector of the Southern Ocean and theirs cover most parts of the Southern Ocean.

3.1.3 Hydrogen isotopic study

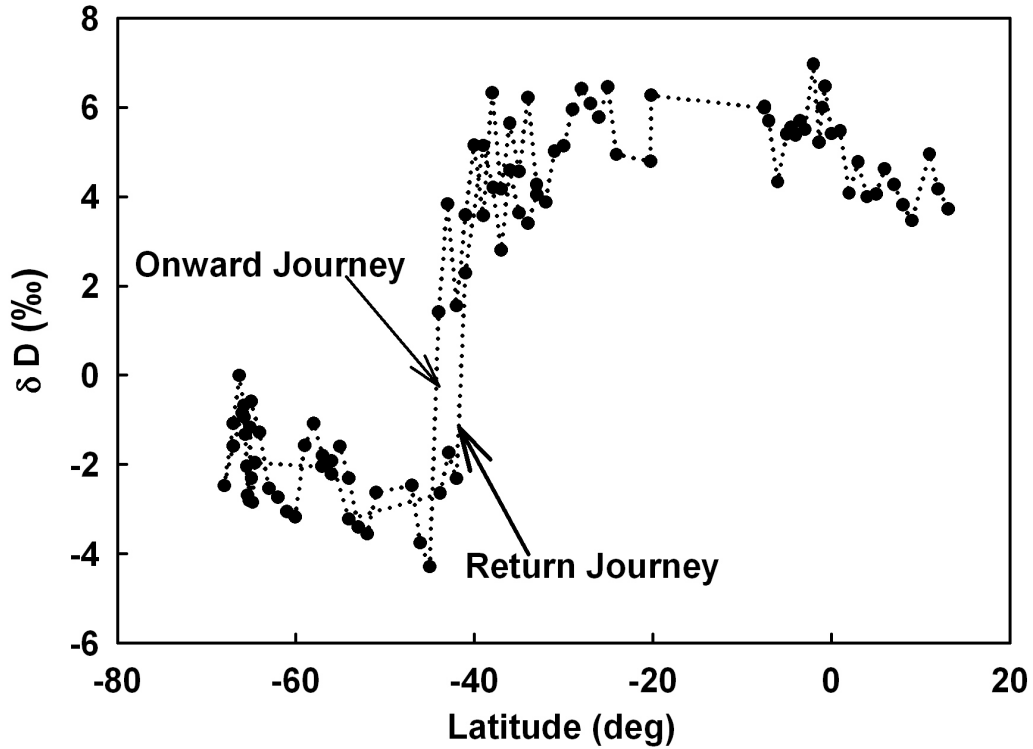


Figure 3.5: Latitudinal variation of δD .

By and large, hydrogen isotopic composition (δD) follows the same trend as $\delta^{18}O$ and salinity (Fig. 3.5) except depleted isotopic values between 4.5°S and 20°S, as observed in the $\delta^{18}O$ and salinity. This may be due to the sparse of sampling in this zone. A sharp decrease in δD of $\sim 8\text{‰}$ from 41°S to 45°S with an increase of $\sim 2\text{‰}$ at 44°S confirms the effect of shoaling of AF and STF. Barring some fluctuations, which are within the experimental uncertainties, δD shows an overall increasing trend, moving towards the south. This increase in the δD values confirms the increasing effect in situ melting of sea ice.

3.1.4 Sea water line over the Southern Ocean

The relation between δD and $\delta^{18}O$ of the ocean surface water gives information about the humidity at the time of evaporation. For worldwide fresh surface waters, Craig [1961] has found that $\delta^{18}O$ and δD exhibit a linear correlation, which defines the global meteoric water line (GMWL). Its slope is ~ 8 and intercept is $\sim 10\text{‰}$. The slope is 8 because this is approximately the value produced by equilibrium Rayleigh fractionation of evaporating water surface at about 90% humidity.

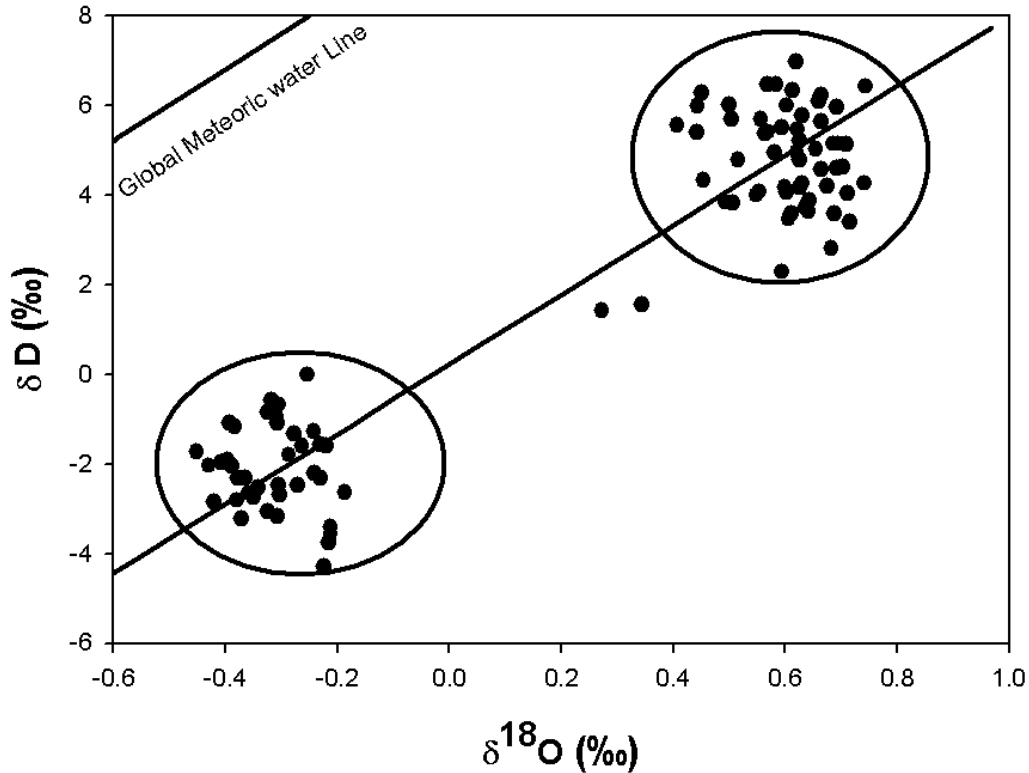


Figure 3.6: Plot of $\delta^{18}O$ vs. δD of surface sea water from the Indian Ocean (best fit line with slope = 7.35 ± 0.29 , intercept = 0.30 ± 0.14 , $r^2 = 0.88$). Global Meteoric Water line is also shown for comparison.

The value of the slope of the GMWL is close to the ratio of the equilibrium fractionation factors for H and O isotopes at 25°C-30°C [Clark and Fritz, 1997].

Slope reduces to less than 8 due to evaporation controlled by ambient humidity (and also due to diffusion through the water vapor boundary layer and exchange with atmospheric water vapor) at the ocean surface. The non-equilibrium evaporation process is characterized [Dansgaard, 1964; Gat, 1981; Mook, 2006] by a slope of less than 8. The relation between δD and $\delta^{18}O$ for the Indian Ocean is depicted in figure 3.6, where data points cluster in two distinct bunches. The best fit line has a slope of (7.35 ± 0.29) , which is significantly lower than the slope of the GMWL (8.12 ± 0.07).

This indicates the Southern Ocean as a whole is evaporating under isotopic non-equilibrium, with a mean ambient humidity significantly less than 95%, as also borne out by humidity observations during the cruise. As a result, the Indian Ocean samples show an intercept of (0.30 ± 0.14) which is much less than the intercept of GMWL (9.20 ± 0.53). The relation between $\delta D - \delta^{18}O$ is similar to two end member mixing (points in the two big circles). This again emphasizes that the region between $41^{\circ}S$ and $45^{\circ}S$ is a transition region between two different types of zones.

3.1.5 Zone demarcation for the Southern Ocean

Thus on the basis of salinity and oxygen (and hydrogen) isotopic data it is inferred that the Indian Ocean north of $41^{\circ}S$ is a zone of dominant evaporation/precipitation whereas south of $47^{\circ}S$ is dominated by melting/freezing. The region between $41^{\circ}S$ and $47^{\circ}S$ is a transition zone between the above mentioned two regions. A schematic representation of these zones is shown in figure 3.7.

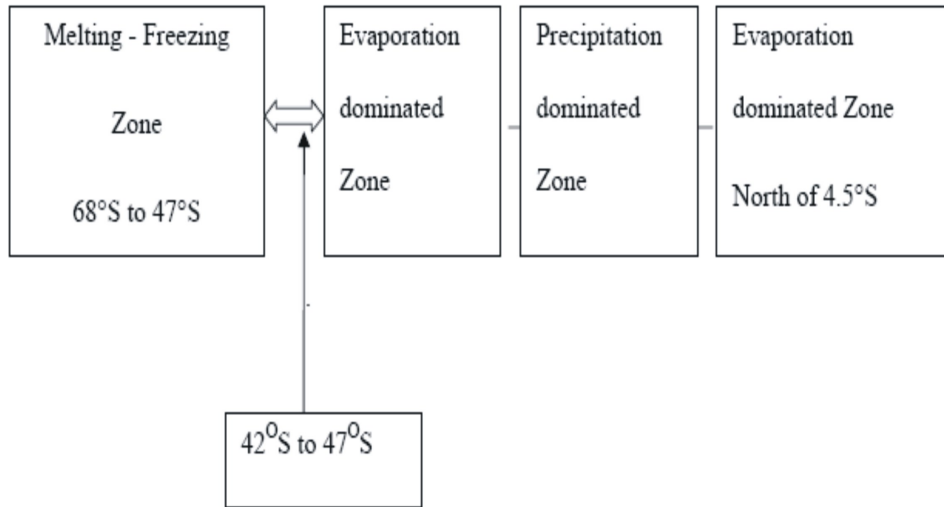


Figure 3.7: Schematic diagram showing different zones in the Southern Indian Ocean depending on domination of different hydrological processes.

3.2 Effect of the Global warming over oceans

Oceans are getting highly affected due to the effect of global warming. Observations shows that $\sim 80\%$ of the total heating of the Earth system (oceans, atmosphere, continents and cryosphere) over the last 40 years has gone into warming the oceans [Levitus et al., 2005]. Due to the effect of warming fresh water input, sea surface level, sea surface temperatures and current structures are significantly changing. But these changes are different for different oceans. A recent model study [Barnett et al., 2005] suggests that ocean warming can not be explained by only taking account the natural internal climate variability or solar and volcanic forcing. To fully explain ocean warming the anthropogenic forcing also has to be taken into the account.

sector of the Southern Ocean as well [Aoki et al., 2003; Aoki et al., 2005] yet such studies are sparse.

To study the effect of global warming on the ocean surface water salinity- $\delta^{18}O$ relation over the Indian sector of the Southern Ocean, a comparative study was done using the previous available stable isotopic and salinity data set (data from Duplessy and Kallel available at <http://data.giss.nasa.gov/o18data> and Archambeau, taken from his paper) [Archambeau et al., 1998; Schmidt et al., 1999]. Sampling points for different studies are shown in figure 3.8. For the comparison, data from the south of 25°S are used as it is common for all studies. NASA data bank does not contain information about the sampling months for Duplessy and Kallel whereas Archabeau and present study were performed in the same season (February-March). All studies were done almost in the same region and likely in the same season. This study demonstrates not only changes in the salinity- $\delta^{18}O$ relation but also changing pattern in the water currents between 40°S and 50°S (sharpness of salinity and $\delta^{18}O$ decrease). This region is very important as it makes demarcation between warm tropical water and Antarctic cold water. Sudden decrease in the salinity and $\delta^{18}O$ between 40°S and 50°S shows the change in the surface water properties. Comparison show that the sharpness of the decrease in the salinity and $\delta^{18}O$ between 40°S and 50°S is increasing from 1969-2006 except during 1993. This may be due to the difference in the study region (Fig. 3.8). This decrease was very fast in 2006 in comparison to the previous data sets. This may be an indication of ocean warming and consequent meridional mixing. The combined effect of these two may shrink the transition zone. More studies are required to confirm this hypothesis.

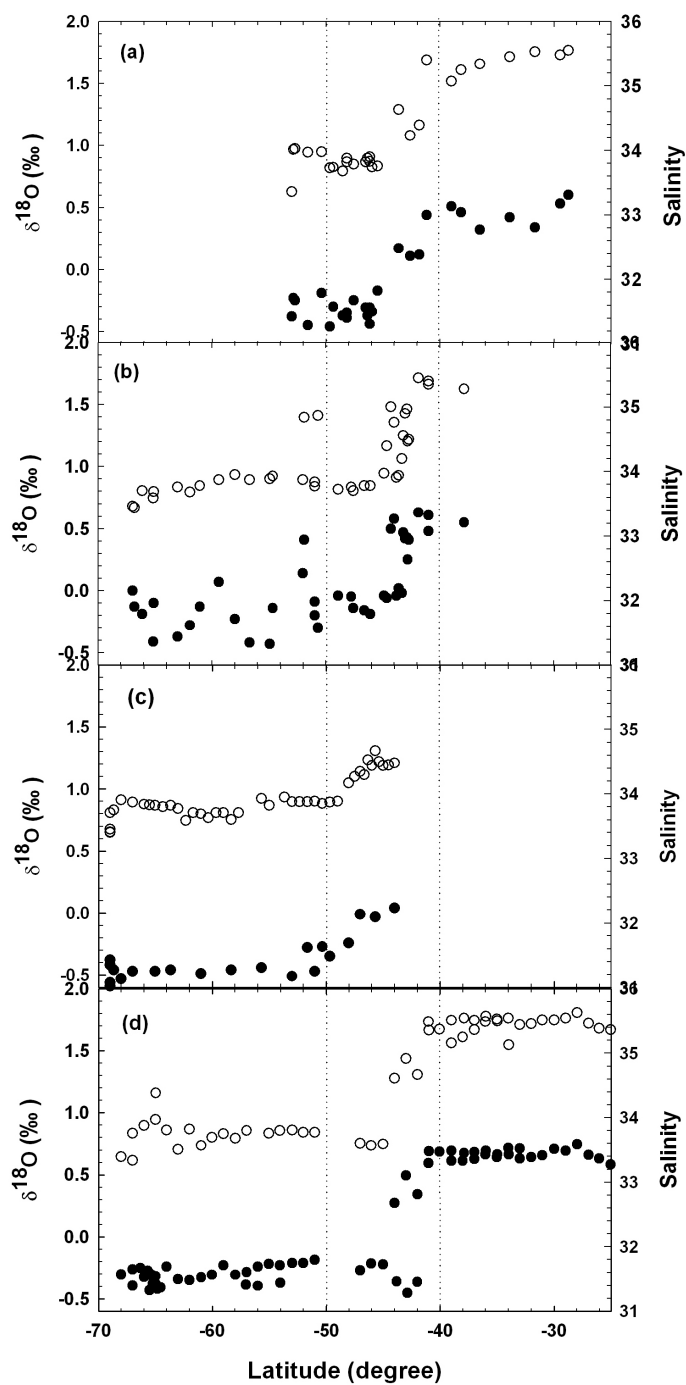


Figure 3.9: Comparison among (a) Duplessy (1969), (b) Kallel (1984), (c) Archambeau (1993) and (d) This work for latitudinal variation of $\delta^{18}\text{O}$ (●) and salinity (○).

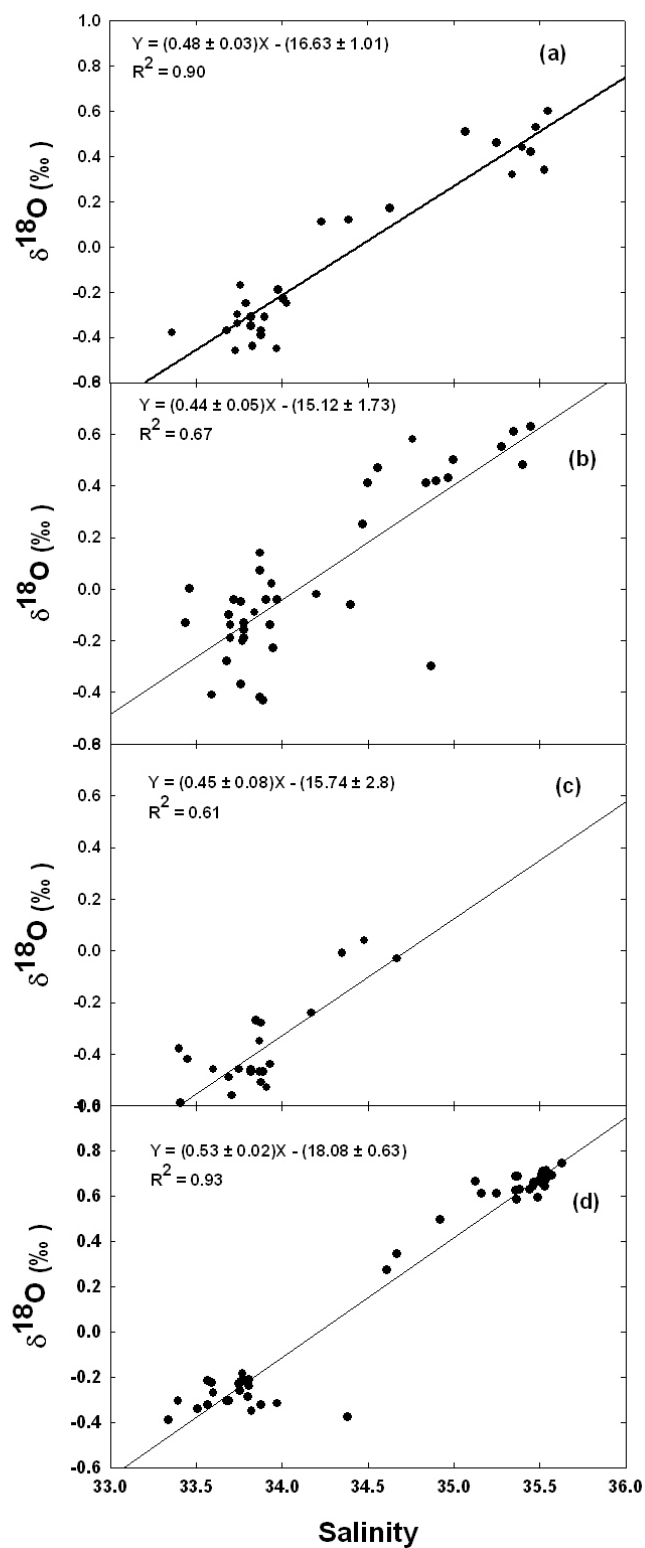


Figure 3.10: Comparison among (a) Duplessy (1969), (b) Kallel (1984), (c) Archambeau (1993) and (d) This work for salinity- $\delta^{18}\text{O}$ relation.

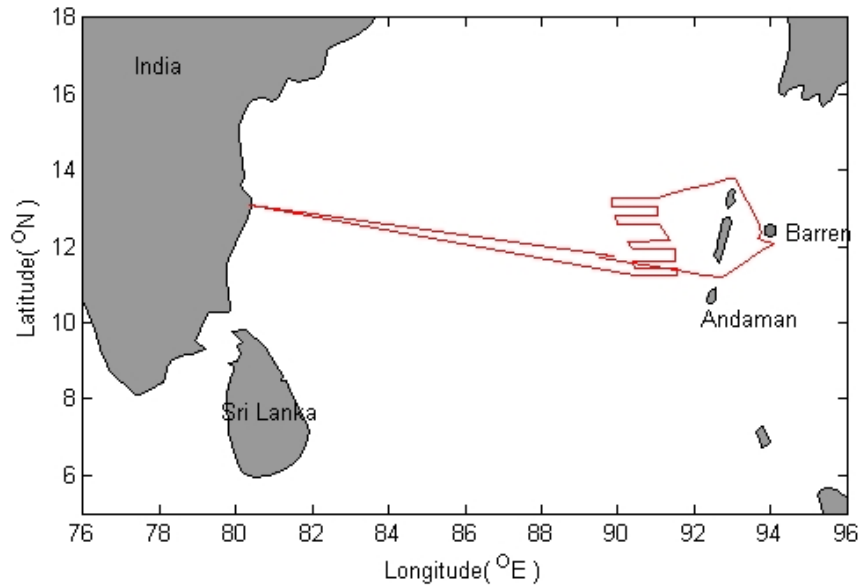
Salinity- $\delta^{18}O$ relation also shows a significant increase in the slope for 2006 study whereas for other studies it is same within the uncertainty limit (Fig. 3.9). This mainly due to the increase of mean $\delta^{18}O$ in the tropics, which could be due to enhanced evaporation in this region, the salinity increase being compensated by influx of ocean water from the surroundings.

3.3 Stable isotopic study of Ocean surface water and Atmospheric water vapor over the Bay of Bengal

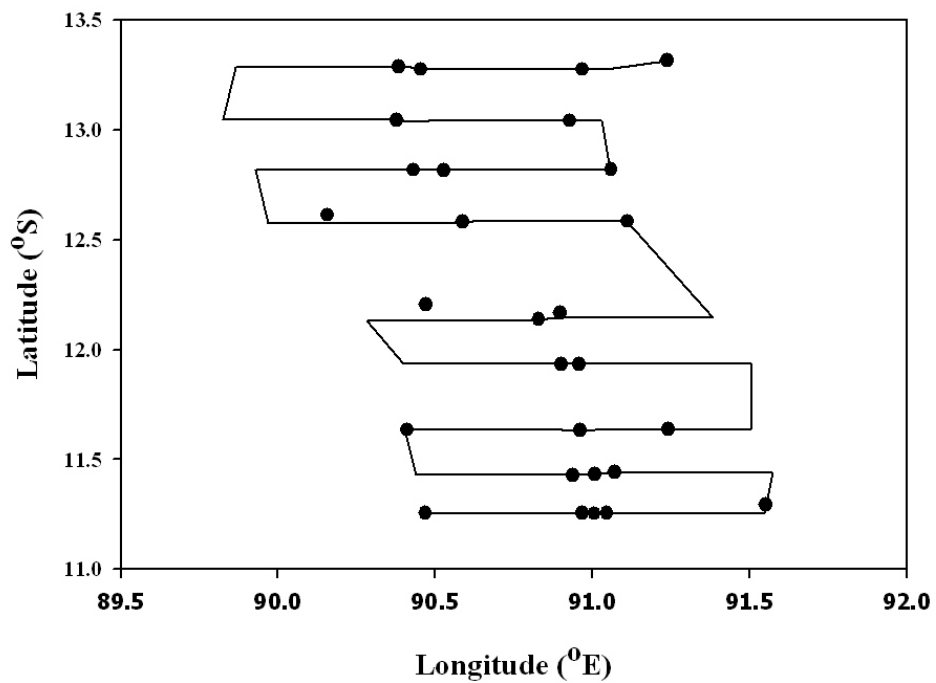
Isotopic equilibrium between ocean surface water (OSW) and atmospheric water vapor (AWV) just above the ocean surface is still an open question. So for very few experimental studies are available [Lawrence, 2003; Lawrence et al., 2004; Uemura et al., 2008] in this regard. For the first time, an experiment was carried out to understand the stable isotopic equilibrium conditions between OSW and AWV over the Bay of Bengal (BOB). Isotopic composition of AWV mainly depends on the isotopic composition of OSW, winds, sea surface temperature, salinity and relative humidity. Literature shows that in the open oceans apart from the equilibrium fractionation, kinetic fractionation is also very prominent. Vapor is assumed to be in stable isotopic equilibrium with the surface water for most of the model inputs. As the BOB is a very important source of moisture for the India monsoon, a cruise was undertaken from 14th May – 4th June 2007 to study OSW and AWV isotopic equilibrium. This is the pre-monsoon period and due to strong heating, evaporation is high during this period.

3.3.1 Cruise track and sampling locations

Sampling was kept limited to a small region ($1^\circ \times 2^\circ$) of the BOB to study small scale temporal and spatial variability of the OSW and AWV. The cruise track is shown in figure 3.11(a) and (b).



(a) Full cruise track started from Chennai and back



(b) Cruise track with sampling locations (\bullet). Left most point on bottom represents sampling location 1. It increases consecutively on moving towards north.

Figure 3.11: Cruise track for the Bay of Bengal study.

Vapor samples and surface water samples were collected twice in a day (0930 Hrs and 1930 Hrs, IST) simultaneously. Morning and evening collections were done for detecting diurnal changes. AWW samples were collected with the help of vapor collection line and liquid nitrogen whereas OSW sampling was done using Niskin bottles or a small, clean plastic bucket. Vapor collection was done for the duration of one hour. So vapor isotopic composition will be the average for one hour. Most of the time ship was stopped during the vapor collection. On a few occasions ship was sailing during the vapor sampling. Thus isotopic composition of AWW comprises of both spatial (10 nautical miles assuming average ship speed of 10 knots) and temporal (one hour) averages.

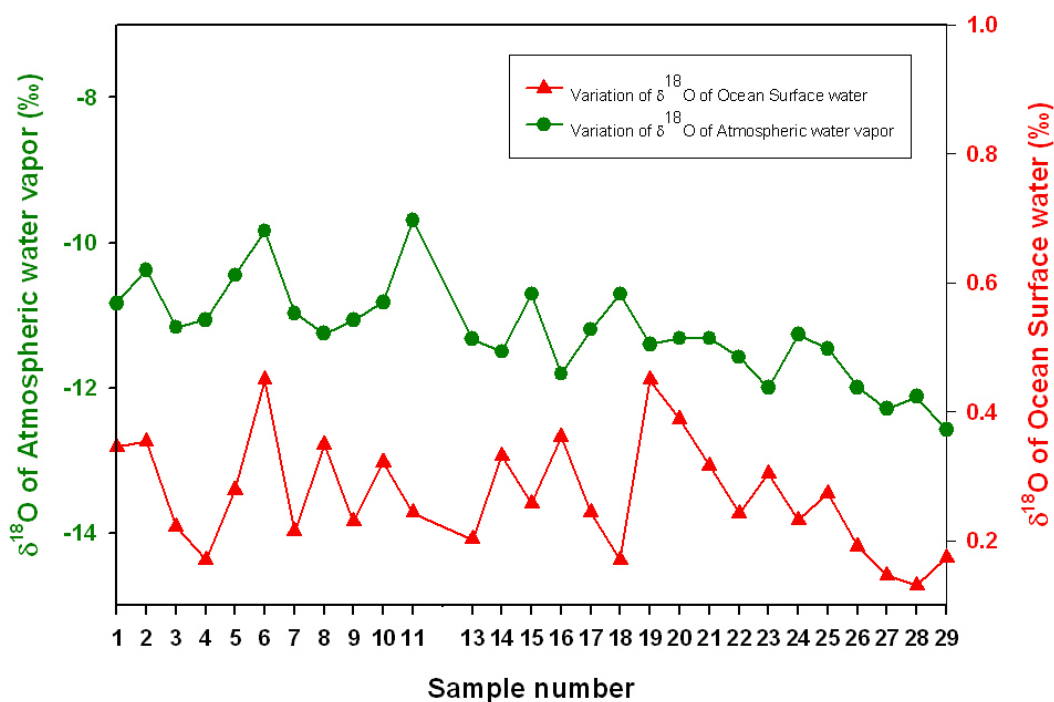


Figure 3.12: Oxygen isotopic variation of vapor and surface water over the BOB. Sample number increases on moving towards north.

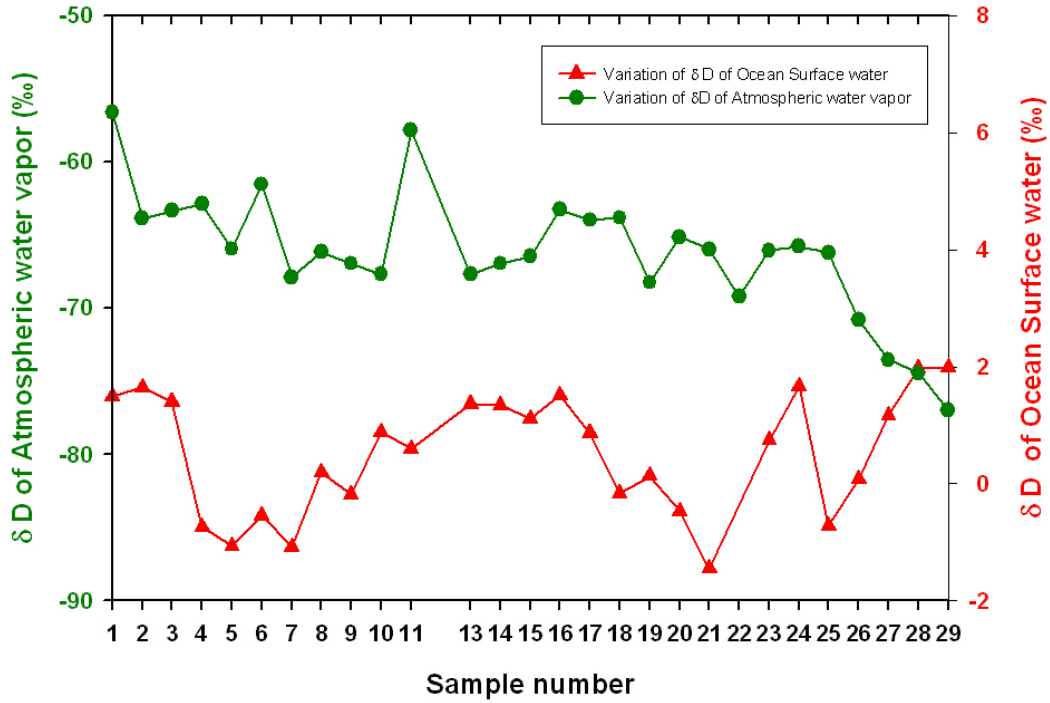


Figure 3.13: Hydrogen isotopic variation of vapor and surface water over the BOB. Sample number increases on moving towards north.

It is a general belief that oceans are homogeneous reservoirs. Our results show that on a small scale ($1^\circ \times 2^\circ$) stable isotopic composition of the OSW and AWV are highly variable with space and time. For all water vapor samples $\delta^{18}O$ ranges between -9.7‰ to -12.5‰ (Fig. 3.12) whereas δD ranges between -56‰ to -76‰ (Fig. 3.13). It shows a large variation ($\sim 2.8\text{‰}$ for $\delta^{18}O$, $\sim 20\text{‰}$ for δD) in the isotopic composition of AWV in a very small region. OSW does not show much variation (0.3‰ for $\delta^{18}O$, 3.4‰ for δD) within the experimental limit. Isotopic composition of AWV shows more fluctuations than the ocean sea surface water. The effect of wind, atmospheric temperature and atmospheric turbulence is less for ocean water because ocean water is a bigger reservoir than atmospheric water vapor. These parameters cause much of variation in the isotopic composition of water vapor.

Overall stable isotopic values of vapor show a decreasing trend on moving towards north. This may be due to the depleted values of OSW. OSW also shows a little decrease on moving towards north but this trend is not as prominent as in the case of AWW especially for the δD . These depleted values of OSW may be due to the effect of fresh water input from the rivers.

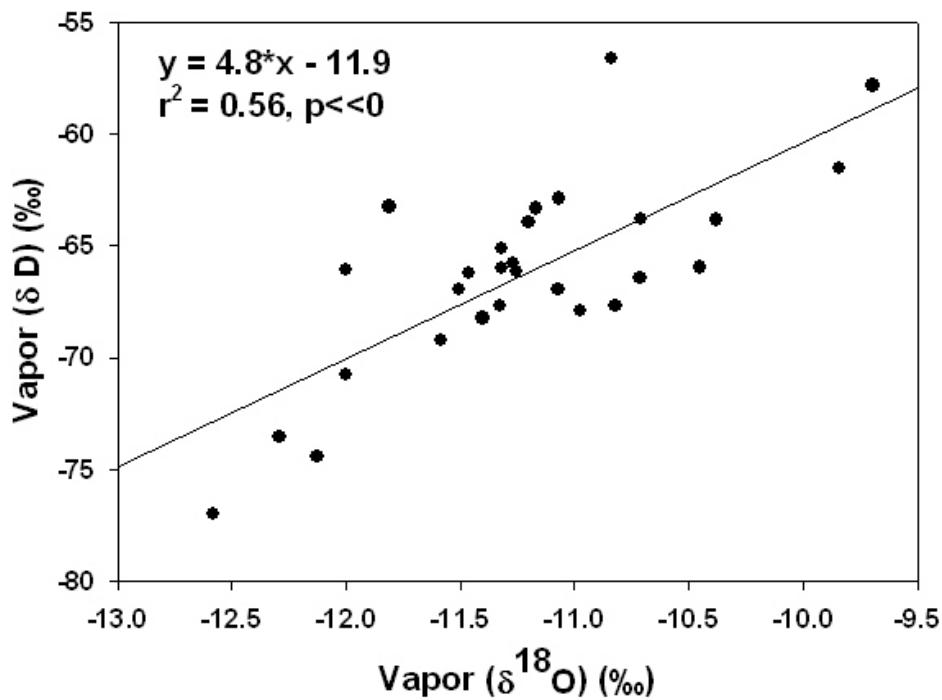


Figure 3.14: Plot of $\delta^{18}\text{O}$ vs. δD for atmospheric water vapor over the BOB.

If evaporation has occurred under isotopic equilibrium (with humidity values higher than 90%) then $\delta^{18}\text{O}$ and δD follow the global meteoric water line ($\delta D = 8 \delta^{18}\text{O} + 10$) with high correlation. Our results show a moderate correlation between $\delta^{18}\text{O}$ and δD ($r^2 = 0.56$) (Fig. 3.14). This moderate correlation may be due to the prominent kinetic effects. These kinetic effects do not permit vapor to completely equilibrate with ocean surface water. The best fit line between δD and $\delta^{18}\text{O}$ for vapor shows a slope of 4.8. This indicates that evaporation has occurred

under strong kinetic effects.

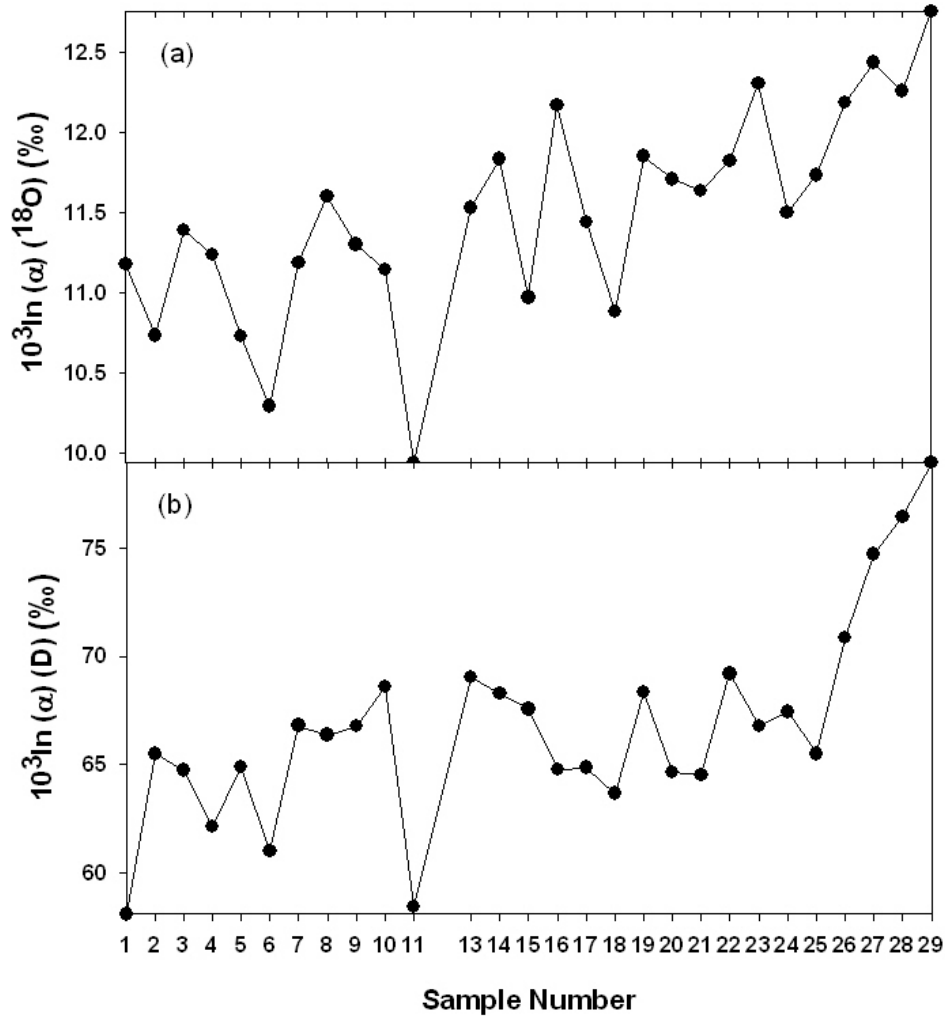


Figure 3.15: Variation of fractionation factor for (a) oxygen and (b) hydrogen over the BOB.

If evaporation occurred at 25°C under isotopic equilibrium condition then the oxygen isotopic fractionation factor ($10^3 \ln \alpha$) expected from theory is 9.3‰ (76‰ for δD) at 25°C [Majoube, 1971]. Our results show an increasing trend in fractionation factor on moving towards north (Fig. 3.15). Overall, variations in the fractionation factor for oxygen and hydrogen are similar. The

minimum value of fractionation factor is 10‰ for the oxygen isotope, close to the equilibrium fractionation factor but the all other values are higher. For hydrogen, the fractionation factor is mostly lower than the equilibrium value, reaching the equilibrium value in the northern most point. This indicates that in general BOB does not evaporate in stable isotopic equilibrium. Fractionation factor depends on sea surface temperature (SST) but in this case it can be ruled out as the overall SST variation is only 1°C which may cause a change in fractionation factor by not more than 0.1‰ for $\delta^{18}O$ and 1‰ for δD . Changing humidity also affects the fractionation factor. Kinetic effects in terms of humidity can be described by the following relationship [Gonfiantini, 1986]:

$$\Delta\epsilon^{18}O_{bl-v} = 14.2(1 - h) \text{ permil}$$

$$\Delta\epsilon^2H_{bl-v} = 12.5(1 - h) \text{ permil}$$

Where ‘bl’ represents boundary layer, ‘v’ vapor and ‘h’ relative humidity. During the cruise period humidity values show a decreasing (max 77% to min 68%) trend on moving northward with some fluctuations. This 9% change in humidity may cause a change of 1.1‰ in fractionation factor for $\delta^{18}O$ and 1‰ for δD . So changes in humidity and temperature are not fully able to explain the changes in the fractionation factor. This show that kinetic fractionation due to the winds also play an important role. As winds get stronger while moving towards north effect of kinetic fractionation factor will increase. So taking into account all the three parameters (temperature, humidity and winds) change in the fractionation factor can be explained.

Our results show that the BOB evaporates under non-equilibrium (isotopic) conditions. This is also confirmed by the slope of $\delta^{18}O - \delta D$. Fractionation factor is higher than the equilibrium fractionation factor for most of the time. Also it

show an increasing trend which can be explained by taking into account all the three parameters (temperature, humidity and winds), responsible for the kinetic fractionation. Although the study region is small, it shows high isotopic variability, especially in the vapor. This suggests that oceans are not a homogeneous reservoir, at least for vapor. Apart from this, the variable nature of fractionation factor proposes to take a distribution (depending upon the degree of kinetic fractionation) of fractionation factors rather than taking a fixed value for the model calculations. This necessitates study of other oceans on wider scale for the better understanding of isotopic fractionation over oceans.

References:

National Hydrographic Organization (IHO), 2000.

Aoki, S., M. Yoritaka and A. Masuyama (2003), Multidecadal warming of subsurface temperature in the Indian sector of the Southern Ocean, *J. Geophys. Res.*, 108 (C4), 8081.

Aoki, S., N. L. Bindoff and C. J. A (2005), Interdecadal water mass changes in the Southern Ocean between 30E and 16E, *GRL*, *J. Geophys. Res.*, 32, L07607.

Archambeau, A. S., C. Pierre, A. Poisson and B. Schauer (1998), Distribution of oxygen and carbon stable isotopes and CFC-12 in the water masses of the southern ocean at 30°E from South Africa to Antarctica: results of CIVA1 cruise, *Journal of Marine System*, 17, 25-38.

Banks, H. T. and N. L. Bindoff (2002), Comparison of Observed Temperature and Salinity Changes in the Indo-Pacific with Results from the Coupled Climate Model HadCM3: Processes and Mechanisms, 2002, 16, *Journal of climate*, 16, 156-166.

Barnett, T. P., D. W. Pierce, K. M. Achuta Rao, P. J. Gleckler, B. D. Santer, J. M. Gregory and W. M. Washington (2005), Penetration of Human-Induced Warming into the World's Oceans, *Science*, 309, 284.

Belkin, I. M. and A. L. Gordon (1996), Southern Ocean fronts from the Greenwich meridian to Tasmania, *J. Geophys. Res.*, 101 (C2), 3675-3696.

Clark, I. D. and P. Fritz. (1997), *Environmental Isotopes in Hydrology*, CRC

Press, Boca Raton, Fla, USA.

Craig, H. (1961), Isotopic Variations in Meteoric Waters, *Science*, 133 (3465), 1702-1703.

Dansgaard, W. (1964), Stable isotopes in precipitation, *Tellus*, 16, 436-468.

Deacon, G. E. R. (1937), The Hydrology of the Southern Ocean, *Discovery Rep.*, 15, 1-124.

Delaygue, G., E. Bard and C. Rollion (2001), Oxygen isotope/salinity relationship in the north Indian Ocean, *J. Geophys. Res.*, 106 (C3), 4565-4574.

Duplessy, J.-C. (1970), Note preliminaire sur les variations de la composition isotopique des eaux superficielles de l'Océan Indien: La relation ^{18}O -Salinité, *C. R. Acad. Sc. Paris*, 271, 1075-1078.

Gat, J. R. (1981), Isotopic Fractionation. In *Stable Isotope Hydrology: Deuterium and Oxygen-18 in the Water Cycle*, Technical Report Series No.210 (eds. Gat J R and Gonfiantini R.), IAEA, Vienna, 21-33.

Gonfiantini, R. (1986), Environmental isotopes in lake studies. In *Handbook of Environmental Isotope Geochemistry*, Vol. 1 (ed. P. Fritz and J. C. Fontes), pp. 113-168. Elsevier.

Gordon, A. L. and B. A. Huber (1984), Thermohaline stratification below the southern ocean sea ice, *J. Geophys. Res.*, 89, 614-648.

Gordon, A. L., E. Molinelli and T. Baker (1978), Large-scale relative dynamic topography of the Southern Ocean, *J. Geophys. Res.*, 83 (C6), 3023-3032.

Kallel, N. (1985), La composition isotopique des eaux du secteur indien de l'océan austral, Master's thesis. Université de Paris Sud.

Lawrence, J. R. (2003), Tropical ice core isotopes: Do they reflect changes in storm activity?, *Geophys. Res. Lett.*, 30 (2), 1072, doi:10.1029/2002GL015906.

Lawrence, J. R., S. D. Gedzelman, D. Dexheimer, H.-K. Cho, G. D. Carrie, R. Gasparini, C. R. Anderson et al. (2004), Stable isotopic composition of water vapor in the tropics, *J. Geophys. Res.*, 109, D06115, doi:06110.01029/02003JD004046.

LeGrande, A. N. and G. A. Schmidt (2006), Global gridded data set of the oxygen isotopic composition in seawater, *Geophys. Res. Lett.*, 33, L12604.

- Levitus, S., J. Antonov and T. Boyer (2005), Warming of the world ocean, 1955–2003, *Geophys. Res. Lett.*, 32, L02604.
- Lutjeharms, J. R. E. (2006), Three decades of research on the greater Agulhas Current, *Ocean Sci. Discuss.*, 939-995.
- Lutjeharms, J. R. E. and H. R. Valentine (1984), Southern Ocean thermal fronts south of Africa, *Deep Sea Res., Part A*, 31, 1461-1475.
- Majoube, M. (1971), Fractionnement en oxygen-18 et en deuterium entre l'eau et sa vapeur, *J. Chem. Phys.*, 68, 1423-1436.
- Michael, D. S., K. J. Heywood, J. Brown and D. P. Stevens (1996), Current structure of south Indian Ocean, *J. Geophys. Res.*, 101 (C3), 6377-6391.
- Mook, W. G. (2006), *Introduction to Isotope Hydrology: Stable and Radioactive Isotopes of Hydrogen, Oxygen and Carbon*, Taylor & Francis.
- Park, Y. H., E. Charriaud and M. Fieux (1998), Thermohaline structure of Antarctic Surface Water/Winter Water in the Indian sector of Southern Ocean, *Journal of Marine Systems*, 5-23.
- Paul, A., S. Mulitza, J. Ptzold and T. Wolff (1999), Simulation of Oxygen Isotopes in a Global Ocean Model. In: Fischer, G & Wefer, G (eds.), *Use of Proxies in Paleoceanography - Examples from the South Atlantic*, Springer-verlag Berlin Heidelberg, 655-686.
- Peterson, R. G. and L. Stramma (1991), Upper-level circulation in the South Atlantic ocean, *Prog. Oceanogr.*, 26, 1-73.
- Read, J. F. and R. T. Pollard (1993), Structure and transport of Antarctic Circumpolar Current and Agulhas Return Current at 40 East, *J. Geophys. Res.*, 98 (C7), 12,281-212,295.
- Rintoul, S. R. and J. L. Bullister (1999), A late winter hydrographic section from Tasmania to Antarctica, *Deep Sea Res.*, 46, 1417-1454.
- Rintoul, S. R. and M. H. England (2002), Ekman Transport Dominates Local Air-Sea Fluxes in Driving Variability of Subantarctic Mode Water, *J. Physical Oceanography*, 32, 1308-1321.
- Schmidt, G. A., G. R. Bigg and E. J. Rohling (1999), Global Seawater Oxygen-18

Database, <http://data.giss.nasa.gov/o18data/>, NASA Goddard Inst. of Space Sci., New York, N. Y.

Uemura, R., Y. Matsui, K. Yoshimura, H. Motoyama and N. Yoshida (2008), Evidence of deuterium excess in water vapor as an indicator of ocean surface conditions, *J. Geophys. Res.*, 113, D19114, doi:19110.11029/12008JD010209.

Whitworth, T., III and W. D. Nowlin, Jr. (1987), Water masses and currents of the Southern Ocean at the Greenwich Meridian, *J. Geophys. Res.*, 92 (C6), 6,462-466,476.

Chapter 4

Rain and Atmospheric water vapor studies over land

4.1 Microphysical studies of rain formation processes over the tropical region

Clouds are very important component of hydrological system. They regulate our hydrological cycle by transporting water away from the earth's surface, redistributing it through the atmosphere and back to the surface by means of precipitation. Not only they produce rain but also influence our atmospheric dynamics by latent heat and cooling. All of these phenomena have their origin in cloud microphysics, whose spatial scale ranges from under a micrometer to a few millimeters. Changes in cloud microphysical processes can modify the spatial extent, spatial distribution and lifetimes of clouds, the water vapor distribution outside of clouds, the fluxes of water and radiation through the atmosphere. Recent research suggests putting more focus on the microphysical processes associated with rain for better predictability. Here, the present study mainly focuses on the microphysical processes associated with the rain formation.

Stable isotopic study of rain water can be an effective tool to get micro-

physical information of rain formation processes as isotopic fractionation is very sensitive to the phase changes. So, temporal variations in the isotopic composition of rain water may provide information about the progressive changes occurring in the cloud parcel. It is important to have high resolution temporal study to understand microphysical processes associated with the rain formation. Large scale variations, both in temporal as well as spatial, of stable isotopic abundances are widely reported [Rozanski et al., 1993]. Mostly they have been used for local hydrological study. But shorter term variations for microphysical processes associated with rain formation are yet to be studied [Celle-Jeanton et al., 2004]. Radar is an important ground based instrument which can penetrate the cloud system and provide information about the cloud dynamics. For obtaining supportive evidence to isotopic variations of rain water, radar was operated simultaneously. Cloud and rain drop size mainly depends on condensation, collision, coalescence and evaporation, all very sensitive to climatic conditions, as is the isotopic composition. So a simultaneous measurement of rain drop size distribution (DSD) and stable isotopic analysis of rain water may provide better insight on cloud precipitation/evaporation processes in the tropical monsoon environment.

An attempt has been made, for the first time, to effectively utilize the synergy of various approaches providing microphysical information of precipitation to study short term variations in the raining cloud system. A campaign has been conducted wherein rain samples are collected during the rain and simultaneously a powerful VHF radar and disdrometer have been operated to infer the characteristics of the vertical structure and rain DSD of precipitation. Here we present results of simultaneous measurements of rain DSD and stable isotope analysis of rain water and discuss implication to the cloud precipitation/evaporation processes in the tropical monsoon environment. The questions addressed include (i) Is there a relationship between DSD and the stable isotope ratios of the rain water and does it depend on the nature of the cloud system (e.g. stratiform versus convective)? (ii) Can a high resolution stable isotopic study of rain water be useful in elucidating

microphysical processes associated with rain formation? (iii) Can the stable isotope ratio be used to differentiate stratiform and convective cloud systems? (iv) Is there significant effect of secondary evaporation or local moisture recycling?

4.1.1 Sampling Location

For the present study rain water samples were collected at National Atmospheric Research Laboratory, Gadanki (13.5°N , 79.2°E) [Fig. 4.1] during September–October 2006. Gadanki is largely influenced by two rainy seasons: Southwest (June–September) and northeast monsoons (October–December). The maximum rainfall occurs generally in October, which is rather a transition month from southwest to northeast monsoon.

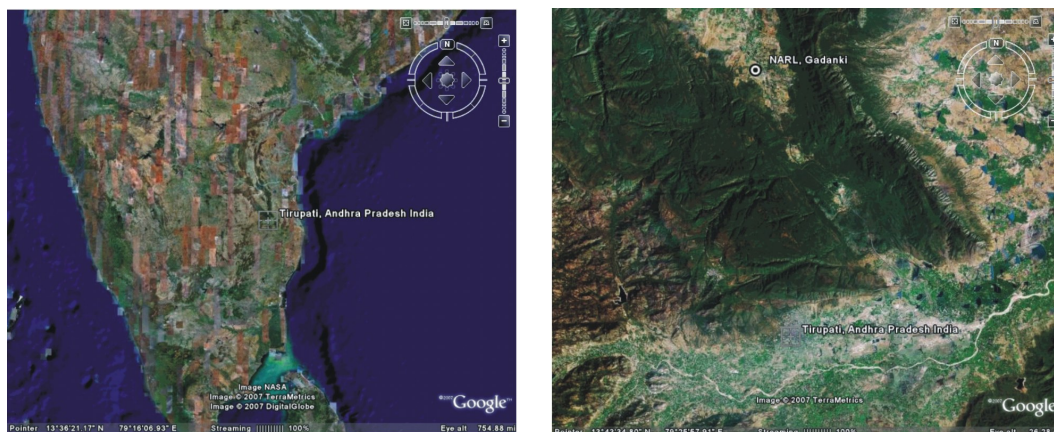


Figure 4.1: Sampling location (NARL, Gadanki).

Rain water collection was done with the help of a rain collector. Several samples were collected for each rain event at different times for the high time resolution stable isotopic study. Rain samples were collected close (about 5 m) to the disdrometer location. The JW (Joss-Waldvogel) disdrometer (RD-69) used in the present study is an impact type disdrometer, which provides the number density of rain drops in 20 diameter classes with a high temporal resolution (1 minute). The prescribed maximum error in the measurement of rain DSD is about

5%. The rainfall rate, reflectivity factor and mass weighted mean diameter are estimated from each 1 minute rain DSD using the standard formulae [Rao et al., 2001]. During campaign period, the Mesosphere–Stratosphere–Troposphere (MST) radar was kept on alert and operated in a special mode, whenever rain occurred over Gadanki. Important operational parameters of radar are presented in chapter 2 of this thesis.

4.1.2 Short term variations in the raining cloud parcel

During the observational period, there were five rain events (12, 14 September 2006 and 05, 17, 26 October 2006), significant in rain amount and duration over Gadanki. Cloud pictures taken from satellite are shown in figure (4.2) (from Kalpana-1, Indian Meteorological Department, India).

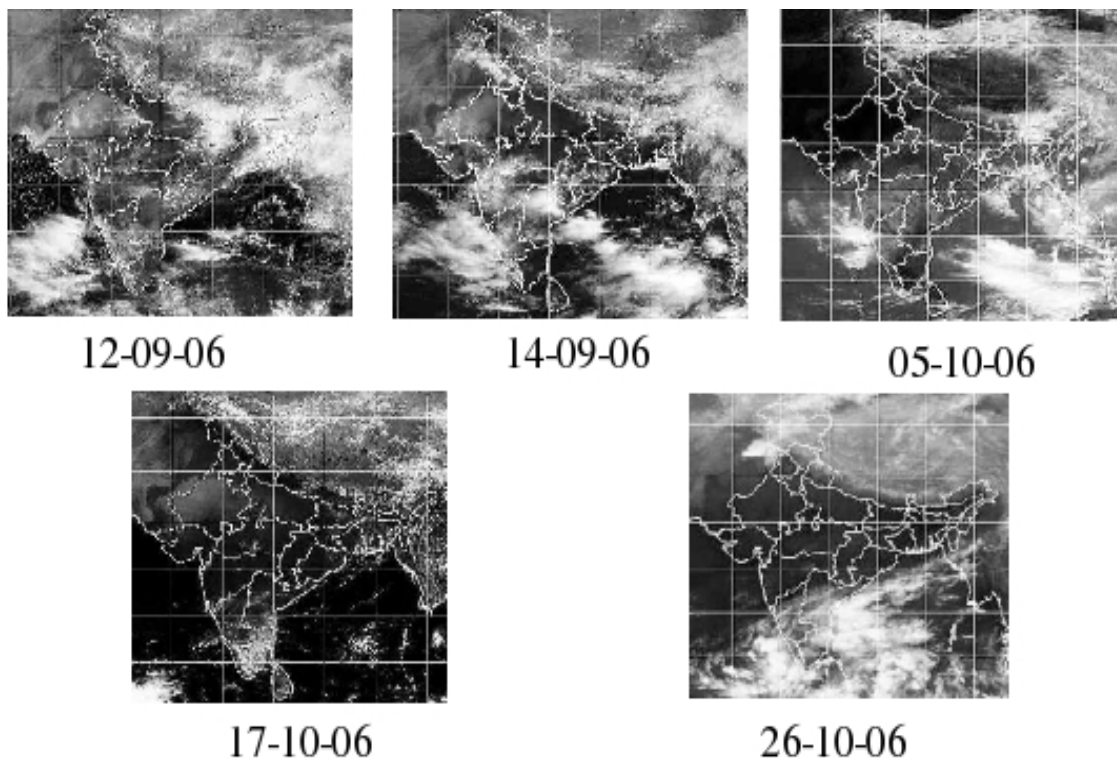


Figure 4.2: Satellite pictures of five major rain events.

A number of samples were collected in each event, and were used for the combined study of rain drop size, $\delta^{18}O$ and δD of rain water.

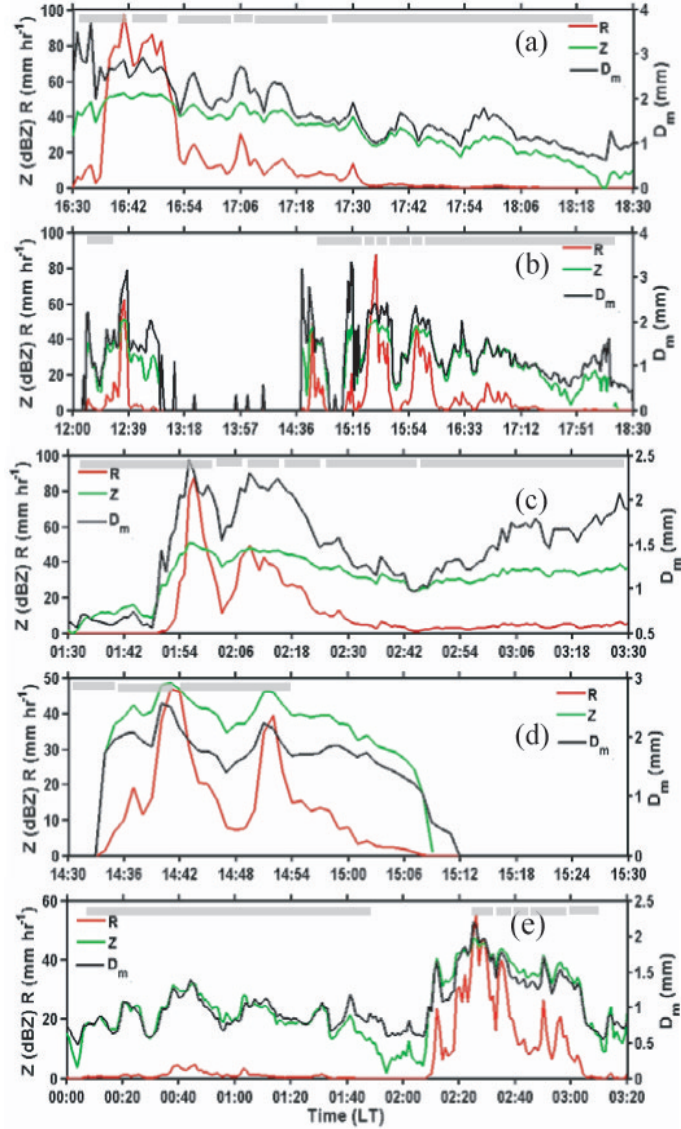


Figure 4.3: Temporal variation of rain integral parameters (R , Z , and D_m) on (a) 12 September, (b) 14 September, (c) 5 October, (d) 17 October and (e) 26 October 2006. Horizontal gray bars represent sampling duration.

The temporal variations of rain integral parameters (reflectivity factor, Z in dBZ, rainfall rate, R in mm hr⁻¹ and mass weighted mean diameter, D_m in mm) are shown in figure (4.3) for all the events. All parameters follow similar patterns.

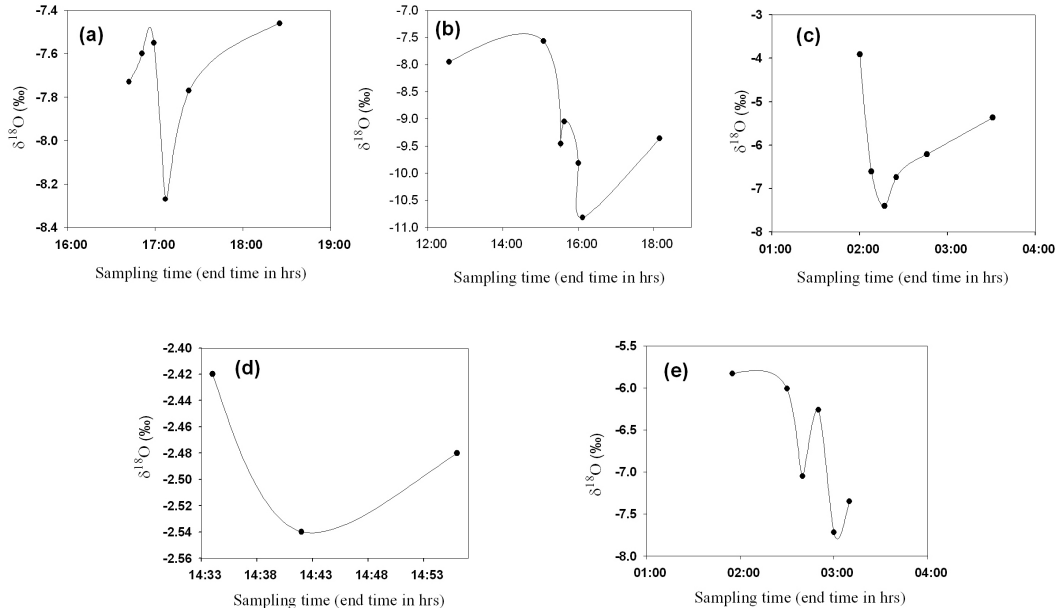


Figure 4.4: Plot of $\delta^{18}\text{O}$ variation with time for (a) 12 September, (b) 14 September, (c) 5 October, (d) 17 October and (e) 26 October 2006.

Both stratiform and convective rain features are present in all the events, however, the duration of convection and the numbers of convective cells vary. Accordingly the number of rain sample vary from 3 (17 October) to 7 (14 September). Time series plots of $\delta^{18}\text{O}$ show a ‘V’ like structure for the rain events of 12 September, 5 and 17 October whereas it shows a ‘W’ like structure on 14 September and 26 October [Fig. 4.4]. On 17 October variations in stable isotopic ratios are very small but still a V-shape is apparent though not very sharp. Schematic diagrams of $\delta^{18}\text{O}$ variations with time are depicted in figure 4.5 (a) and (b). The first condensation starts at the topmost part of the cloud because of low temperature and high saturation level. While moving vertically up in the cloud the stable isotopic ratio of the vapor decreases. Thus the vapor in the upper most part is more depleted in the heavier isotope (^{18}O and D) [He and Smith, 1999; Smith et al., 2006]. In this case due to (i) low temperature, (ii) high condensation rate and (iii) depleted vapor isotopic values at the top of cloud parcel, the first rain sample is more depleted than the second. Part “A” of figure 4.5 (a) shows this. Here this effect is so strong

that it dominates over other effects (such as evaporation during fall). This trend is more prominent in the deep convective systems whose specified vertical extent is larger than the horizontal extent and the first rain forms at the upper part than the later rain that forms at the lower part of the cloud parcel [Fig. 4.4(a)].

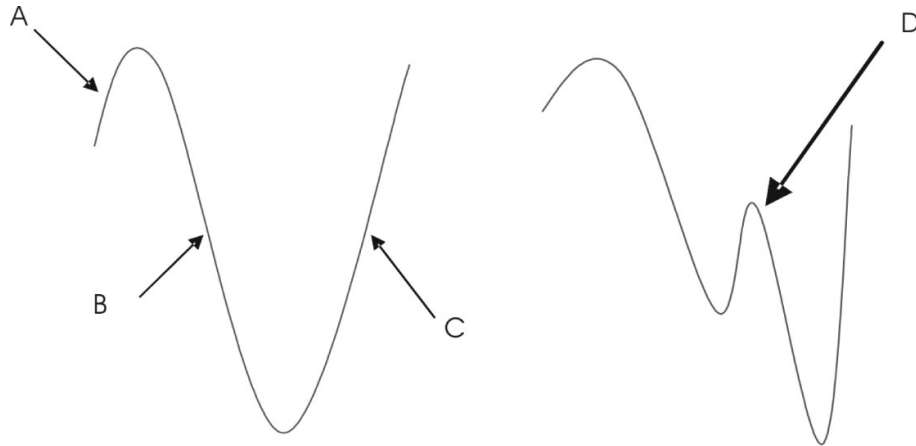


Figure 4.5: Schematic diagram of $\delta^{18}O$ variation of (a) type 1 and (b) type 2.

The isotopic composition of the drop changes due to (i) condensational growth (ii) evaporation or (iii) re-condensation of the atmospheric moisture on the drop on its way down. If the condensational growth of the cloud drop follows the Rayleigh isotopic fractionation it continues to be enriched in the heavier isotope (^{18}O and D) with its growth, because the heavier isotopologues prefer the liquid state (the isotopic composition of the remaining vapor is not likely to change due to its large amount). The initial rain samples are more affected by evaporation than the later samples, because as rain progresses, the atmosphere below the cloud base gets saturated and also cools down. Thus the initial samples are isotopically more enriched than the later ones. Re-condensation on the falling drop can also deplete the isotopic composition of the drop. This is also seen in the stable isotopic data. “B” in figure 4.5 (a) could be the combined effect of condensational growth of the drop in cloud parcel, re-condensation of the atmospheric moisture on the falling drop and evaporation where applicable. Once the atmosphere saturates,

effect of evaporation decreases and the signature of condensational growth starts manifesting. “C” in figure 4.5(a) shows the domination of condensational growth over evaporation. If convective nature dominates then condensational growth of the cloud drop would be less prominent, as in high turbulence, the drop would preferentially grow by collision-coalescence process. In stratiform clouds, drops would have enough time to grow by the condensation from vapor [Rogers and Yau, 1976]. This condensational growth makes the drops more enriched in the heavier isotope which is seen as “C” of figure 4.5(a). Thus a dip in the time series plot of isotopes might be a good indication of the changing nature of the cloud parcels from convective to stratiform type. Isotopic time series plot on 14 September and 26 October show a special structure which is shown as “D” in figure 4.5(b). This sudden increase in the isotopic composition could be due to the replacement of first cloud by another at the location by horizontal advection. A detailed study was done for the rain event of 5 October. On this day a Mesoscale Convective System (MCS) passed over Gadanki producing ~ 26 mm of rainfall (accumulated) in 3 hours. For about 90 minutes (02:05 – 03:35 LT (LT = UT+5:30)), the MST radar spectra have shown a clear bimodal structure up to 6 (8) km after (before) 02:13 LT, except during 02:28 – 02:51 LT, when the bimodality is seen intermittently both in time and height. Spectral moments are estimated independently after separating the clear air and precipitation echoes and are depicted as time–height contours in figure (4.6). Positive velocities indicate upward motion. It clearly shows the typical structure of mesoscale convective system [Houze, 2004]. In convection (before 02:13 LT), both clear air and precipitation echo powers are large and extend up to 9 km. Corresponding to this time, strong updrafts of the order of 8 ms^{-1} [Fig. 2.5(b)] and moderate to intense turbulence [Fig. 2.5(c)] are observed.

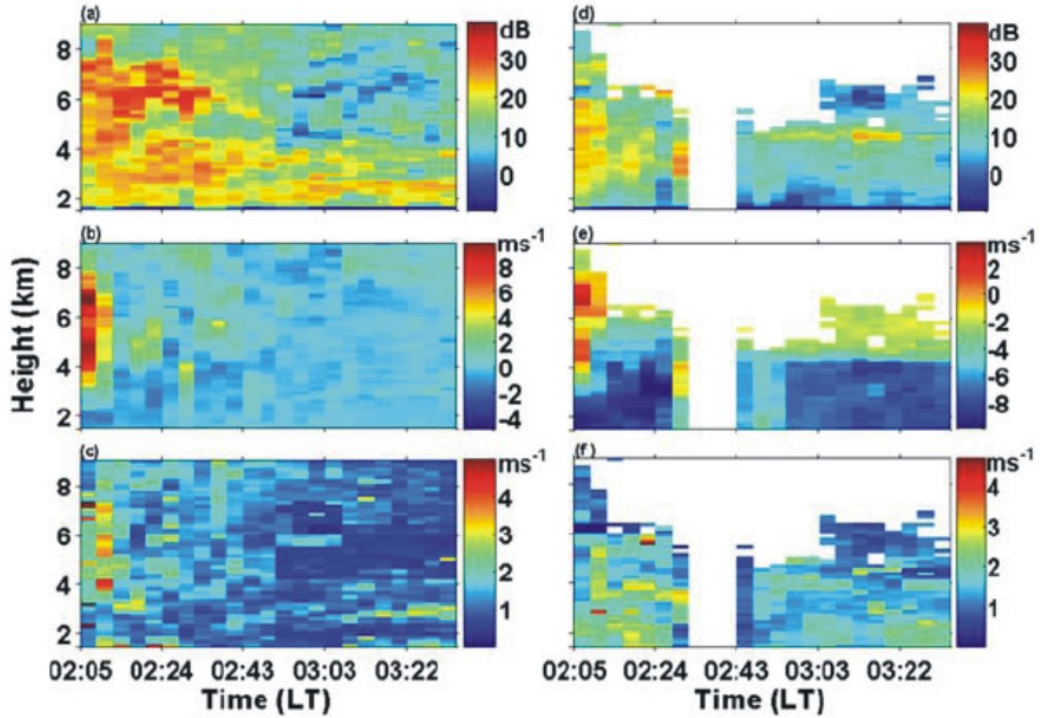


Figure 4.6: Time-height contours of profiler spectral moments at vertical incidence: (a) and (d) range corrected SNR, (b) and (e), Doppler velocity, and (c) and (f) spectral width for (left) clear air and (middle) precipitation echoes observed on 5 October 2006. Note that color scales of Doppler velocity contours are different for clear air and precipitation.

A clear bright band, signature of stratiform precipitation, with enhanced precipitation echo power at around 4.35 km is observed after 02:51 LT [Fig. 2.5(d)]. Above 4 km, the Doppler velocity of precipitation [Fig. 2.5(e)] (resultant of fall velocity of hydrometeors and vertical air motion) shows upward motion in convection which indicates that raindrops are carried aloft because of strong updrafts [Fig. 2.5(b)]. As expected, strong gradients in Doppler velocity of hydrometeors are seen around the bright band in stratiform region. The spectral width of precipitation echo, which represents the rain DSD (after correcting it for beam broadening and turbulence), is wide below 4 km in two time intervals (before 02:28 LT and after 03:19 LT). The precipitation observed after the intense convection and before the

stratiform rain (i.e., during 02:13 – 02:51 LT) can be considered as transition rain with properties intermediate to convection and stratiform rain [Rao et al., 1999].

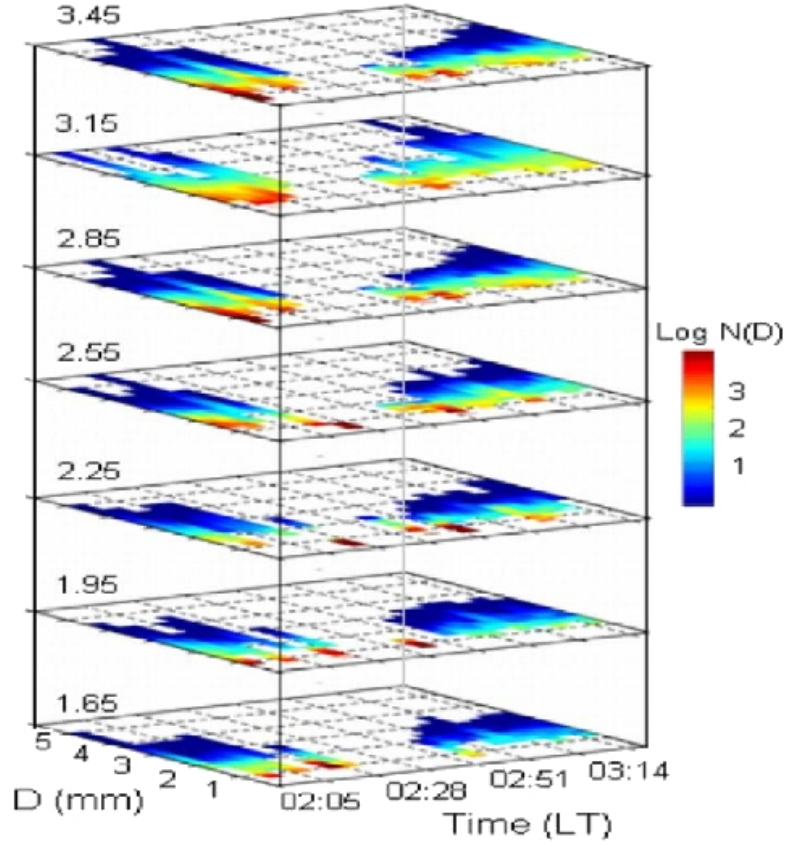


Figure 4.7: Temporal and vertical variation of rain DSD.

The precipitation echoes are used to retrieve DSD in rain region (3.6-1.65 km). DSD retrievals are not performed in the later part of transition rain and early stratiform rain at a few range gates, where the precipitation echo is too noisy to get meaningful rain DSD. The temporal and vertical variation of rain DSD is shown in figure 4.7. The temporal variation of DSD at all heights shows a common feature with wide distribution during convection and initial part of transition rain and also in later part of stratiform rain and narrow distribution in the initial stages of stratiform rain. Vertical variation of DSD displays marked variation with height

as well from convection to stratiform rain. Number of smaller drops is generally high in both rain regimes at higher altitudes (above 2.85 km), however, gradually reduces to small at lower altitudes. The reduction of smaller drops is significant in the stratiform rain.

Dip in the V-shape [Fig. 4.4(c)] of temporal variations in stable isotopic composition of rain sample corresponds to the transition point from the convective nature to the stratiform nature of the cloud parcel as shown by the radar data. Radar observations clearly support our cloud evolution hypothesis which is based on the isotopic composition of rain. This indicates that stable isotopic composition of rain water is a good indicator of microphysical processes happening inside cloud.

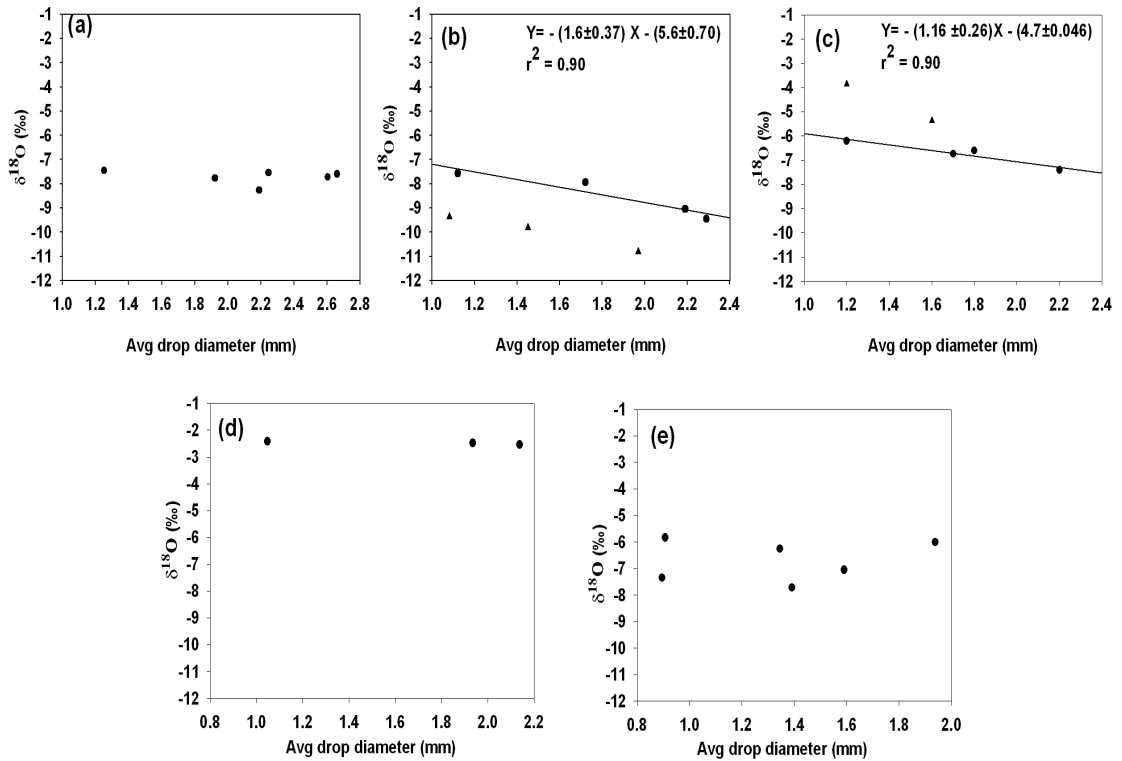


Figure 4.8: Scatter plot between $\delta^{18}\text{O}$ and mass weighted mean diameter of rain drops on (a) 12 September, (b) 14 September, (c) 5 October, (d) 17 October and (e) 26 October 2006. ▲ indicate samples either start or end of the rain events. So they have not been taken into the account while calculating regression.

Stable isotopic ratio shows a negative correlation with mean drop size for the rain events of 14 September and 5 October [Fig. 4.8 (b) and (c)]. The change in the isotopic composition of the drop due to the evaporation will be the combined effect of surface evaporation (proportional to a^2 , where a is the radius of the falling drop) and inversely proportional to the volume of the drop ($1/a^3$). Therefore bigger rain drops are less affected by evaporation (i.e. less enrichment in ^{18}O) than smaller drops. Since smaller drops are affected more by evaporation, they are more enriched relative to bigger drops. For most of the time the isotopic composition of smaller drops is affected by evaporation rather than by condensational growth. For the rain events on 12 September, 17 and 26 October oxygen isotopic ratio ($\delta^{18}\text{O}$) does not change with drop size [Fig. 4.8 (a), (d) and (e)]. This could be a case of cancellation of evaporation effect to the condensational growth effect on the isotope ratio.

The relation between δD and $\delta^{18}\text{O}$ of the rain water gives information about the humidity at the time of evaporation (slope) and effect of re-evaporation of rain drops during fall (intercept) (Craig, 1961) . Slope 8 of global meteoric water line (GMWL) can be achieved only when humidity approaches to 90% [Gat, 1971]. In the present study similar slope of $\delta D - \delta^{18}\text{O}$ line (7.87 ± 0.47) [Fig. 4.9] as GMWL shows that condensational growth of cloud drop has occurred under close to isotopic equilibrium. Intercept of the meteoric water line over Gadanki is also similar to the GMWL with this error.

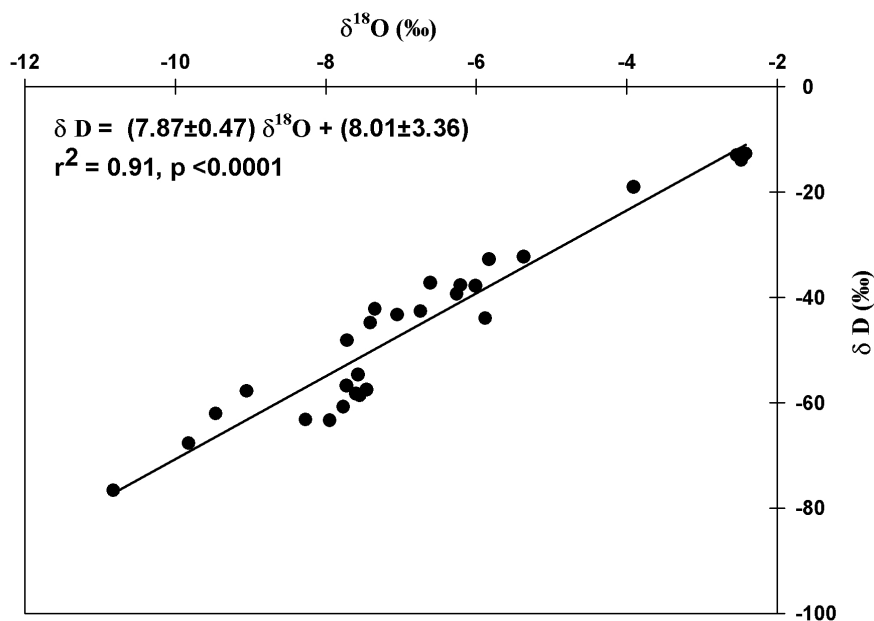


Figure 4.9: Plot of $\delta^{18}\text{O}$ vs. δD .

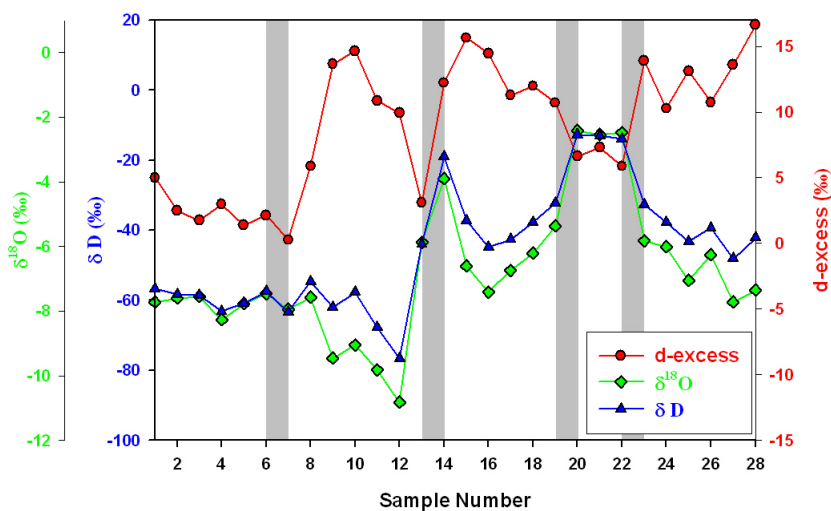


Figure 4.10: Variation of stable oxygen ($\delta^{18}\text{O}$) and hydrogen (δD) isotopic compositions of rain water with d-excess. X-axis is labeled from first sample on 12 September (1) to the last sample on 26 October 06 (28). Gray bands demarcate different rain events.

Local moisture recycling is an important component of regional rainfall. The combined use of hydrogen and oxygen isotopes in the rain leads to an additional parameter, deuterium excess (the d-excess, calculated by $d = \delta D - 8\delta^{18}O$) [Dansgaard, 1964], which provides information on moisture recycling. As a water body goes through successive evaporation and precipitation cycles, the d-excess would consequently increase [Lachniet and Patterson, 2002]. Isotopic variations (δD and $\delta^{18}O$) of rain and d-excess with sample numbers are depicted in figure 4.10. Gray bands demarcate different rain events. After the first rain event (12 September), all parameters (d-excess, $\delta^{18}O$ and δD) show an increasing trend. This increase is most likely due to the increasing effect of recycled moisture because as monsoon progresses, due to availability of more water on land through rain, recycling of moisture increases. Increasing trend in the isotopic composition of rain indicates that rain is derived from the initial extraction from a vapor mass. One explanation for this may be as follows: In the starting phase of monsoon, due to hot land surface, clouds mature and die very fast. So the maximum rain occurs near the coastal regions. Whereas as monsoon progresses land cools and cloud system reaches more inland without raining much at coastal regions.

Stable isotope measurements were carried out to characterize the effects of evaporation and condensational growth aimed at gaining insight into cloud processes. Temporal variation of $\delta^{18}O$ along with DSD suggests that the strong turbulence during the initial phases of the cloud system changes to less turbulent, stratiform system with time in most cases. For two rain events temporal variation of $\delta^{18}O$ shows the replacement of first air mass with second one after some time. Rain over Gadanki shows a dominant effect of secondary evaporation. An increasing trend in d-excess parameter indicates the increasing effect of recycled moisture as monsoon advances. The results of this study are an important input for isotope based models which seldom consider the evolving nature of cloud systems (convective to stratiform, in the same day).

4.2 Characterization of Atmospheric Water Vapor and Rain over the tropical region (Ahmedabad)

Lower tropospheric water vapor reservoir is very dynamic, quickly responding to the changes in external conditions such as temperature and relative humidity. Increase of water vapor in the lower troposphere induces precipitation (rain) by providing saturation to the unsaturated cloud systems, specially in convective zones. Measurements of changing atmospheric water vapor (AWV) may be useful in determining the frequency of rain events in monsoon regions. An additional motivation for this study is the fact that for a country like India where most of the precipitation occurs during the monsoon period (June, July, August and September), it is very important to know the water vapor cycle in the lower troposphere. The simultaneous determination of the isotopic compositions of rain and atmospheric water vapor is a sound approach to assess not only the water vapor cycle but also to determine the changes in local moisture due to the monsoon system. Ground-based observations of isotopic compositions of AWV provide an opportunity to validate satellite data and could help verify their accuracy. This study focuses on the isotopic compositions of both rain and water vapor (for an extended period of time, one year) over the tropical monsoon region. Thus, for the first time in India high resolution (daily) rain water and atmospheric water vapor samples were collected. A special sampling campaign was conducted for a period of one year between April 2007 and April 2008 at Ahmedabad, India (23.03°N, 72.56°E). Monsoon was normal during 2007 (Indian Meteorological Department). These samples were analyzed for their stable isotopic compositions. The main objectives of this study are to characterize the temporal variability in the isotopic compositions of rain and water vapor, and to understand the effect of rain on local water vapor isotopic composition. The questions addressed include (i) Is there a significant change in the stable isotopic composition of AWV during the onset of the monsoon? (ii) Is there an isotopic equilibrium between rain and water vapor? (iii) If yes, then on what time scales

and does it tally with that predicted from the observed temperatures? (iv) what is the magnitude of annual/seasonal change in stable isotopic composition of AWW? Such data are relevant for the study of plant-water isotopic relationship using models and thus in tree ring based paleoclimatology [Sheshshayee et al., 2005].

4.2.1 Vapor sources over Ahmedabad

Probable sources of moisture in the Indian region are shown in figure 4.11.

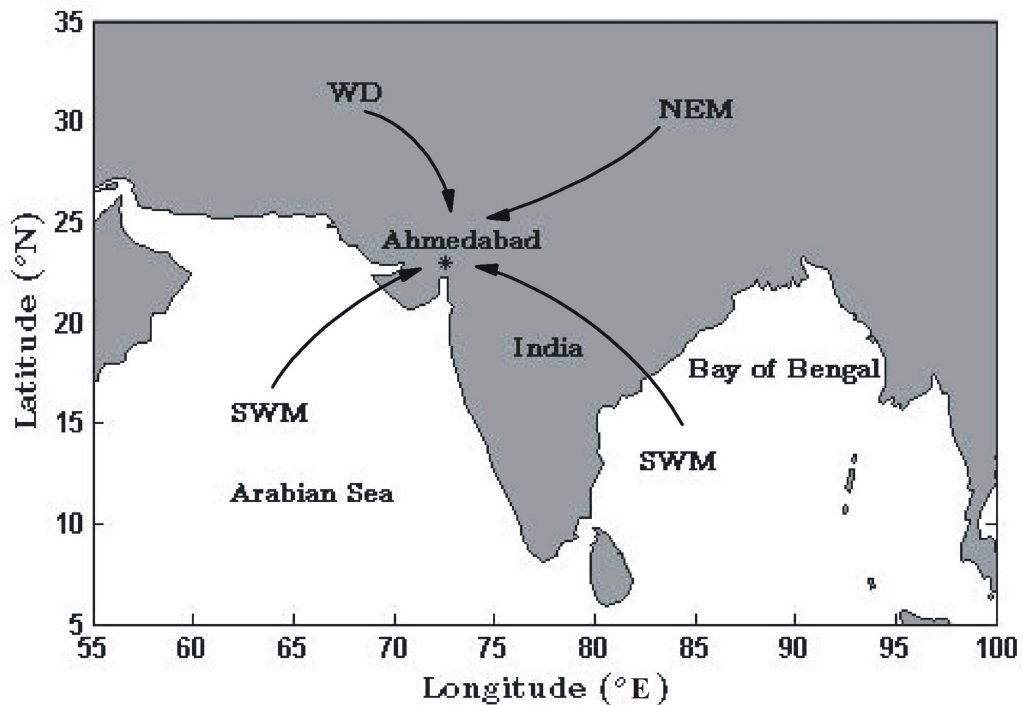


Figure 4.11: Sampling location (Ahmedabad) and possible water vapor sources marked by arrows: SWM, South west monsoon (mid Jul to end Sep.); NEM, North east monsoon (Oct-Jan); WD, Western disturbance (Nov-Mar).

During the boreal winter mostly dry winds from the Asian landmass pick up moisture from the Bay of Bengal (BOB), bringing rains to north-eastern and southern India (north-east monsoon). During the summer, the south-west monsoon brings moisture both from the BOB and the Arabian Sea. Ahmedabad, being

located in the west, gets vapor mainly from the Arabian Sea, and seldom from the BOB. Additionally, vapor highly depleted in ^{18}O from the Mediterranean region also gets transported by the ‘western disturbances’ during winter [Yurtsever and Gat, 1981; Das, 1995].

4.2.2 Annual water vapor cycle

Stable oxygen isotopic compositions of atmospheric water vapor ($\delta^{18}\text{O}_{av}$) during the 2007-08 are shown in figure (4.12).

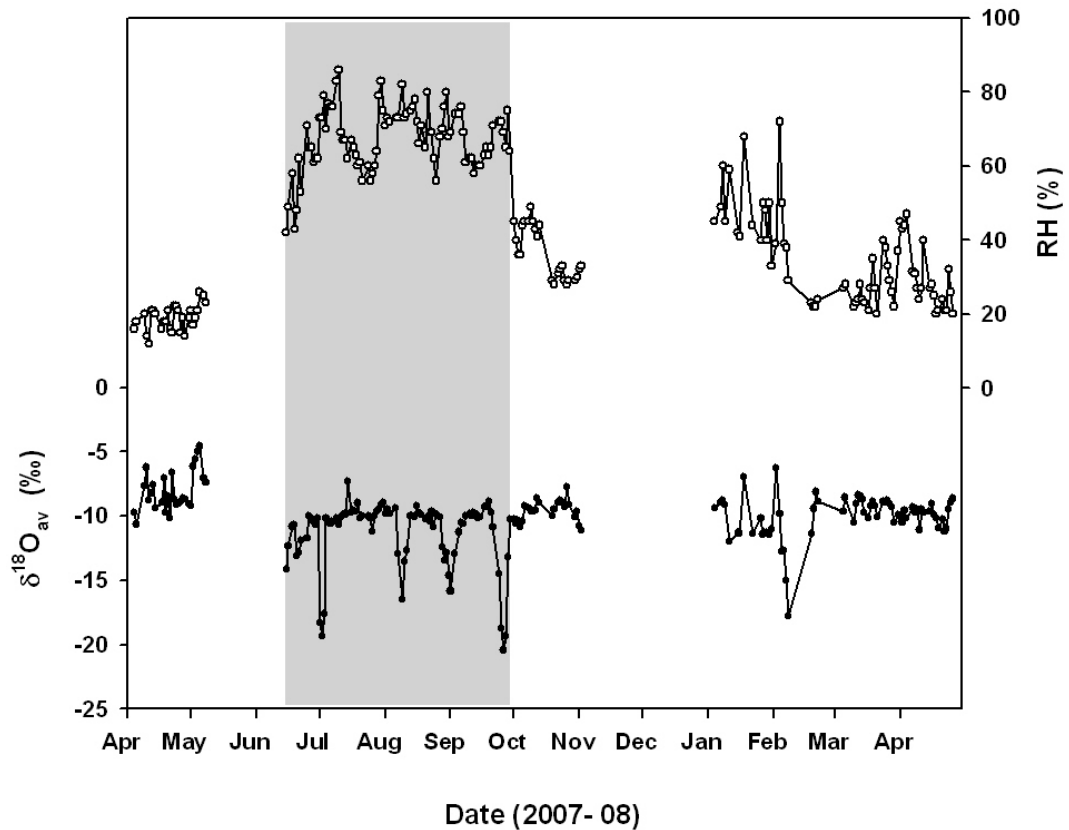


Figure 4.12: Variation of stable oxygen isotopic composition of atmospheric water vapor ($\delta^{18}\text{O}_{av}$) (\bullet) and relative humidity (RH) (o) over Ahmedabad from April 2007 –April 2008. Gray shade indicates the monsoon season. Beginning of each month is marked by a pip.

Between the first week of April and the first week of May, $\delta^{18}O_{av}$ values were higher than in the later months, and a slight increasing trend is seen, which may be due to the increase in humidity during this period (from 12% in April to 26% in May). A large impact of rain water on the local water vapor is clearly marked by a sharp decrease of $\sim 3\text{‰}$ in $\delta^{18}O_{av}$ and a sharp increase of 20% in relative humidity (RH) from May to the second week of June [Fig. 4.12].

During the monsoon $\delta^{18}O_{av}$ attained an average value of $\sim -11\text{‰}$ and persisted till the end of October, even though the last rain of the year was received on 27 September. This may be due to the carry over effect of rain on $\delta^{18}O_{av}$. From October onwards $\delta^{18}O_{av}$ started stabilizing (fewer fluctuations) and reached an average value of -9.5‰ [Fig. 4.12]. Between 2 Feb and 8 Feb 08, $\delta^{18}O_{av}$ values showed a decreasing trend. From 9 February onwards an increasing trend was observed and the average $\delta^{18}O_{av}$ value was attained on 20 Feb 08. This may be due to the short term effect of western disturbances as it brings moisture highly depleted in heavy isotopes [Pande et al., 2000]. Back trajectory analysis using NOAA Hysplit Model confirms that during this period air mass is transported from Pakistan and Arabian countries. A typical example back trajectory analysis on 8 Feb 08 is shown in figure 4.13. From 20 Feb 08 to 31 March 08 a slight decreasing trend was observed in $\delta^{18}O$ which may be due to the continuous decrease of humidity in the atmosphere. End of the monsoon can be clearly marked by a sharp decrease in RH values.

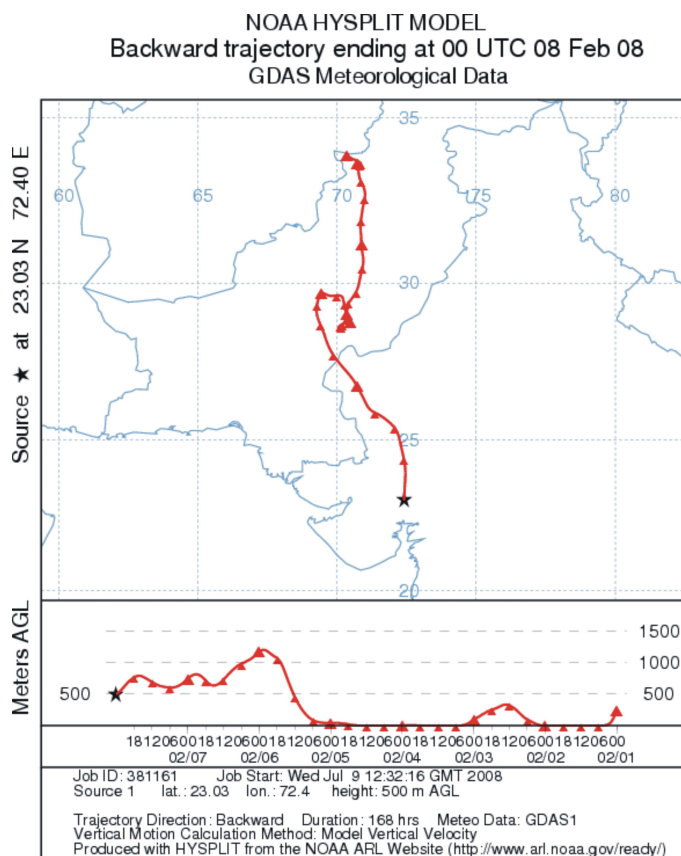


Figure 4.13: Back trajectory analysis on 8 Feb 08 to trace western disturbances.

4.2.3 Modifications in AWW due to monsoonal rain

On the 20 June, 2007 first rain of the year was received over Ahmedabad [Fig. 4.14]. Stable oxygen isotopic compositions of rain ($\delta^{18}O_r$, daily average) with the amount collected (total amount collected for the whole day) is shown in figure 4.14. Preferential removal of ^{18}O during the rainout processes leaves behind ^{18}O depleted vapor in the cloud: intense rain leads to ^{18}O depleted cloud vapor and consecutively ^{18}O depleted rain. This mechanism is well explained by the Rayleigh fractionation during rainout and is known as the amount effect [Dansgaard, 1964]. During the monsoon, amount of rain varied between 0.1-28.1 mm d⁻¹. $\delta^{18}O_r$ showed a large range of variations from 0.3‰ to -10‰. Amount weighted average $\delta^{18}O_r$ value for the whole monsoon season was found to be -4.5‰. Except for the first few

rains, major variations in the $\delta^{18}O_r$ can be attributed to the amount effect, i.e., whenever the amount of rain was less, $\delta^{18}O_r$ values of rain was less negative (i.e., higher) and vice versa.

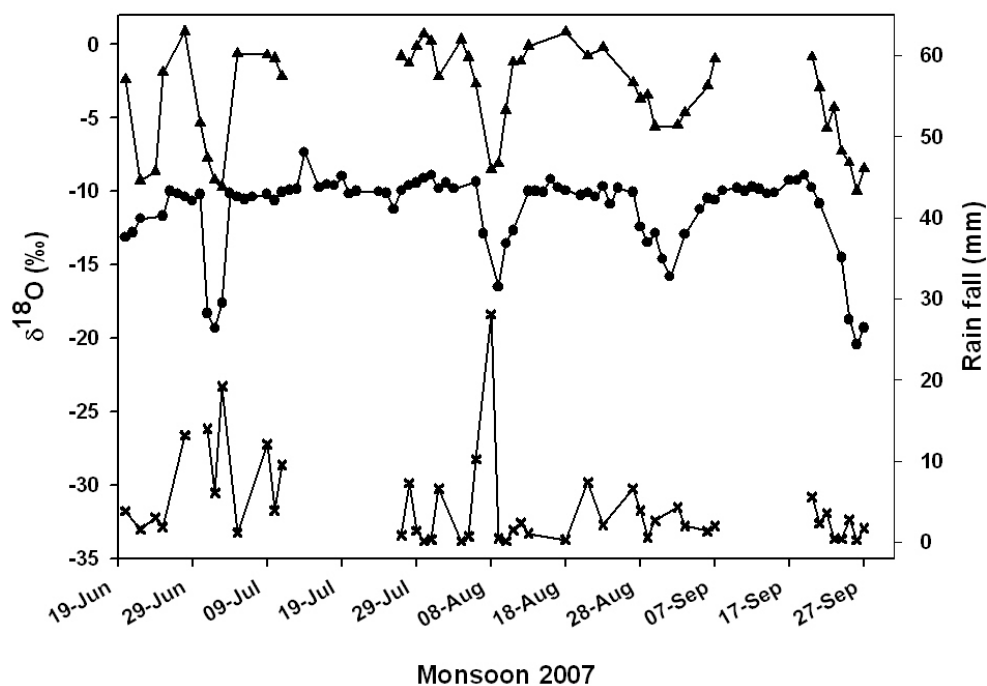


Figure 4.14: Stable oxygen isotopic composition of rain water (\blacktriangle), atmospheric water vapor (\bullet) and rainfall (\times) during monsoon 2007. Gaps in the data represent days when it did not rain.

The maximum daily rain (28.2 mm) occurred on 8 August 07 and $\delta^{18}O_r$ decreased upto -8.6‰ , the minimum $\delta^{18}O_r$ obtained for the monsoon season except for the last few (less rain) events. At the onset of monsoon, $\delta^{18}O_r$ was significantly more negative though the amount of rain was less. This may be due to the effect of local moisture which can be highly depleted due to the strong evaporation and mixing from regional water bodies as the air temperature reaches its maximum ($>40^\circ\text{C}$). Once monsoon sets in, the effect of local moisture decreases and the effect of monsoonal rain takes over. The former dominates again after the withdrawal

of the monsoon. Although the amount of rain was less during the retreat, $\delta^{18}O_r$ was still depleted. Equilibration of rain drops with ^{18}O depleted local moisture probably decreases $\delta^{18}O_r$. Rain samples were also collected ~ 4 km way from PRL by Dr. M. G. Yadava. Almost similar $\delta^{18}O_r$ values of his rain samples gives an additional confidence to the present data.

4.2.4 Stable isotopic equilibrium between vapor and rain

The co-variation of $\delta^{18}O_{av}$ and $\delta^{18}O_r$ is also shown in figure 4.14. Five major rain events (22 June, 2 July, 9 August, 1 and 26 September) were marked by more negative $\delta^{18}O_{av}$. During all of these events rain and vapor were found to be in isotopic equilibrium, except on 22 June, when $\delta^{18}O$ of rain was highly depleted (-9.3‰) but that of vapor was only -11.9‰ . One explanation for this anomaly may be as follows. During the onset of monsoon air temperatures are high ($>40^\circ\text{C}$) resulting in strong evaporation of rain drops. The high temperatures and evaporation may not permit the quick attainment of isotopic equilibrium between rain and water vapor. For the rest of the events after the onset of monsoon, atmospheric humidity has already increased ($>80\%$) and this additional vapor dominates over local vapor. Thus, the $\delta^{18}O_{av}$ initially decreases due to the depleted rain samples (due to the amount effect) and remains in isotopic equilibrium with rain, but once it stops raining, $\delta^{18}O_{av}$ bounces back to its normal value during no rain of $\sim -10\text{‰}$. This observation shows that the atmospheric water vapor is in isotopic equilibrium with rain at all times on a diurnal scale. It is also seen that isotopic equilibrium between rain and vapor occurs quite fast with negligible time lag. $\delta^{18}O_{av}$ shows a high stability between two consecutive rain events.

Apart from the regular vapor collection, a few (N=30) vapor and rain samples were collected simultaneously to assess the instantaneous isotopic equilibrium between rain and water vapor; results are presented in Table 4.1.

Date (2007)	Time (hrs)	Sampling duration (hrs)	Temp (°C)	Rh (%)	$\delta^{18}O$ (Vapor) (‰)	$\delta^{18}O$ (Rain) (‰)	$\delta^{18}O$ (Vapor - Rain) (‰)
19-Apr	23:15	01:00	34.0	18	-4.7	10.9	15.5
20-Jun	18:30	02:00	29.0	74	-11.7	-2.4	9.3
1-Jul	20:00	01:00	30.0	78	-15.6	-6.3	9.4
2-Jul	21:15	01:00	26.5	82	-17.2	-8.9	8.3
3-Jul	10:00	02:00	26.5	79	-17.6	-8.2	9.4
3-Jul	14:30	01:00	25.5	86	-17.2	-8.3	8.9
9-Jul	10:00	02:00	27.5	83	-10.2	-0.9	9.3
9-Jul	16:00	02:00	26.0	85	-9.7	-1.1	8.7
9-Jul	22:00	01:00	26.0	87	-9.6	0.2	9.8
10-Jul	17:00	01:00	27.0	85	-9.5	-0.2	9.3
28-Jul	15:00	01:30	28.5	76	-11.5	-1.3	10.2
29-Jul	10:00	02:00	28.5	79	-9.4	-0.1	9.3
30-Jul	10:00	02:00	28.0	83	-9.1	0.7	9.8
31-Jul	10:00	02:00	29.0	75	-8.9	0.2	9.1
6-Aug	19:30	01:00	27.0	83	-11.9	-2.7	9.3
8-Aug	10:00	02:00	26.5	83	-19.2	-9.8	9.4
8-Aug	14:15	01:00	26.5	86	-15.1	-5.8	9.3
8-Aug	18:30	01:00	27.0	85	-17.3	-8.6	8.8
12-Aug	20:30	01:00	26.0	86	-10.9	-1.3	9.7
21-Aug	10:00	02:00	26.5	80	-10.1	-1.1	9.0
21-Aug	14:30	01:00	26.0	80	-10.4	-0.8	9.6
27-Aug	15:30	01:00	25.0	85	-12.5	-0.7	11.8
27-Aug	18:45	01:00	27.0	80	-14.6	-4.3	10.3
28-Aug	19:45	01:00	26.0	82	-13.5	-3.8	9.7
29-Aug	20:15	01:00	26.5	80	-13	-3.8	9.2
2-Sep	11:30	01:00	28.5	81	-13.2	-4.2	9.0
6-Sep	21:00	01:00	26.5	80	-13.0	-2.7	10.3
20-Sep	23:15	01:00	27.5	75	-10.8	-1.0	9.8
24-Sep	22:30	01:00	27.5	76	-14.9	-7.8	7.1
27-Sep	16:00	01:00	27.0	89	-17.4	-7.8	9.6
Mean			27.1	81.5	-12.9	-3.5	9.4
Sdv			1.2	4	3.1	3.3	0.8

Table 4.1: Simultaneous rain and vapor collection: date of collection (column 1), starting time (column 2), duration of collection (column 3), temperature and relative humidity at start (columns 4 and 5 respectively), $\delta^{18}O$ value of vapor and rain relative to V-SMOW (columns 6 and 7 respectively) and difference between the $\delta^{18}O$ value of vapor and rain (columns 8). Mean and standard deviation calculated neglecting the first row of (pre-monsoon) data as it is not a monsoonal rain sample.

Temperature and RH were measured using a digital hygrometer (calibrated using a wet and dry bulb thermometer). It can be seen that for most cases (except 19 April, 27 August and 24 September 2007) atmospheric water vapor was $\sim 9\text{‰}$ depleted compared to that of the rain water during the monsoon. A mean difference of 9.4‰ between $\delta^{18}\text{O}$ values of vapor and rain is consistent with isotopic equilibrium at the observed mean temperature of $\sim 27^\circ\text{C}$, within uncertainties [Clark and Fritz, 1997]. For the pre-monsoon rain event of 19 April 07, vapor was 15.5‰ depleted compared to rain. At that time air temperature was higher (34°C), humidity lower (18%) and rain was enriched in ^{18}O possibly due to strong evaporation during fall. In general the atmospheric water vapor remained in instantaneous isotopic equilibrium with rain water during the monsoon season (Table 4.1).

The present study shows significant impact of monsoonal rain over local atmospheric water vapor. Stable isotopic composition of rain and vapor show that they are in the isotopic equilibrium at least during monsoon. It appears that by monitoring the isotopic composition of atmospheric vapor using satellite sensors, one may be able to detect the onset of monsoons over India.

References

- Celle-Jeanton, H., R. Gonfiantini, Y. Travi and B. Sol (2004), Oxygen-18 variations of rainwater during precipitation: application of the Rayleigh model to selected rainfalls in Southern France, *J. Hydrol.*, 289, 165-177.
- Clark, I. D. and P. Fritz. (1997), *Environmental Isotopes in Hydrology*, CRC Press, Boca Raton, Fla, USA.
- Craig, H. (1961), Isotopic Variations in Meteoric Waters, *Science*, 133 (3465), 1702-1703.
- Dansgaard, W. (1964), Stable isotopes in precipitation, *Tellus*, 16, 436-468.
- Das, P. K. (1995), *The Monsoons*, National Book Trust, India, p. 252.
- Gat, J. R. (1971), Comments on the stable isotope method in regional groundwater investigation, *Wat. Resour. Res.*, 7, 980-993.

- He, H. and R. B. Smith (1999), Stable isotope composition of water vapor in the atmospheric boundary layer above the forests on New England, *J. Geophys. Res.*, 104 (D9), 11,657-611,673.
- Houze, R. A., Jr. (2004), Mesoscale convective systems, *Rev. Geophys.*, 42, RG4003, doi:4010.1029/2004RG000150.
- Lachniet, M. S. and W. P. Patterson (2002), Stable isotope values of Costa Rican surface waters, *Journal of Hydrology*, 260, 135-150.
- Pande, K., J. T. Padia, R. Ramesh and K. K. Sharma (2000), Stable isotope systematics of surface water bodies in the Himalayan and Trans-Himalayan (Kashmir) region, *Proc. Indian Acad. Sci. (Earth Planet. Sci.)*, 109 (1), 109- 115.
- Rao, T. N., D. N. Rao, K. Mohan and S. Raghavan (2001), Classification of tropical precipitating systems and associated Z-R relationships, *J. Geophys. Res.*, 106, 17699-17711.
- Rao, T. N., D. N. Rao and S. Raghavan (1999), Tropical precipitating systems observed with Indian MST radar, *Radio Sci.*, 34, 1125 –1139.
- Rogers, R. R. and M. K. Yau. (1976), *A short course in cloud physics*, Pergamon Press.
- Rozanski, K., L. Araguas-Araguas and R. Gonfiantini (1993), Isotopic patterns in modern global precipitation, in *Climate Change in Continental Isotopic Records*, *Geophys. monogr. Ser.*, vol 78, edited by P. K. Swart et al., pp 1-36, AGU, Washington, D. C.
- Sheshshayee, M. S., H. Bindumadhava, R. Ramesh, T. G. Prasad, M. R. Lakshminarayana and M. Udayakumar (2005), Oxygen isotope enrichment ($\delta^{18}O$) as a measure of time-averaged transpiration rate, *Journal of Experimental Botany*, 56 (422), 3033-3039.
- Smith, J. A., A. S. Ackerman, E. J. Jensen and O. B. Toon (2006), Role of deep convection in establishing the isotopic composition of water vapor in the tropical transition layer, *J. Geophys. Res.*, 33, L06812, doi: 06810.01029/02005GL024078.
- Yurtsever, Y. and J. R. Gat (1981), *Atmospheric waters. Stable Isotope Hydrology Deuterium and Oxygen-18 in the Water Cycle*. Technical Report Series No.210. (Gat, J. R. and Gonfiantini, R. Eds.), 103-142. IAEA, Vienna.

Chapter 5

Summary and Scope for Future Work

Atmospheric moisture cycling is an important aspect of the earth's climate system. Global warming makes the study of atmospheric moisture more essential. Increasing load of atmospheric moisture has been predicted to increase frequency of severe storms. Stable isotopes of water deuterium (D) and oxygen (^{18}O) already have been proved important tracers of the natural hydrological processes. So to study hydrological cycle using stable isotope based models, information of fractionation factor at each phase change is highly essential. So far only a few studies are available to characterize this and most of these are laboratory experiments. This study provides first experimental information about the fractionation factor over ocean and land by direct collection of atmospheric water vapor, ocean surface water and rain water. Also for the first time this study demonstrates potential of the stable isotopes to trace microphysical processes associated with rain formation. The present thesis also provides a new stable isotopic dataset of the ocean surface water and atmospheric water vapor over the Southern Ocean and the Bay of Bengal.

5.1 Ocean Studies

5.1.1 Stable isotopic study of the Southern Ocean surface water

Results from the isotopic study of ocean surface water over the Southern Ocean:

1. Near the equator: a very clear signature of the domination of evaporation-precipitation process is seen, while a precipitation dominated zone is located between two evaporation dominated zones south of the equator.
2. Signature of the Agulhas Front and the Subtropical Front (recognizable by the sharp decrease in salinity and $\delta^{18}O$) in the surface waters are identified at 41°S and 44°S in February. During the return journey (March) these two fronts merged and are located at 41°S.
3. Region between 63°S and 67°S found affected by freezing of ocean water. From 67°S onwards both $\delta^{18}O$ and salinity start decreasing possibly due to mixing of continental melt ice to the coastal ocean water.
4. The region between 41°S and 45°S works as a transition zone: the region lying north of 41°S is dominated by evaporation/precipitation processes while that south of 45°S (upto Antarctica) is dominated by melting/freezing processes.
5. The best fit line between δD and $\delta^{18}O$ indicates the Southern Ocean evaporates under the isotopic non-equilibrium condition.

5.1.2 Stable isotopic study of ocean surface water (OSW) and atmospheric water vapor (AWV) over the Bay of Bengal (BOB)

Results from the isotopic study of OSW and AWV over the BOB:

1. Stable isotopic composition of the OSW and AWV found highly varying with space and time. For all vapor samples $\delta^{18}O$ ranges between -9.7‰ to -12.5‰ whereas δD ranges between -56‰ to -76‰ .
2. $\delta^{18}O$ and δD follow the same trends with the r^2 value of 0.56. This moderate correlation may be due to the prominent kinetic effects.
3. Overall stable isotopic values of vapor show a decreasing trend on moving towards north. This may be due to the depleted values of OSW. OSW also shows a little decrease on moving towards north but this trend is not as prominent as in the case of AWV. These depleted values of OSW may be due to the effect of fresh water input from the rivers.
4. The best fit line between δD and $\delta^{18}O$ for vapor (with the slope of 4.84) indicates that evaporation has occurred under strong kinetic effects.
5. Isotopic composition of AWV shows more fluctuations than the ocean sea surface water.
6. Increasing trend in d-excess values on moving towards the north again verifies the increasing effect of kinetic fractionation.
7. Fractionation factors between OSW and AWV for both oxygen and hydrogen were found different than their equilibrium value which indicates that in general the BOB does not evaporate in stable isotopic equilibrium.
8. Our results show that the deviation in the fractionation factor from their equilibrium value can be explained by taking into account all the three parameters (temperature, humidity and winds), responsible for the kinetic fractionation.

5.2 Land Studies

5.2.1 Simultaneous study of rain drop size distribution (DSD) and stable isotopic composition of rain water

Results from the simultaneous study of the rain drop size distribution, MST radar and stable isotopic composition of rain water:

1. Time series plot of $\delta^{18}O$ shows a specific 'V' or 'W' structure for all the rain events.
2. For the first time the simultaneous study of cloud parcel turbulence (using MST radar) and stable isotopic composition of rain water has been done. This study reveals that the single rain parcel can also have both stratiform and convective nature; however, the duration of convection is varying from case to case.
3. The temporal variations of rain integral parameters: reflectivity factor (Z in dBZ), rainfall rate (R in mm hr^{-1}) and mass weighted mean diameter (D_m in mm) also confirm both stratiform and convective rain features in all the events.
4. Stable isotopic study of rain water suggests the formation of the first condensate at the topmost part of the cloud parcel due to (1) low temperature, (2) high condensation rate and (3) depleted isotopic values at the top of cloud parcel.
5. The initial rain samples show more evaporation effect than the later samples. Effect of evaporation decreases and the signature of condensational growth start manifesting once the atmosphere saturates at the later part of rain event.

6. Turbulence and strong vertical motion in the first phase of the cloud system is also confirmed by the MST radar data. It clearly shows the typical structure of mesoscale convective system in the starting. This turbulence decreases with time and cloud parcel attains a typical structure of stratiform system. A clear bright band, signature of stratiform precipitation, with enhanced precipitation echo power at around 4.35 km. This is the same time when a sharp dip is observed in the time series plot of the $\delta^{18}O$ of the rain water. So a dip in the time series plot of isotopes may be the good indication of the changing nature of the cloud parcels form convection to stratiform type.
7. A ‘W’ structure in the time series plot of $\delta^{18}O$ might be due to the replacement of first cloud parcel by another one at the site of sample collection.
8. Isotopic ratio shows a negative correlation with mean drop size for the rain events of 14 September and 5 October. It shows that most of the time smaller drops were dominated by evaporation over condensational growth. For the rain events on 12 September, 17 and 26 October isotopic ratio ($\delta^{18}O$) do not change with drop size. This may be due to the cancellation of evaporation effect to the condensational growth effect for the whole event.
9. Intercept of δD - $\delta^{18}O$ line (7.87 ± 0.47) indicate that the effect of secondary evaporation (i.e. re-evaporation of rain drops) is prominent during the rain events at Gadanki.

5.2.2 Stable isotopic study of rain water and atmospheric water vapor (AWV) at Ahmedabad

Results from the stable isotopic study of rain water and atmospheric water vapor at Ahmedabad:

1. Between the first week of April and the first week of May, oxygen isotopic composition of AWV ($\delta^{18}O_{av}$) values are higher than in the later months,

and a slight increasing trend is seen, which may be due to the increase in relative humidity (RH) during this period.

2. A large impact of rain water on the local water vapor is clearly marked by a sharp decrease of $\sim 3\%$ in $\delta^{18}O_{av}$ and a sharp increase of $\sim 20\%$ in RH values of AWV from May to the second week of June.
3. During the monsoon $\delta^{18}O_{av}$ attained an average value of $\sim -11\%$ and persisted till the end of October, even though the last rain of the year is received on 27 September. This may be due to the carry over effect of rain on $\delta^{18}O_{av}$. From October onwards $\delta^{18}O_{av}$ started stabilizing (fewer fluctuations) and reached an average value of -9.5% .
4. Short term effect of western disturbances is also traced by the $\delta^{18}O_{av}$ between 2 and 20 Feb. Back trajectory analysis confirms that during this period air mass is transported from Pakistan and Arabian countries.
5. Amount weighted average of oxygen isotopic composition of rain water ($\delta^{18}O_r$) for the whole monsoon season is found to be -4.5% .
6. Except for the first few rains, major variations in the $\delta^{18}O_r$ can be attributed to the amount effect. The maximum daily rain (28.2 mm) occurred on 8 August 07 and $\delta^{18}O_r$ decreased up to -8.6% , the minimum $\delta^{18}O_r$ obtained for the monsoon season except for the last few (less rain) events.
7. At the onset of monsoon, strong effect of local moisture observed which decreases as monsoon progresses and the effect of monsoonal rain takes over during the monsoon period. The former dominates again after the withdrawal of the monsoon.
8. Five major rain events (22 June, 2 July, 9 August, 1 and 26 September) are marked by more negative $\delta^{18}O_{av}$. During all of these events rain and vapor

are found to be in isotopic equilibrium, except on 22 June. One explanation for this anomaly may be as follows. During the onset of monsoon air temperatures are high ($>40^{\circ}\text{C}$) resulting in strong evaporation of rain drops. The high temperatures and evaporation may not permit the quick attainment of isotopic equilibrium between rain and water vapor. For the rest of the events after the onset of monsoon, atmospheric humidity has already increased ($>80\%$) and this additional vapor dominates over local vapor. Thus, the $\delta^{18}\text{O}_{av}$ initially decreases due to the depleted rain samples (due to the amount effect) and remains in isotopic equilibrium with rain, but once it stops raining, $\delta^{18}\text{O}_{av}$ bounces back to its normal value during no rain of $\sim -10\text{‰}$. This observation shows that the atmospheric water vapor is in isotopic equilibrium with rain at all times on a diurnal scale. It is also seen that isotopic equilibrium between rain and vapor occurs quite fast with almost no time lag. $\delta^{18}\text{O}_{av}$ shows a high stability between two consecutive rain events.

9. Simultaneous collection of rain water and AWV demonstrate instantaneous isotopic equilibrium between rain and water vapor. It is found that for most cases atmospheric water vapor is $\sim 9\text{‰}$ depleted compared to that of the rain water during the monsoon.
10. For the pre-monsoon rain events AWV is not found in stable isotopic equilibrium with rain. This may be due to the strong evaporation of rain drops.
11. In general atmospheric water vapor remained in instantaneous isotopic equilibrium with rain water during the monsoon season.

5.3 The future scope of the present work

Stable isotopes of water have been proved powerful tracers for the hydrological cycle but for the first time present study demonstrates the potential of these isotopes to trace microphysical processes occurring during rain formation. This suggests the

additional use of these isotopes to understand finer physical processes happening inside the cloud parcel. This study provides experimental data on the fractionation factor over land and ocean both which is essential for the isotope based cloud models. Though a few stable isotopic studies of atmospheric water vapor over ocean and land have been done but they are limited to small regions. It requires more experimental studies for the remaining parts for better understanding of hydrological cycle. Results of the present thesis give motivation to address the following interesting issues:

- More stable isotopic studies of ocean surface water and deep waters over unexplored regions will help better understand ocean surface processes and under water currents. Ocean surface show large seasonal influence. So seasonal study of ocean surface water and deep water may provide valuable inputs to our current understanding. Several isotopic studies have been done in this regards but they are sparse over the Southern Ocean. This may also help to understand monsoon system.
- Proper understanding of ocean-atmosphere interaction is not only important for the hydrological cycle but also for the earth's energy budget. Present study show that the stable isotopes of atmospheric water vapor over oceans can be an efficient tracers to study energy exchange between ocean and atmosphere. So stable isotopic study of atmospheric water vapor over different parts of oceans will help to understand changing nature of ocean-atmospheric interaction with space and time. Present study also demonstrates dependence of isotopic fractionation factor on various environmental parameters. So the temporal isotopic study of atmospheric water vapor will help to understand this and will provide inputs to the isotope based hydrological models. This study will also be helpful to trace changes due to the effect of global warming in the ocean-atmosphere interaction.
- A big network for the stable isotopic study of rain water is established (Global

network for isotopes in precipitation) but no such work is done for the vapor isotopic studies. Such isotopic study of atmospheric water vapor are very sparse. Isotopic studies of atmospheric water vapor provide better insight to the monsoon system. Not only it gives information about the source of moisture but also tells about the water vapor recharge during the monsoon period. This necessitates isotopic study of atmospheric water vapor over different parts of continents for the longer period. This may be helpful to understand and predict monsoon better.

- Present study shows that the microphysical processes occurring inside the cloud parcel can be traced using stable isotopes. Proper understanding of rain formation processes is necessary for better predictability. So the high resolution isotopic study of rain water along with radar and disdrometer observations during different seasons (e.g. pre-monsoon, monsoon and post-monsoon) will provide better understanding of these microphysical processes for the various cloud types.
- Recently satellite based observations of atmospheric water vapor (hydrogen isotopic composition only) have become available. Using present dataset with some assumptions, satellite observation can be validated.
- On the basis of experimental inputs such as information of fractionation factor, isotopic composition of ocean surface water, atmospheric water vapor and rain water, microphysical processes associated with rain formation, effect of local moisture and amount of secondary evaporation, a good isotope based model to study hydrological cycle can be developed. Also other existing models can be tested and modified using the present data and information.

List of Publications

Papers in Refereed journals:

- **Rohit Srivastava**, R. Ramesh, Satya Prakash, N. Anilkumar and M. Sudhakar, (2007), Spatial variation of oxygen isotopes and salinity in the Southern Indian Ocean, *Geophys. Res. Lett.*, Vol. 34, doi:10.1029/2007GL031790.
- T. Narayana Rao, B. Radhakrishna, **Rohit Srivastava**, T. Mohana Satyanarayana, D. Narayana Rao and R. Ramesh (2008), Inferring microphysical processes occurring in mesoscale convective systems from radar measurements and isotopic analysis, *Geophys. Res. Lett.*, Vol. 35, L09813, doi:10.1029/2008GL033495.
- **Rohit Srivastava**, R. Ramesh, R. A. Jani, N. Anilkumar and M. Sudhakar, Stable oxygen, hydrogen isotope ratios and salinity variations of the surface Southern Indian Ocean waters (Accepted in *Current Science*).
- **Rohit Srivastava**, R. Ramesh, R. A. Jani and Ashutosh K. Singh, Is the monsoon rain in oxygen isotopic equilibrium with ambient water vapor? (Under review, *Geophys. Res. Lett.*).
- **Rohit Srivastava**, R. Ramesh, T. Narayana Rao, B. Radhakrishna, T. Mohan Satyanarayana and D. Narayana Rao, Relationship between stable oxygen isotope ratio and drop size distribution in tropical rainfall (Under review, *Tellus B*).

Abstracts in National/International conferences:

- **Rohit Srivastava** and R. Ramesh, "Effect of global warming on the salinity- $\delta^{18}O$ relationship in the Southern Ocean", National Space Science Symposium, RAC, Udagamandalam (Ooty), India, 26th - 29th 2008.

- **Rohit Srivastava** and R. Ramesh, "Investigation of cloud processes using stable oxygen/ hydrogen isotopes in tropical rainfall", European Research Course on Atmosphere (ERCA), Grenoble, France, 7th Jan - 8th Feb.
- **Rohit Srivastava**, R.Ramesh, T. Narayana Rao and D. Narayana Rao, "Investigation of the relationship between stable oxygen/ hydrogen isotopes and the drop size distribution in tropical rainfall", MST 11, Eleventh International Workshop on Technical and Scientific aspects of MST 11, Gadanki, Tirupati, India, December 11-15, 2006.
- Satya Prakash, **Rohit Srivastava**, R. Ramesh, Rahul Mohan and M. Sudhakar, "First Nitrogen-based Production Measurement in the Southern Ocean", International Workshop on Sustained Indian Ocean Biogeochemical and Ecological Research (SIBER), Goa, India, 3-6 October, 2006.
- Ramesh Rengaswamy, Satya Prakash, **Rohit Srivastava**, Naveen Gandhi and Sanjeev Kumar, "Nitrogen Assimilation and f-Ratios in the Indian Ocean", International Workshop on Sustained Indian Ocean Biogeochemical and Ecological Research (SIBER), Goa, India, 3-6 October, 2006.



Oxygen isotope and salinity variations in the Indian sector of the Southern Ocean

Rohit Srivastava,¹ R. Ramesh,¹ Satya Prakash,¹ N. Anilkumar,² and M. Sudhakar²

Received 1 September 2007; revised 24 October 2007; accepted 9 November 2007; published 20 December 2007.

[1] A combined study of stable oxygen isotopes ($\delta^{18}\text{O}$) and salinity of surface ocean waters collected from the Southern Indian Ocean during the late austral summer and early fall (25th January to 1st April, 2006) helped to trace atmospheric and oceanic processes: near the equator, a very clear signature of the domination of evaporation-precipitation process was seen, while a precipitation dominated zone was located between two evaporation dominated zones south of the equator. The signature of the Agulhas Front (AF) and the Subtropical Front (STF, recognizable by the sharp decrease in salinity and $\delta^{18}\text{O}$) in the surface waters were identified at 41°S and 44°S in February; during the return journey (March) these two fronts had merged and were located at 41°S . South of 45°S , the slope of the $\delta^{18}\text{O}$ -salinity relationship was close to zero; while north of 62°S could have some precipitation/evaporation effect, south of 63°S was clearly dominated by freezing/melting. **Citation:** Srivastava, R., R. Ramesh, S. Prakash, N. Anilkumar, and M. Sudhakar (2007), Oxygen isotope and salinity variations in the Indian sector of the Southern Ocean, *Geophys. Res. Lett.*, *34*, L24603, doi:10.1029/2007GL031790.

1. Introduction

[2] Stable isotopes of light elements, deuterium (D) and oxygen (^{18}O) are important tracers of the natural hydrological processes [Friedman *et al.*, 1964; Craig and Gordon, 1965; Clark and Fritz, 1997; Duplessy *et al.*, 1991]. In the modern ocean, $\delta^{18}\text{O}$ has been used as a tracer for sea ice melt [Macdonald *et al.*, 1999], glacial and river run-off, deep ocean water masses [Meredith *et al.*, 1999] and deep water formation [Jacobs *et al.*, 1985]. A simultaneous study of $\delta^{18}\text{O}$ and salinity provides specific information about sea surface processes such as (1) evaporation/precipitation, (2) melting/freezing, (3) upwelling/advection, and (4) continental runoff. In the case of the Southern Ocean, changes due to continental run off are very small. Salinity and $\delta^{18}\text{O}$ co-vary in the case of evaporation-precipitation because both parameters decrease due to precipitation whereas evaporation increases both. Salinity and $\delta^{18}\text{O}$ exhibit a linear relationship and its slope depends on regional climate, but in the case of melting/freezing, $\delta^{18}\text{O}$ does not change much while salinity changes significantly. For a proper understanding of the processes and salinity- $\delta^{18}\text{O}$ slope, large spatial and temporal data coverage is needed. In the Southern Ocean, such data sets are limited (e.g., GISS &

GNIP data bases) [Schmidt *et al.*, 1999; International Atomic Energy Agency (IAEA), 2001].

[3] The Southern Ocean is characterized by the presence of several fronts; fronts are defined as water masses with marked changes in the properties [Park *et al.*, 1998]. The Indian sector of the Southern Ocean is characterized by the presence of two such major fronts: the Agulhas Front (AF) and the Subtropical Front (STF, Figure 1) [Sparrow *et al.*, 1996; Belkin and Gordon, 1996; Rintoul and Bullister, 1999; Rintoul and England, 2002]. The former is the connecting link between the generically similar Southern Atlantic and Southern Indian Ocean Currents [Deacon, 1937]. It is a major source of water exchange between the Atlantic and the Indian Oceans [Peterson and Stramma, 1991; Read and Pollard, 1993; Lutjeharms, 2006]. It is characterized by the temperature gradient between 15.7 to 21.0°C at 200 m depth [Gordon *et al.*, 1978]. AF can merge with the STF or form a separate front to the north of STF between 39°S to 40°S [Lutjeharms and Valentine, 1984]. STF makes an interface between Subtropical Surface Waters and Subantarctic Surface Water [Deacon, 1937]. It is characterized by the horizontal surface temperature and salinity transitions of 10 – 14°C and 34.6 to 35.1 , respectively with the mean location of 42°S [Whitworth and Nowlin, 1987]. While these criteria may be useful to recognize the positions of AF and STF at depths, in the surface they are traceable using $\delta^{18}\text{O}$ as well, as we show here.

2. Sampling and Methodology

[4] Surface seawater samples were collected during the second expedition to the Southern Ocean and Larsemann Hills, Antarctica on board R/V *Akademik Boris Petrov* during January to March, 2006. We reached the Prydz Bay area, Antarctica, on 25th February, a time when freezing started in the Antarctic Zone. This cruise covered a large area (from 13°N to 68°S and 71°E to 77°E). 97 ocean surface water samples were collected at one degree intervals. The cruise track is shown in Figure 1. Using a small, clean plastic bucket, sea surface water samples were collected. The bottles were filled to the brim. Samples were stored in 100 ml plastic bottles with tight-fitting double caps to prevent evaporation. The bottles were taped at the neck as a further precaution. Salinity was measured on board using a salinometer (Autosal) with a reproducibility of 0.001. The accuracy was checked by using IAPSO Standard sea water of salinity 34.995, conductivity 1.997435, conductivity ratio (K15) 0.99987.

[5] An isotope ratio mass spectrometer (PDZ-Europa, Geo 20-20) was used for isotopic analysis, by the CO_2 equilibration method [Epstein and Mayeda, 1953; Gonfiantini,

¹Physical Research Laboratory, Navrangpura, India.

²National Centre for Antarctic and Ocean Research, Vasco-da-Gama, India.

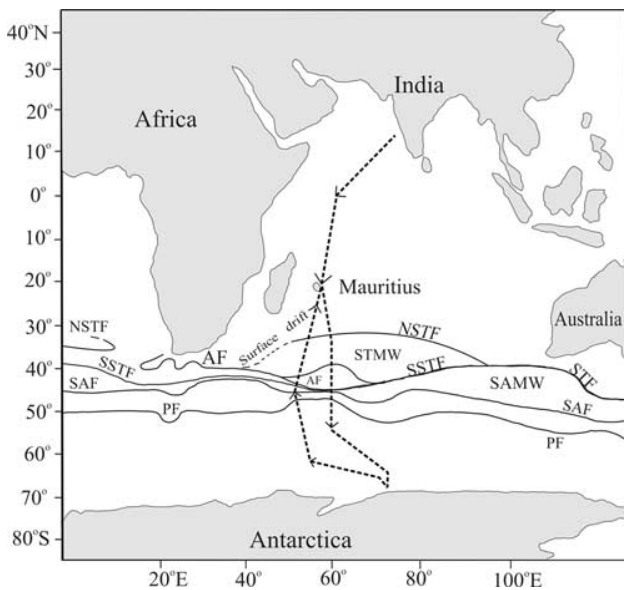


Figure 1. Cruise track along which sampling was done. Approximate locations of the various fronts are marked [after *Belkin and Gordon, 1996*]: AF, Agulhas Front; NSTF and SSTF, North and South Sub-Tropical Fronts; PF, Polar Front; SAF, Sub-Antarctic Front; and SAMW and STMW, Sub-Antarctic and Sub-Tropic Mode Waters. Onward and return journeys are shown by arrows.

1981]. The isotopic compositions were expressed in the conventional units defined by:

$$\delta^{18}\text{O} = \left[\frac{(^{18}\text{O}/^{16}\text{O})_{\text{sample}}}{(^{18}\text{O}/^{16}\text{O})_{\text{standard}}} - 1 \right] * 1000 \text{ permil} (\text{‰})$$

V-SMOW was used as a reference [*Gonfiantini, 1981; Coplen, 1996*]. The overall reproducibility of $\delta^{18}\text{O}$ measurement was better than $\pm 0.1\text{‰}$. Two IAEA standards GISP and SLAP gave mean $\delta^{18}\text{O}$ values of -54.56 and -24.43 , while the recommended values are -55.5 and -24.85 respectively, indicating that a stretching of 1.7% is needed for isotopically depleted samples. However, since we are only measuring ocean water and the values fall within the range of -1 to $+1\text{‰}$, no correction was applied to the measured values.

3. Results and Discussion

[6] The observed latitudinal variations of $\delta^{18}\text{O}$, salinity and Sea Surface Temperature (SST) are shown in Figures 2a, 2b, and 2c, respectively (see auxiliary material).¹ From 5°N to 45°S salinity follows the $\delta^{18}\text{O}$ pattern. North of 4.5°S lies a high salinity and high $\delta^{18}\text{O}$ region, indicating a positive E-P (i.e. evaporation dominates). Between 4.5°S to 20°S lies a low salinity and low $\delta^{18}\text{O}$ region, with a negative E-P (i.e. precipitation dominates). Moving further south of 20°S , the salinity and $\delta^{18}\text{O}$ values again start increasing. This indicates again the domination of evapo-

ration. It appears that due to solar heating, water around the equator (from 13°N to 4.5°S) evaporates and rains south of 4.5°S upto 20°S in the austral summer, when the ITCZ (Inter Tropical Convergence Zone) is located south of the equator.

[7] AF and STF have been reported earlier to be at subsurface; but during our poleward journey (February) we could observe their signature at the very surface. At 41°S there is a change in salinity by 0.69 while $\delta^{18}\text{O}$ changes by 0.35‰ , showing the presence of AF. Again at 44°S sharp changes in the salinity and oxygen isotopic composition occur. Between 44°S and 45°S , salinity changes by 1.02 and $\delta^{18}\text{O}$ by 0.49‰ , indicating the position of STF. SST too decreases by 2°C (from 18°C to 16°C) at AF whereas a decrease of 4.5°C (from 15°C to 10.5°C) at

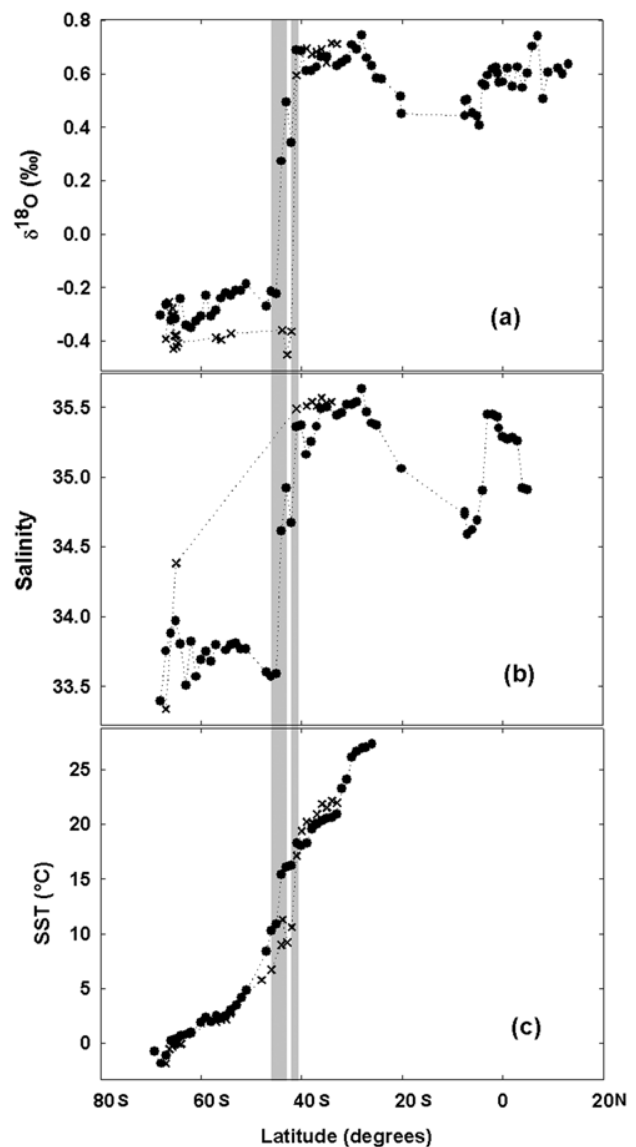


Figure 2. Latitudinal variation of (a) $\delta^{18}\text{O}$, (b) salinity, and (c) SST of surface waters. The two vertical bands refer to positions of the fronts: (left) STF and (right) AF. The solid circles and crosses refer to data collected during onward and return journeys, respectively.

¹Auxiliary materials are available in the HTML. doi:10.1029/2007GL031790.

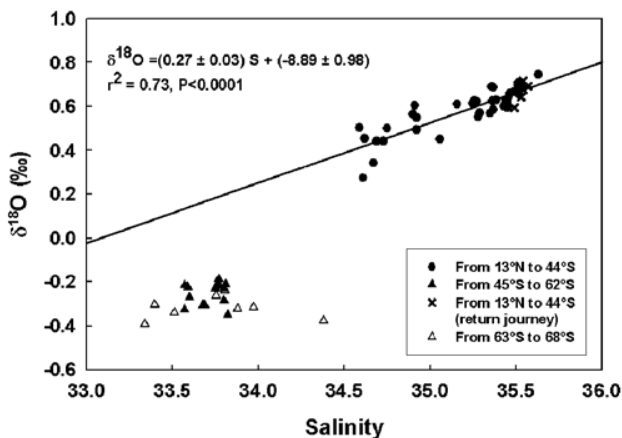


Figure 3. The $\delta^{18}\text{O}$ -salinity relationship for the Indian Ocean, 2006.

STF is seen Figure 2c. During the return journey (March) a sharp increase in $\delta^{18}\text{O}$ by 0.95‰ was noticed at 41°S. This indicates that both fronts (AF and STF) had merged at least at the surface; SST too decreased sharply by 9°C at 41°S (Figure 2c).

[8] In the case of freezing/melting of in situ ice, sea water $\delta^{18}\text{O}$ does not change much whereas the salinity varies significantly. Since the fractionation factor for water to ice transition is very small, freezing does not change the $\delta^{18}\text{O}$ of the remaining water or ice significantly. But salinity changes as during freezing ice discards salt; the salt content in the remaining water increases; during melting salinity decreases due to fresh water input from ice. The case of continental ice melt is different. The ice forms by precipitation which is highly depleted in the heavier isotope. So mixing of continental melt water decreases salinity as well as $\delta^{18}\text{O}$ of the ocean surface water [e.g., Archambeau et al., 1998]. The region from 45°S to 68°S shows much less variation in $\delta^{18}\text{O}$ (between -0.2‰ and -0.4‰) than salinity. From 45°S to 61°S salinity follows the same trend as $\delta^{18}\text{O}$ except for some minor variations. From 47°S to 51°S increases of 0.17 in salinity and 0.08‰ in $\delta^{18}\text{O}$ are observed. This is a cyclonic area. Winds are very strong (about 10 to 14 m/s) in this region. Due to strong winds evaporation is also high and thus salinity and $\delta^{18}\text{O}$ increase. From 51°S (58.8°E) to 62°S (67°E) $\delta^{18}\text{O}$ covary, indicating minor effect of precipitation/evaporation. The region between 63°S to 67°S exhibits high salinity (increase in salinity by 0.25 for first region and 0.49 for second region) while $\delta^{18}\text{O}$ remains constant. This region is affected by ocean water freezing; we observed freezing during the cruise south of 63°S. From 67°S onwards both $\delta^{18}\text{O}$ and salinity start decreasing possibly due to mixing of continental melt ice to the coastal ocean water. During the return journey (March) we have only one sample for salinity up to 41°S (48°E) at 65°S. This high value of salinity (34.38) is due to a strong freezing effect, as visually observed. This is also the beginning of the austral fall. $\delta^{18}\text{O}$ shows a constant value from 68°S to 42°S but for small variations between -0.25‰ to -0.45‰ during the return journey. From 41°S to 33°S salinity and $\delta^{18}\text{O}$ are both constant except for small variations. Figure 3 shows the relationship between $\delta^{18}\text{O}$ and salinity. All points plotted as circles and crosses are

from north of 44°S (13°N to 44°S). In the graph, best fit line has a slope of 0.27 ± 0.03 (best fit line: $\delta^{18}\text{O} = (0.27 \pm 0.03)S - (8.89 \pm 0.98)$, $r^2 = 0.73$, $P \sim 0$), indicating that this region is governed by local evaporation and precipitation. On the other hand, points plotted as triangles from 45°S to 68°S, lie in a line of negligible slope (best fit line: $\delta^{18}\text{O} = -(0.01 \pm 0.06)S + (0.04 \pm 2.10)$, $r^2 = 0.0011$, $P = 0.88$). The data points are further distinguished as solid (up to 62°S) and open triangles (south of 63°S). While the freezing effect is clearly seen for the latter, some evaporation effect can not be ruled out for the former.

[9] *LeGrande and Schmidt* [2006] presented global gridded data set of sea water $\delta^{18}\text{O}$ values, with variable number of observations for different oceanic regions. They reported $\delta^{18}\text{O}$ -salinity relationships for different oceanic regions, whose definition was somewhat arbitrary, according to them. They cautioned that their data set was too sparse to capture consistently seasonal or longer variability except in localized regions. Our $\delta^{18}\text{O}$ data fall in a similar range reported by them. Our results are consistent with their general observations that (1) the $\delta^{18}\text{O}$ -salinity slope is greatest at mid-latitudes and shallowest at low latitudes and the Southern Ocean and (2) in areas of sea ice formation and melting, the slopes tend to be shallow. They reported slopes of 0.24 and 0.16 respectively for the Southern Ocean and the Indian Ocean. A direct comparison of the slopes obtained by us is difficult because (1) our data are seasonal and theirs pertain to long term means and (2) our data pertain only to the Indian sector of the Southern Ocean and theirs cover most parts of the Southern Ocean.

4. Summary

[10] A new set of $\delta^{18}\text{O}$ and salinity data are presented for the Southern Indian Ocean. The data show an evaporation/precipitation dominated region near the equator whereas from 63°S onwards towards Antarctica, melting/freezing processes are more prominent. South of 45°S is characterized by minor effects of evaporation/precipitation. Signature of Agulhas Front (AF) and Subtropical Front are found at 41°S (57.5°E) and 44°S (57.5°E), respectively, in February whereas during the return journey (March) these fronts had merged at 41°S.

[11] **Acknowledgments.** The initiative of T. V. P. Bhaskara Rao to take up the Special Expedition to Southern Ocean and Larsemann Hills, Antarctica (formulated by NCAOR) and the encouragement of P. S. Goel, Secretary, Ministry of Earth Sciences, Govt. of India, and Director, NCAOR, are gratefully acknowledged. Thanks are also due to S. Pednekar, the scientific team, Captain and officers onboard R. V. Boris Petrov for all the support and R. A. Jani for laboratory assistance.

References

- Archambeau, A. S., C. Pierre, A. Poisson, and B. Schauer (1998), Distribution of oxygen and carbon stable isotopes and CFC-12 in the water masses of the Southern Ocean at 30°E from South Africa to Antarctica: results of CIVA1 cruise, *J. Mar. Syst.*, *17*, 25–38.
- Belkin, I. M., and A. L. Gordon (1996), Southern Ocean fronts from the Greenwich meridian to Tasmania, *J. Geophys. Res.*, *101*, 3675–3696.
- Clark, I. D., and P. Fritz (1997), *Environmental Isotopes in Hydrology*, 331 pp., CRC Press, Boca Raton, Fla.
- Coplen, T. B. (1996), Editorial: More uncertainty than necessary, *Paleoceanography*, *11*, 369–370.
- Craig, H., and L. I. Gordon (1965), *Stable Isotope in Oceanographic Studies and Paleotemperatures*, 122 pp., V. Lischii Figli, Pisa, Italy.
- Deacon, G. E. R. (1937), The hydrology of the Southern Ocean, *Discovery Rep.*, *15*, 1–124.

- Duplessy, J.-C., L. Labeyrie, A. Juillet-Leclerc, F. Maitre, J. Duprat, and M. Sarnthein (1991), Surface salinity reconstruction of the North Atlantic Ocean during the Last Glacial Maximum, *Oceanol. Acta.*, *14*, 311–324.
- Epstein, S., and T. Mayeda (1953), Variation of ^{18}O content of water from natural sources, *Geochim. Cosmochim. Acta.*, *4*, 213–224.
- Friedman, I., A. C. Redfield, B. Schoen, and J. Harris (1964), The variation of deuterium content of natural waters in the hydrological cycle, *Rev. Geophys.*, *2*, 177–224.
- Gonfiantini, R. (1981), The δ -notation and the mass-spectrometric measurement techniques, in *Stable Isotope Hydrology: Deuterium and Oxygen-18 in the Water Cycle*, *Tech. Rep. Ser. 210*, edited by J. R. Gat and R. Gonfiantini, pp. 103–142. Int. At. Energy Assoc., Vienna, Austria.
- Gordon, A. L., E. Molinelli, and T. Baker (1978), Large-scale relative dynamic topography of the Southern Ocean, *J. Geophys. Res.*, *83*, 3023–3032.
- International Atomic Energy Agency (IAEA) (2001), GNIP Maps and Animations, <http://isohis.iaea.org/>, Vienna, Austria.
- Jacobs, S. S., R. G. Fairbanks, and Y. Horibe (1985), Origin and evolution of water masses near the Antarctic continental margin: Evidence from $\text{H}_2^{18}\text{O}/\text{H}_2^{16}\text{O}$ ratios in seawater, *Oceanology of the Antarctic Continental Shelf*, *Antarct. Res. Ser.*, edited by S. S. Jacobs, pp. 59–85, AGU, Washington, D. C.
- LeGrande, A. N., and G. A. Schmidt (2006), Global gridded data set of the oxygen isotopic composition in seawater, *Geophys. Res. Lett.*, *33*, L12604, doi:10.1029/2006GL026011.
- Lutjeharms, J. R. E. (2006), Three decades of research on the greater Agulhas Current, *Ocean Sci. Discuss.*, *3*, 939–995.
- Lutjeharms, J. R. E., and H. R. Valentine (1984), Southern Ocean thermal fronts south of Africa, *Deep Sea Res., Part A*, *31*, 1461–1475.
- Macdonald, R. W., E. C. Carmack, F. A. McLaughlin, K. K. Falkner, and J. H. Swift (1999), Connections among ice, runoff and atmospheric forcing in Beaufort Gyre, *Geophys. Res. Lett.*, *26*, 2223–2226.
- Meredith, M. P., K. J. Heywood, R. D. Frew, and P. F. Dennis (1999), Formation and circulation of the water masses between the southern Indian Ocean and Antarctica: Results from $\delta^{18}\text{O}$, *J. Mar. Res.*, *57*, 449–470.
- Park, Y. H., E. Charriaud, and M. Fieux (1998), Thermohaline structure of Antarctic Surface Water/Winter Water in the Indian sector of Southern Ocean, *J. Mar. Syst.*, *17*, 5–23.
- Peterson, R. G., and L. Stramma (1991), Upper-level circulation in the South Atlantic Ocean, *Prog. Oceanogr.*, *26*, 1–73.
- Read, J. F., and R. T. Pollard (1993), Structure and transport of Antarctic Circumpolar Current and Agulhas Return Current at 40°E , *J. Geophys. Res.*, *98*, 12,281–12,295.
- Rintoul, S. R., and J. L. Bullister (1999), A late winter hydrographic section from Tasmania to Antarctica, *Deep Sea Res., Part 1*, *46*, 1417–1454.
- Rintoul, S. R., and M. H. England (2002), Ekman transport dominates local air-sea fluxes in driving variability of Subantarctic Mode Water, *J. Phys. Oceanogr.*, *32*, 1308–1321.
- Schmidt, G. A., G. R. Bigg, and E. J. Rohling (1999), Global Seawater Oxygen-18 Database, <http://data.giss.nasa.gov/o18data/>, NASA Goddard Inst. of Space Sci., New York.
- Sparrow, M. D., K. J. Heywood, J. Brown, and D. P. Stevens (1996), Current structure of the south Indian Ocean, *J. Geophys. Res.*, *101*, 6377–6391.
- Whitworth, T., III, and W. D. Nowlin Jr. (1987), Water masses and currents of the Southern Ocean at the Greenwich Meridian, *J. Geophys. Res.*, *92*, 6462–6476.
-
- N. Anilkumar and M. Sudhakar, National Centre for Antarctic and Ocean Research, Vasco-da-Gama, Goa, India 403 804.
S. Prakash, R. Ramesh, and R. Srivastava, Physical Research Laboratory, Navrangpura, Ahmedabad, India 380 009. (rohit@prl.res.in)

Auxiliary Material for Paper Geophys. Res. Lett. , doi:10.1029/2007GL031790, 2007

- 1.1 Column "Lat", degrees, latitude from where sample was collected.
- 1.2 Column "Lon", degrees, longitude from where sample was collected.
- 1.3 Column "SST", Sea surface temperature (in °C).
- 1.4 Column "Salinity", Ocean surface water salinity.
- 1.5 Column " $\delta^{18}\text{O}$ ", $\delta^{18}\text{O}$ value of the samples.

Lat(°)	Lon(°E)	SST*(°C)	Salinity	$\delta^{18}\text{O}$(‰)
13.11	71.00	NULL**	NULL	0.64
11.96	70.54	NULL	NULL	0.60
11.00	70.02	NULL	NULL	0.62
9.01	68.91	NULL	NULL	0.61
8.03	68.38	NULL	NULL	0.51
7.01	67.84	NULL	NULL	0.74
5.97	67.25	NULL	NULL	0.70
5.00	66.70	NULL	34.91	0.60
4.00	66.21	NULL	34.92	0.55
2.99	65.68	NULL	35.26	0.63
2.00	65.09	NULL	35.28	0.55
0.99	64.60	NULL	35.27	0.62
0.01	64.02	NULL	35.29	0.57
-0.72	63.67	NULL	35.35	0.57
-1.01	63.51	NULL	35.43	0.60
-1.37	63.30	NULL	NULL	0.63
-2.00	62.94	NULL	35.45	0.62
-2.99	62.42	NULL	35.45	0.59
-3.48	62.19	NULL	NULL	0.56
-4.00	61.92	NULL	34.9	0.56
-4.54	61.59	NULL	NULL	0.41
-5.01	61.30	NULL	34.69	0.44
-6.01	60.75	NULL	34.62	0.45
-7.00	60.22	NULL	34.59	0.50
-7.50	59.96	NULL	34.75	0.50
-7.50	60.95	NULL	34.73	0.44
-20.17	57.35	NULL	35.06	0.45
-20.27	57.29	NULL	NULL	0.52
-24.10	57.52	NULL	NULL	0.58
-25.03	57.51	NULL	35.37	0.58
-26.04	57.50	27.31	35.39	0.63
-26.96	57.51	27.00	35.47	0.66

-27.98	57.50	26.93	35.63	0.74
-29.00	57.50	26.67	35.54	0.69
-29.98	57.49	26.08	35.52	0.71
-31.04	57.50	24.05	35.52	0.66
-32.01	57.51	23.24	35.46	0.64
-33.02	57.50	20.91	35.44	0.63
-34.96	57.50	20.56	35.50	0.66
-36.03	57.51	20.31	35.49	0.66
-37.00	57.50	19.99	35.36	0.63
-38.02	57.50	19.51	35.25	0.61
-39.00	57.50	18.25	35.16	0.61
-40.04	57.50	18.05	35.37	0.69
-41.00	57.50	18.26	35.36	0.69
-42.00	57.50	16.25	34.67	0.34
-43.00	57.50	16.06	34.92	0.49
-43.99	57.50	15.37	34.61	0.27
-45.00	57.50	10.86	33.59	-0.22
-46.05	57.50	10.24	33.57	-0.22
-47.02	57.50	8.35	33.60	-0.27
-51.00	58.79	4.82	33.77	-0.19
-52.02	59.51	4.15	33.77	-0.21
-53.00	60.25	3.44	33.81	-0.21
-54.06	61.07	2.99	33.80	-0.23
-55.04	61.86	2.49	33.76	-0.22
-56.02	62.63	2.28	NULL	-0.24
-56.99	63.44	2.46	33.80	-0.29
-58.00	64.30	1.94	33.68	-0.31
-59.01	65.18	2.33	33.75	-0.23
-60.05	66.11	1.88	33.69	-0.31
-60.98	66.97	1.00	33.57	-0.33
-62.02	67.96	0.91	33.82	-0.35
-63.01	68.99	0.80	33.51	-0.34
-64.04	70.03	0.66	33.81	-0.24
-65.00	71.03	0.40	33.97	-0.32
-66.00	72.16	0.23	33.88	-0.32
-66.99	73.95	-1.13	33.75	-0.26
-68.01	77.54	-1.85	33.40	-0.30
69.33	76.09	-0.77	NULL	NULL
-67.01	71.12	-1.83	33.34	-0.39
-66.34	69.06	-0.54	NULL	-0.25
-65.79	64.96	-0.29	NULL	-0.30
-65.79	64.96	-0.29	NULL	-0.31
-65.66	64.00	-0.18	NULL	-0.28
-65.50	62.94	-0.06	NULL	-0.43

-65.39	62.00	0.17	NULL	-0.30
-65.23	60.99	0.25	NULL	-0.38
-65.10	59.97	0.21	NULL	-0.38
-64.97	58.99	0.04	34.38	-0.38
-64.82	58.01	0.16	NULL	-0.42
-64.56	56.09	0.02	NULL	-0.41
64.01	52.72	-0.05	NULL	NULL
62.95	51.86	0.81	NULL	NULL
-57.05	49.91	1.96	NULL	-0.39
-56.00	50.01	2.20	NULL	-0.40
-54.05	50.00	2.18	NULL	-0.37
54.03	50.03	2.90	NULL	NULL
54.23	50.08	2.73	NULL	NULL
54.05	50.00	2.91	NULL	NULL
47.99	48.26	5.77	NULL	NULL
46.03	49.07	6.72	NULL	NULL
44.07	49.53	8.99	NULL	NULL
-43.82	49.20	9.22	NULL	-0.36
-42.87	48.12	11.30	NULL	-0.45
-42.01	48.01	10.60	NULL	-0.36
-41.01	48.02	17.13	35.49	0.59
-39.00	48.00	20.22	35.51	0.70
-37.90	48.00	20.18	35.54	0.67
-37.00	48.00	20.91	35.51	0.68
-36.00	48.00	21.86	35.57	0.69
-35.02	48.00	21.53	35.53	0.64
-34.02	48.00	22.15	35.54	0.72
-32.99	48.00	21.96	NULL	0.71

*SST=Sea Surface Temperature

**NULL = no data available



Inferring microphysical processes occurring in mesoscale convective systems from radar measurements and isotopic analysis

T. Narayana Rao,¹ B. Radhakrishna,¹ Rohit Srivastava,² T. Mohan Satyanarayana,¹
D. Narayana Rao,¹ and R. Ramesh²

Received 1 February 2008; revised 20 March 2008; accepted 1 April 2008; published 15 May 2008.

[1] An attempt has been made, for the first time, to effectively utilize the synergy of various approaches providing microphysical information of precipitation to study short term variations in a Mesoscale Convective System (MCS). A campaign has been conducted wherein rain samples are collected during the passage of MCSs over Gadanki, India, and simultaneously a powerful VHF radar and disdrometer have been operated to infer the characteristics of the vertical structure and rain drop size distribution (DSD) of precipitation. Besides the convection and transition rain, two distinctly different phases of the stratiform rain are identified. Evaporation of rain drops seems to be significant in both convection and stratiform portions of MCS. Observed changes in the temporal variation of the stable oxygen isotope ratios ($\delta^{18}\text{O}$) of precipitation are interpreted in terms of microphysical processes leading to isotopic fractionation. The pattern of variability in isotopic abundance is found to be different from convection to transition and to stratiform rain. The present analysis clearly shows that the height (or temperature) and the rain regime of condensation are of paramount importance in determining $\delta^{18}\text{O}$. Correlations of $\delta^{18}\text{O}$ with rainfall integral parameters stress the need for caution in interpreting the depleted isotopic ratios are due to high rainfall and/or bigger drops. **Citation:** Narayana Rao, T., B. Radhakrishna, R. Srivastava, T. Mohan Satyanarayana, D. Narayana Rao, and R. Ramesh (2008), Inferring microphysical processes occurring in mesoscale convective systems from radar measurements and isotopic analysis, *Geophys. Res. Lett.*, 35, L09813, doi:10.1029/2008GL033495.

1. Introduction

[2] The Mesoscale Convective System (MCS) is one of the highly intriguing features in the earth's atmosphere, given its links to hydrological cycle, dynamics, and radiation budget [Houze, 2004]. Wind profiling radars operating at VHF/UHF bands have contributed significantly to our understanding of the kinematics [Cifelli and Rutledge, 1994] and microphysical characteristics of MCS [Rajopadhyaya et al., 1993; Cifelli et al., 2000; Rao et al., 2006]. Most of the studies mentioned above focused on the variability of rain DSD from one rain regime to the other in a statistical sense. However, the vertical and temporal variability of rain DSD within a storm can provide better insight on microphysical processes occurring in MCS. This approach is

highly relevant considering significant evaporation observed below 2.5 km in convective systems within Australian [Cifelli et al., 2000] and Asian [Rao et al., 2006] monsoons.

[3] Stable isotopic analysis of rain water is another promising way of getting microphysical information, because the isotopic fractionation of rain water depends, primarily, on phase changes of hydrometeors and evaporation. Temporal changes in the isotopic content of rain water, thus, provide clues to the microphysical processes occurring within the cloud and precipitation below the cloud base. While large scale variations, both temporal as well as spatial, of stable isotopic abundances are widely reported [Rozanski et al., 1993, and references therein], short term variations are not properly documented [Celle-jeanton et al., 2004].

[4] A special campaign has been conducted during September - December 2006 wherein rain samples, during the passage of several MCS over Gadanki (13.5°N, 79.2°E), are collected. Simultaneously, disdrometer and the Indian MST radar, located at the same location, have been operated to obtain rain DSD at the surface and aloft, respectively. These measurements are used to (1) study short term variations of rain DSD in MCS, (2) investigate temporal changes in stable isotopic abundance within MCS, and (3) investigate the relationship between the isotopic composition of rain water and rain integral parameters to better understand microphysical processes occurring in the MCS.

2. Data and Analysis

[5] In each rain event, several rain samples were collected with the help of rain collector. Enough care was taken to prevent the evaporation during and after the sample collection. An isotope ratio mass spectrometer (PDZ-Europa, Geo 20-20) is used for isotopic analysis, by the CO_2 equilibration method. The stable isotopic (^{18}O) abundance is presented in conventional delta notation (δ) (with V-SMOW as reference). The external precision of $\delta^{18}\text{O}$ is better than $\pm 0.1\%$ [Srivastava et al., 2007]. The rain DSD at the surface are measured with a RD-69 Joss-Waldvogel (JW) disdrometer, located ~ 5 m away from rain collection spot.

[6] The Indian MST radar located at Gadanki is a powerful VHF Doppler radar, which provides not only 3D wind and turbulence information but is also useful to study the precipitation [Rao et al., 1999]. During campaign period, the radar was kept on alert and operated in a special mode, whenever rain occurred over Gadanki. The important parameters of the radar for this experiment are as follows: pulse width - 1 μs , inter pulse period - 250 μs , coherent integrations - 128, incoherent integrations - 4, FFT points

¹National Atmospheric Research Laboratory, Gadanki, India.

²Physical Research Laboratory, Navrangpura, Ahmedabad, India.

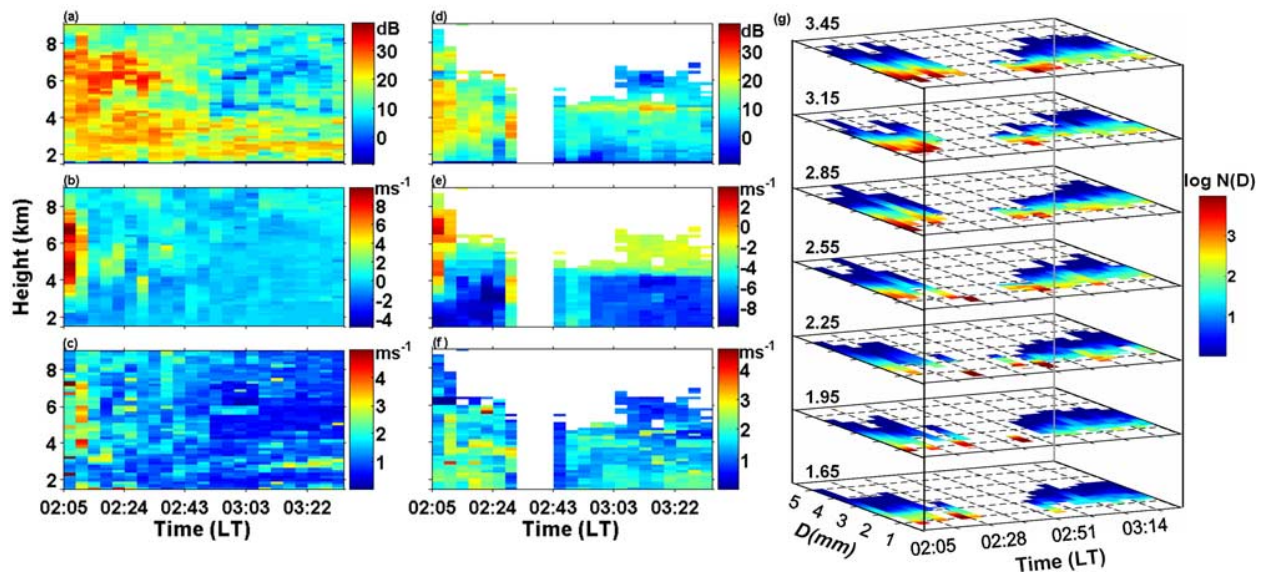


Figure 1. Time-height contours of profiler spectral moments at vertical incidence: (a) and (d) range corrected SNR, (b) and (e), Doppler velocity, and (c) and (f) spectral width for (left) clear air and (middle) precipitation echoes observed on 5 October 2006. Note that color scales of Doppler velocity contours are different for clear air and precipitation. Positive velocities indicate upward motion. (g) Temporal and vertical variation of rain DSD.

– 512, number of radar beams –3 (zenith and 10° off-zenith towards west and south), temporal resolution – 4 min, and range resolution – 150 m. Echoes due to refractive index fluctuations and hydrometeors are identified in the spectral domain and are separated [Rao *et al.*, 1999]. Direct deconvolution method has been employed to retrieve rain DSD. The JW disdrometer is used for absolute calibration of the radar power. Modeling and experimental studies have shown that DSD retrieval with VHF radars may not, always, be able to resolve drops smaller than 1 mm [Rajopadhyaya *et al.*, 1993].

3. Results

[7] On 5 October, an MCS passed over Gadanki producing ~ 26 mm of rainfall (accumulated) in 3 hours. For about 90 minutes (02:05–03:35 LT (LT = 5.30 + UT)), the MST radar spectra have shown a clear bimodal structure up to 6 (8) km after (before) 02:13 LT, except during 02:28–02:51 LT, when the bimodality is seen intermittently both in time and height. Spectral moments are estimated independently after separating the clear air and precipitation echoes, as discussed above, and are depicted as time–height contours in Figure 1. It clearly shows the typical structure of mesoscale convective system [Houze, 2004]. In convection (before 02:13 LT), both clear air and precipitation echo powers are large and extend up to 9 km. Corresponding to this time, strong updrafts of the order of 8 ms^{-1} (Figure 1b) and moderate to intense turbulence (Figure 1c) are observed. A clear bright band, signature of stratiform precipitation, with enhanced precipitation echo power at around 4.35 km is observed after 02:51 LT (Figure 1d). Above 4 km, the Doppler velocity of precipitation (Figure 1e) (resultant of fall velocity of hydrometeors and vertical air motion) shows upward motion in convection, which indicates that raindrops are carried aloft because of

strong updrafts (Figure 1b). As expected, strong gradients in Doppler velocity of hydrometeors are seen around the bright band in stratiform region. The spectral width of precipitation echo, which represents the rain DSD (after correcting it for beam broadening and turbulence), is wide below 4 km in two time intervals (before 02:28 LT and after 03:19 LT). The precipitation observed after the intense convection and before the stratiform rain (i.e., during 02:13–02:51 LT) can be considered as transition rain with properties intermediate to convection and stratiform rain [Rao *et al.*, 1999].

[8] The precipitation echoes are used to retrieve DSD in rain region (3.6–1.65 km) following the method discussed in section 2. DSD retrievals are not performed in the later part of transition rain and early stratiform rain at a few range gates, where the precipitation echo is too noisy to get meaningful rain DSD. The temporal and vertical variation of rain DSD is shown in Figure 1g. The temporal variation of DSD at all heights shows a common feature with wide distribution during convection and initial part of transition rain and also in later part of stratiform rain and narrow distribution in the initial stages of stratiform rain. Vertical variation of DSD displays marked variation with height as well from convection to stratiform rain. Number of smaller drops is generally high in both rain regimes at higher altitudes (above 2.85 km), however, gradually reduces to small at lower altitudes. The reduction of smaller drops is significant in the stratiform rain.

[9] The rain DSD at the surface observed with disdrometer (Figure 2a) is largely consistent with profiler DSD, being broader during 3 time intervals (01:53–02:21, 03:05–03:33 and 04:30–04:40 LT). Reasons for the reduction of smaller drops in strong rain during 01:53–02:21 LT are partly geophysical and partly associated with instrumental problem (JW disdrometer severely underestimates smaller drops in strong rain). For about 40 minutes between 01:50 and 2:30 LT, large values of rainfall integral parameters

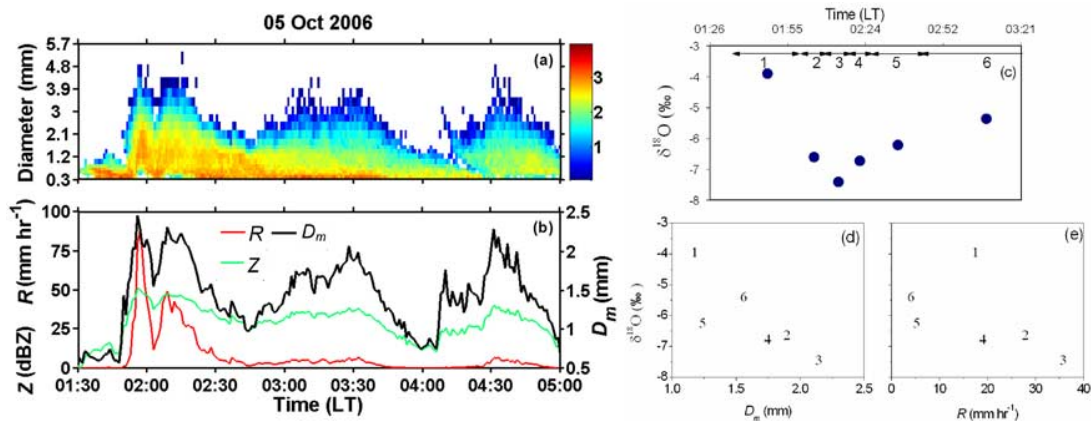


Figure 2. Temporal variation of (a) rain DSD, (b) rain integral parameters (R , Z , and D_m), and (c) $\delta^{18}\text{O}$ during the passage of MCS on 5 October 2006. The sampling time of each sample is also shown in Figure 2c. Scatterplots between $\delta^{18}\text{O}$ and (d) D_m and (e) R . Numbers represent the rain water sample number in the order in which they were collected.

(rainfall rate (R), Reflectivity factor (Z), and mass weighted mean diameter (D_m)) are observed. After 2:30 LT, R and Z varied gradually, while D_m shows large variations with time and reached local maxima of 2.06 and 2.27 mm at 03:28 and 04:31 LT, respectively (Figure 2b).

[10] Six rain samples were collected during 01:30–03:30 LT, and were later subjected to isotopic analysis. Figure 2c shows temporal variation of $\delta^{18}\text{O}$ along with sampling time of each rain sample. Note that the sampling time is not uniform and also more samples were collected during stronger rains. The temporal variation in $\delta^{18}\text{O}$ is significant during convection-initial phase of transition rain, with changes as large as 4‰ in 30 minutes. During this period, $\delta^{18}\text{O}$ clearly shows a rapid negative trend (more depletion) with time, however, recovers gradually and shows enriched values in samples collected during the later half of the transition-stratiform rain. The $\delta^{18}\text{O}$ measured at different stages of a MCS are plotted as a function of D_m and R (Figures 2d and 2e) to understand the relation between them. In general, $\delta^{18}\text{O}$ is correlated (linear correlation coefficient, $r^2 = -0.8$ significant at 95% confidence level) better with D_m than that with R ($r^2 = -0.5$). From these negative correlations, it has been found that the rate of depletion of $\delta^{18}\text{O}$ with D_m and R are 1.32‰ per 0.5 mm and 0.5‰ per 10 mm hr^{-1} , respectively.

[11] The stable isotopic analysis (in terms of $\delta^{18}\text{O}$, δD and d-excess) has been carried out on rain samples collected in a few other rain events (see Table S1¹). The $\delta^{18}\text{O}$ trend is nearly similar in all the rain events considered here.

4. Discussion

[12] MCS is a conglomerate of stratiform and convective clouds and precipitation with varying mesoscale circulations induced by these clouds [Houze, 2004]. The intense updrafts of the order of 8–10 ms^{-1} observed in convection carries hydrometeors aloft into divergent regions at higher altitudes (Figures 1b and 1e). Hydrometeors heavier enough

to overcome the updraft will fall out instantly in convective cores. A large number of smaller drops are also seen in the radar retrieved DSD at 3.45 km and below. It is hard to decide the source of these drops as the radar measurements are available only from 02:05 LT. Breaking of rain drops due to collision with other drops or spontaneous breaking of bigger drops could be one possibility with advection from surrounding regions being the other possibility. The decreasing trend of smaller and medium size drops (≤ 3 mm) from 3.45 km to 1.65 km seen in the radar DSD maps during convection could be attributed to evaporation. Earlier experimental results have shown significant rain evaporation of 20–50% in tropics near convection [Worden et al., 2007], primarily because of the presence of unsaturated air below the cloud base.

[13] The hydrometeors transported into divergent regions due to intense updrafts in convection fall in the neighboring regions and set up the stratiform environment. From Figure 1, it is clear that these hydrometeors are falling from different height regions. The hydrometeors during the first phase of stratiform rain may be falling from a few km above the bright band and as a result the time for drop growth due to vapor deposition, which is the main mechanism in stratiform rain, is not much. On the other hand, in the later half of the stratiform rain, hydrometeors seem to fall from higher altitudes, growing steadily by vapor deposition resulting into bigger drops. Owing to the strong dependence of the radar backscatter on drop diameter, one would expect strong backscatter from bigger drops. Indeed, strong radar backscatter is clearly evident from Figure 1d, in particular, near the radar bright band. The rain DSD retrieved from the radar and disdrometer at aloft and ground, respectively, also confirms the absence (presence) of bigger drops before (after) 03:11 LT. The vertical variation of rain DSD in stratiform region clearly shows reduction of smaller drops with height, indicating strong rain evaporation in this region. Although collision-coalescence mechanism occurs at the expense of smaller drops, it is unlikely, as there is no increase in the number of drops in medium-large drop size. Note that the MST radar may not always be able to detect drops ≤ 1 mm. However, disdrometer measurements showing considerable reduction of smaller drops in the stratiform

¹Auxiliary materials are available in the HTML. doi:10.1029/2008GL033495.

precipitation supports MST radar observations, and reconfirms the evaporation of rain drops. In convection, the break-up of rain drops seems to partially offset the reduction of drops due to evaporation, and as a result still sizeable number of smaller drops exists in lower altitudes (< 2 km).

[14] Microphysical processes such as condensation and evaporation can be well traced by the oxygen isotopes because they fractionate during these processes. Variation of $\delta^{18}\text{O}$ within the system shows a 'V' type structure with sharp depletion initially in the convection and initial phase of transition rain followed by gradual enrichment in later half of transition rain and stratiform rain. The variability of isotopic fractionation is traditionally described with the Rayleigh fractionation model [Dansgaard, 1964], in which evaporation of raindrops is not included. Present observations clearly indicate that evaporation is significant in MCS observed over Gadanki. The evaporation of rain drops causes enrichment of $\delta^{18}\text{O}$ as can be seen in the first sample (maximum enriched value during sampling). In the subsequent samples the effect of evaporation reduces as ambient air saturates, as inferred from a decreasing trend in d-excess (Table S1). In the convective systems due to the intense rain rate, very soon the amount effect dominates over the evaporation effect. Here the main process causing amount effect is related to Rayleigh distillation. Fractional removal of heavy isotopes in the condensate is high during intense precipitation, leading to increasingly ^{18}O depleted vapor in the cloud because ^{18}O prefers the condensed phase compared to ^{16}O . This high degree of rainout results in low $\delta^{18}\text{O}$ in the remaining vapor and ensuing condensate at cloud level. Therefore, the depletion trend of $\delta^{18}\text{O}$, seen in the first 3 samples, could be attributed to the amount effect [Dansgaard, 1964], which is a common mechanism in tropical precipitation. $\delta^{18}\text{O}$ is relatively enriched ($\sim 2\%$ more than the most depleted value) in the stratiform rain regime. It is generally accepted that the hydrometeors form at lower altitudes in a growing convective cloud, and are then carried aloft by strong updrafts. The hydrometeors observed in stratiform rain might have originated in such convective cores and later transported into trailing stratiform regions. It is most likely that these condensates retain the basic isotopic composition acquired at the time of condensation. Observational and recent modeling studies have shown enriched stable isotopes in convection relative to its surroundings, which is thought to be due to the lofting of enriched condensates from lower altitudes [Webster and Heymsfield, 2003; Smith et al., 2006]. Further, isotopic fractionation of rain drop can occur below the cloud base by the effects of evaporation and isotope exchange with unsaturated vapor. Smaller hydrometeors generally re-equilibrate with the vapor during their descent, as their adjustment distance [Friedman et al., 1962] is small. Large number of medium to bigger drops observed in the later part of stratiform rain, perhaps, retains their original isotopic composition [Stewart, 1975]. These bigger drops contribute to most of the rain water (in terms of volume) collected at the surface and decide the isotopic composition of rain samples. The other important process for isotopic fractionation, evaporation of rain drops, seems to be significant during stratiform rain, which results in the enrichment of ^{18}O [Stewart, 1975].

[15] An inverse relation is seen between rainfall integral parameters (D_m and R) and $\delta^{18}\text{O}$, albeit with some scatter. It

is now widely known that the isotopic content of ^{18}O in rain water strongly depends on the raindrop size (and rainfall rate) [Dansgaard, 1964; Jouzel, 1986], through condensation, evaporation and isotopic equilibration processes. The adjustment distance is relatively shorter for smaller drops and, therefore, equilibration is more for smaller drops. Enrichment due to the evaporation is more for the smaller drops (evaporative enrichment is diluted in drops of larger volume). Of course, both these processes depend on the ambient temperature and humidity and also reduce the depletion of $\delta^{18}\text{O}$. As a result, negative correlation between $D_m(R)$ and $\delta^{18}\text{O}$ is anticipated as seen in Figures 2d and 2e. A closer look at the figure, however, indicates the need for caution in generalizing such relations. For instance, the average rainfall rate for samples 1 and 4 is nearly the same (17.6 and 19.1 mm hr $^{-1}$) but the $\delta^{18}\text{O}$ values differ by $\sim 3\%$. Similarly, $\delta^{18}\text{O}$ values for samples 2 and 5 are nearly equal ($\sim 6.5\%$) but their D_m (1.9 and 1.24 mm) and R (27.9 and 5.4 mm hr $^{-1}$) values are distinctly different. Further, considerable number of bigger drops is observed with large D_m values in the later half of stratiform precipitation, but with moderate $\delta^{18}\text{O}$ values. This clearly indicates that the stage at which rain samples are collected is also important and needs to be considered while describing the variability of $\delta^{18}\text{O}$ and comparing $\delta^{18}\text{O}$ values at different locations.

5. Summary and Conclusions

[16] The present report is the first of its kind, where combination of radar and disdrometer measurements along with isotopic analysis has been used to address several key questions related to short term variations of MCS and also to infer meteorological processes occurring in MCS at shorter scale. From the radar and disdrometer measurements, different stages (convection, transition, stratiform) of MCS are discerned. Interestingly, the first half of the stratiform region is distinctly different from the second half in terms of radar backscatter, rain DSD, and variability of rainfall integral parameters in general and D_m in particular. In the later half of the stratiform rain, hydrometeors, carried upward by strong updrafts during convection, seem to fall from higher altitudes, growing steadily by vapor deposition. The increase in the size of drops, in turn, produces strong radar backscatter as evident from Figure 1d. The presence of bigger rain drops during this period, as seen by radar aloft and disdrometer at the surface also confirms this. The 4D plot of rain DSD, obtained from radar measurements, reveals that the evaporation is significant both in convection and stratiform rain regimes of MCS in monsoonal rains.

[17] The temporal variation of $\delta^{18}\text{O}$ within the MCS shows oft-seen 'V' shape structure in frontal systems [Celle-jeanton et al., 2004] with a rapid depletion of $\delta^{18}\text{O}$ at the rate of 4‰ in 30 minutes during convection-initial phases of transition and a gradual increase from transition to stratiform rain. The amount effect [Dansgaard, 1964] seems to explain the observed initial depleting trend of $\delta^{18}\text{O}$. The increasing trend is interesting as there exists several mechanisms in the literature to explain this feature. Earlier studies on short term variations of $\delta^{18}\text{O}$ in frontal systems attributed the enrichment in stable isotopic abundance in small rain samples to evaporation of rain drops [Peng et al., 2007], isotopic re-equilibration between the vapor and raindrops

[Gedzelman and Arnold, 1994], a different mechanism from the descending phase [Celle-Jeanton et al., 2004], intrusion of new air masses with rich stable isotopes into the cloud, and formation of hydrometeors at a lower altitude. In the present study, it has been shown that the increase in stable isotopic abundance is due to the transport of hydrometeors, which are condensed at lower altitudes in convective cloud, from convective region to trailing stratiform region. It is most likely that the condensates retain their basic character acquired at the time of condensation. The above process coupled with evaporation of rain drops below the cloud base dictates the isotopic value of $\delta^{18}\text{O}$. The isotopic re-equilibration of rain drops with vapor below the cloud base is most unlikely given the bigger size of hydrometeors ($D_m \approx 2$ mm).

[18] The correlation between $\delta^{18}\text{O}$ and rainfall parameters seems to be significant; however, there is some scatter. Moreover, for the same rain rate, the $\delta^{18}\text{O}$ values vary considerably depending on the phase of the MCS at which the samples were collected. Therefore, caution has to be exercised while generalizing such correlations describing short term variations and comparing $\delta^{18}\text{O}$ values at different locations.

References

- Celle-Jeanton, H., R. Gonfiantini, Y. Travi, and B. Sol (2004), Oxygen-18 variations of rainwater during precipitation: Application of the Rayleigh model to selected rainfalls in southern France, *J. Hydrol.*, *289*, 165–177.
- Cifelli, R., and S. A. Rutledge (1994), Vertical motion structure in maritime continent mesoscale convective systems: Results from a 50-MHz profiler, *J. Atmos. Sci.*, *51*, 2631–2652.
- Cifelli, R., et al. (2000), Drop-size distribution characteristics in tropical mesoscale convective systems, *J. Appl. Meteorol.*, *39*, 760–777.
- Dansgaard, W. (1964), Stable isotopes in precipitation, *Tellus*, *16*, 436–468.
- Friedman, I., L. Machta, and R. Soller (1962), Water-vapor exchange between a water droplet and its environment, *J. Geophys. Res.*, *67*, 2761–2766.
- Gedzelman, S. D., and R. Arnold (1994), Modeling the isotopic composition of precipitation, *J. Geophys. Res.*, *99*, 10,455–10,471.
- Houze, R. A., Jr. (2004), Mesoscale convective systems, *Rev. Geophys.*, *42*, RG4003, doi:10.1029/2004RG000150.
- Jouzel, J. (1986), Isotopes in cloud physics: Multiphase and multistage condensation process, in *Handbook of Environmental Isotope Geochemistry*, vol. 2, *The Terrestrial Environment*, edited by P. Fritz and J. C. Fontes, pp. 61–105, Elsevier, Amsterdam.
- Peng, H., B. Mayer, S. Harris, and H. R. Krouse (2007), The influence of below-cloud secondary effects on the stable isotope composition of hydrogen and oxygen in precipitation at Calgary, Alberta, Canada, *Tellus, Ser. B*, *59*, 698–704.
- Rajopadhyaya, D. K., P. T. May, and R. A. Vincent (1993), A general approach to the retrieval of raindrop size distributions from wind profiler Doppler spectra: Modeling results, *J. Atmos. Oceanic Technol.*, *10*, 710–717.
- Rao, T. N., D. N. Rao, and S. Raghavan (1999), Tropical precipitating systems observed with Indian MST radar, *Radio Sci.*, *34*, 1125–1139.
- Rao, T. N., N. V. P. Kirankumar, B. Radhakrishna, and D. N. Rao (2006), On the variability of the shape-slope parameter relations of the gamma raindrop size distribution model, *Geophys. Res. Lett.*, *33*, L22809, doi:10.1029/2006GL028440.
- Rozanski, K., L. Araguas-Araguas, and R. Gonfiantini (1993), Isotopic patterns in modern global precipitation, in *Climate Change in Continental Isotopic Records*, *Geophys. Monogr. Ser.*, vol. 78, edited by P. K. Swart et al., pp. 1–36, AGU, Washington, D. C.
- Smith, J. A., A. S. Ackerman, E. J. Jensen, and O. B. Toon (2006), Role of deep convection in establishing the isotopic composition of water vapor in the tropical transition layer, *Geophys. Res. Lett.*, *33*, L06812, doi:10.1029/2005GL024078.
- Srivastava, R., R. Ramesh, S. Prakash, N. Anilkumar, and M. Sudhakar (2007), Oxygen isotope and salinity variations in the Indian sector of the Southern Ocean, *Geophys. Res. Lett.*, *34*, L24603, doi:10.1029/2007GL031790.
- Stewart, M. K. (1975), Stable isotope fractionation due to evaporation and isotopic exchange of falling water drops: Applications to the atmospheric processes and evaporation of lakes, *J. Geophys. Res.*, *80*, 1133–1146.
- Webster, C. R., and A. J. Heymsfield (2003), Water isotope ratios D/H, $^{18}\text{O}/^{16}\text{O}$, $^{17}\text{O}/^{16}\text{O}$ in and out of clouds map dehydration pathways, *Science*, *302*, 1742–1745.
- Worden, J., et al. (2007), Importance of rain evaporation and continental convection in the tropical water cycle, *Nature*, *445*, 528–532, doi:10.1038/nature05508.

T. Mohan Satyanarayana, D. Narayana Rao, T. Narayana Rao, and B. Radhakrishna, National Atmospheric Research Laboratory, Gadanki 517 112, India. (tnrao@narl.gov.in)

R. Ramesh and R. Srivastava, Physical Research Laboratory, Navrangpura, Ahmedabad, 380 009, India.

राष्ट्रीय अंटार्कटिक एवं
समुद्री अनुसंधान केन्द्र
पृथ्वी विज्ञान मंत्रालय
(भारत सरकार)
हेड लैण्ड सडा, वास्को-डा-गामा
गोवा - ४०३८०४, भारत



**NATIONAL CENTRE FOR
ANTARCTIC & OCEAN RESEARCH**
Ministry of Earth Sciences
(Government of India)
Headland Sada, Vasco-da-Gama
Goa - 403 804, INDIA

Dr M. Sudhakar
Group Director & Scientist 'G'
Ocean Sciences & Services Group

12th June, 2009

Sub: Acceptance of manuscript for publication in Current Science Special Section—Reg.

Ref: MANUSCRIPT NO. CSSS-SOL-MS02

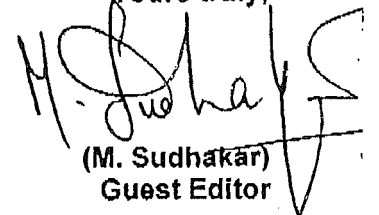
Dear Mr Srivastava,

The following paper submitted by you incorporating the suggestions of the reviewers for consideration in the special section of 'Current Science' on the "Results of Southern Ocean and Larsemann Hills Expeditions" has been accepted for publication. We will send you the proof for correction in due course of time.

Title: *Spatial variation of hydrogen isotopes and salinity in the Southern Indian Ocean*
Authors: R. Srivastava, R. Ramesh, R. A. Jani, Anil Kumar and M. Sudhakar

With best regards

Yours truly,


(M. Sudhakar)
Guest Editor

To

Mr Rohit Srivastava
Senior Research Fellow
Physical Research Laboratory
Navarangpura
Ahmedabad--380 009.

Stable oxygen, hydrogen isotope ratios and salinity variations of the surface Southern Indian Ocean waters

Rohit Srivastava¹, R. Ramesh¹, R. A. Jani¹, N. Anilkumar² and M. Sudhakar²

¹Physical Research Laboratory, Navrangpura, Ahmedabad 380 009, India

²National Centre for Antarctic and Ocean Research, Vasco da Gama, Goa 403 804, India.

Stable isotope ($\delta^{18}\text{O}$ and δD) and salinity measurements were made on the surface waters collected from the Southern (Indian) Ocean during the austral summer (25th January to 1st April, 2006) on board *R/V Akademik Boris Petrov* to investigate the relative dominance of the various hydrological processes namely evaporation, precipitation, melting and freezing over different latitudes. The region between 41°S and 45°S is a transition zone: the region lying north of 41°S is dominated by evaporation/precipitation process while that south of 45°S (up to Antarctica) is dominated by melting/freezing processes. Further, the combined study of stable oxygen and hydrogen isotope ($\delta^{18}\text{O}$ and δD) indicates that the Southern Ocean evaporates in non-equilibrium conditions.

Keywords: Southern Indian Ocean, stable oxygen and hydrogen isotopes, global meteoric water line, mass spectrometry.

The Southern Ocean, defined as the region between the south of 60°S and Antarctica¹, is an important region that affects the climate of the earth. The main bottom and intermediate water masses of the world ocean originate here. The Antarctic Zone of the

Southern Ocean refers to the vast area between the polar front and the Antarctic continent. The surface water in this zone, characterized by a commonly observed summer minimum surface temperature, is the Antarctic Surface Water (AASW)². The thermohaline structure of this water mass is determined by seasonally changing air-sea interaction (air-sea fluxes of momentum, heat, and fresh water), advection, and formation and melting of sea ice³. Despite its close relationship with changing atmospheric conditions, the vertical and horizontal structures of AASW of the Indian sector of the Southern Ocean, as a whole, have not been studied to any extent, although some detailed studies exist for limited locations.

Stable isotopes of oxygen and hydrogen have been used as very reliable tracers for hydrological processes for long. In the modern ocean they have been used as tracers for melting of sea ice⁴, glacial and river run-off, deep ocean water masses⁵, and deep-water formation processes⁶. The isotopic compositions at various stages of the hydrological cycle help constrain different water masses as well as their movement. Isotopic compositions of ice cores have become the most important tools for paleotemperature reconstructions^{7, 8}. The variation in the isotopic composition of deep-sea water is relatively smaller than that in freshwater and mainly determined by freshwater input and mixing between water masses⁹.

Several expeditions have been made earlier to explore the Indian Ocean as well as the Southern Ocean¹⁰⁻¹³. But due to high spatial and temporal variability this region needs more studies to characterize its physical (such as temperature and salinity), chemical, and isotopic properties adequately. Some studies have shown that due to global warming, parts of Antarctic ice sheet are melting and the Southern Ocean is getting more and more

melt water¹⁴⁻¹⁷. This makes the isotopic study of the Southern Ocean all the more urgent. Combined study of stable hydrogen (δD) and oxygen ($\delta^{18}\text{O}$) isotopes and salinity can be ideal to monitor various processes happening in the oceans. Here new δD and salinity data pertaining to the Indian sector of the Southern Ocean are presented and discussed (details of the oxygen isotope data will be presented elsewhere).

About a hundred samples of ocean surface water were collected during the second expedition to the Southern Ocean and Larsemann Hills, Antarctica on board R/V “Akademik Boris Petrov” (25th January to 1st April, 2006). A vast area (from 13°N to 68°S and 71°E to 77°E) was covered for sampling (Figure 1). The collection of surface sea water samples was done with the help of a small, clean plastic bucket. Before sample collection, the bucket was rinsed with the surface water of the sampling site. This collected water was stored in 100 ml plastic bottles with tight-fitting double caps to prevent evaporation. Bottles were filled up to the brim to facilitate easy identification of any later evaporation/leakage and taped at the neck as a further precaution. Measurement of salinity (in Practical Salinity Unites, PSU) was done by a Salinometer (Autosal) on board with an accuracy of 0.001‰. When the water temperature was close to 0°C, the salinity measurements were not made (Table 1).

A dual-inlet isotope ratio mass spectrometer (PDZ-Europa Geo 20-20) was used for isotopic analysis. Equilibration of the water samples was achieved with H₂ gas for δD analysis¹⁸. Platinum coated beads (known as Hoko Beads) were used as catalyst for the equilibration in about two hours. The equilibrated gas was let into the mass spectrometer for isotopic analysis. The isotopic composition is expressed in the conventional units defined by:

$$\delta = [(R/R_{\text{standard}}) - 1] * 1000 \quad \text{per mil (‰)}$$

Where $R = D / H$ (or $^{18}\text{O} / ^{16}\text{O}$). We used VSMOW (Vienna Standard Mean Ocean Water) as a reference¹⁹. Standard deviation of the δD measurement is about $\pm 1\%$.

The δD values of ocean waters are very sensitive to variations in the evaporation-precipitation processes. The isotopic compositions of the surface waters of the ocean are determined by the amount of rainfall (precipitation) and the amount of water that evaporates from the ocean. In regions where the amount of precipitation or river run off is higher than evaporation ($P > E$, negative net evaporation), the ocean surface becomes diluted in the heavier isotopes (D and ^{18}O) and the net isotopic composition becomes lighter. Conversely, a higher rate of evaporation compared to that of precipitation ($E > P$, positive net evaporation) leads to the enrichment of heavier isotopes. This is due to the preferential removal of lighter isotopes (H and ^{16}O) from the ocean surface. Similarly, a positive net evaporation leads to an increase in salinity, while negative net evaporation leads to a decrease in salinity. These processes cause linear relationships between the stable isotopes (δD and $\delta^{18}\text{O}$) and salinity, the slopes depending on climatic constraints²⁰.

At higher latitudes, the effect of freezing at the ocean surface increases salinity as salt is excluded while freezing. However, it causes only a weak depletion in the δD values of the remaining liquid sea water. This is because the isotopic fractionation between ice and water is much smaller than that between vapour and water. The melting of sea ice causes large changes in salinity and leaves δD almost unchanged (the resulting mixture may be only slightly enriched in δD), while melting of continental-ice causes large drops both in salinity and δD ²¹. So the combined study of stable isotopic composition (δD or $\delta^{18}\text{O}$) and salinity provides a unique method to trace ocean surface processes.

We observe a large variation in the surface water salinity (from 35.63 PSU to 33.34 PSU) throughout the cruise. Near the equator, between 60°E and 70°E, salinity variations exhibit high and low salinity regions very near each other (Figure 2). In the present study 4°S makes a clear demarcation between the evaporation dominated zone (i.e. high salinity due to positive E-P) to the precipitation dominated zone (i.e. low salinity due to negative E-P). More samples are required from other sites in the same latitude range to confirm the longitudinal extent of this effect.

An increase in salinity is observed to the south of 20°S, which reaches a maximum of 35.6 ‰ and stays constant in the region between 28°S and 41°S. However, it shows a sharp decrease between 41°S and 45°S. This decrease can either be due to (1) heavy precipitation or (2) underwater current which breaks at the surface. With a small increase of 0.17PSU between 47°S to 51°S, from 51°S onwards salinity shows a decreasing trend with some small fluctuations. This small increase can be due to vertical mixing caused by high winds in this region.

Hydrogen isotopic composition follows same trend as salinity (Figure 3). A sharp decrease at (41°S-45°S) confirms the effect of precipitation or shoaling of an underwater current. Barring some fluctuations, which are within the experimental uncertainties, δD shows an overall increasing trend, moving towards the south. This increase in the δD values reflects the increasing effect *in situ* melting of sea ice. In other words, as we move towards the Antarctic continent the effect of melting/freezing processes increases. Thus on the basis of salinity and hydrogen isotopic data it is inferred that the Indian Ocean north of 41°S is a zone of dominant evaporation/precipitation whereas south of 47°S it is dominated by melting/freezing. The region between 41°S and 47°S is a transition zone

between the above two regions. A schematic representation of these zones is shown in Figure 4.

The relation between δD and $\delta^{18}O$ of the ocean surface water gives information about the humidity at the time of evaporation. For worldwide fresh surface waters, Craig²¹ has found that $\delta^{18}O$ and δD exhibit a linear correlation, which defines the global meteoric water line (GMWL). Its slope is ~ 8 and intercept is $\sim 10\%$. The slope is ~ 8 because this is approximately the value produced by equilibrium Rayleigh fractionation of evaporating water surface at about 100% humidity. The value of ~ 8 is also close to the ratio of the equilibrium fractionation factors for H and O isotopes at 25-30°C^{22, 23, 18}. The slope reduces to less than ~ 8 due to evaporation controlled by ambient humidity (and also due to diffusion through the water vapor boundary layer and exchange with atmospheric water vapor) at the ocean surface. The non-equilibrium evaporation process is characterized²⁴⁻²⁶ by a slope of less than ~ 8 . The relation between δD and $\delta^{18}O$ for the Indian Ocean is depicted in Figure 5, where data points cluster in two distinct bunches. The best fit line has a slope of (7.77 ± 0.06) , which is significantly lower than the slope of the GMWL (8.12 ± 0.07) . This indicates the Southern Ocean as a whole is evaporating under the non-equilibrium condition, with a mean ambient humidity significantly less than 95%, as also borne out by humidity observations during the cruise. As a result, the Indian Ocean samples show an intercept of (0.22 ± 0.18) which is much less than the intercept of GMWL (9.20 ± 0.53) . The relation between $\delta D - \delta^{18}O$ shows the two end point mixing type of phenomenon (points in the two big circles). This again emphasizes that the region between 41°S and 45°S is a transition region between two different types of zones.

In summary in the Southern (Indian) Ocean, the region between 41°S and 45°S makes a demarcation between an evaporation/precipitation zone (north of 41°S) and a melting freezing zone (south to 45°S). The sharpness of the transition zone could be dependent on season. A little lower slope of the $\delta D - \delta^{18}O$ line than 8 reveals that evaporation occurs in the Southern Ocean under isotopic non-equilibrium condition i.e. kinetic effects (due to diffusion related fractionation) during vapor formation are more prominent. Future studies may throw light on the seasonal and spatial variations in the Southern Ocean.

ACKNOWLEDGEMENTS: We thank the Department of Ocean Development and National Institute Antarctic and Oceanographic Research for opportunity to participate in the expedition to the Southern Ocean. We also thank the captain, chief scientist and the crew of R/V *Akademik Boris Petrov*. We thank the reviewers for their critical comments.

References

1. National Hydrographic Organization (IHO), 2000.
2. Park, Y.H., Charriaud, E. & Fieux, M., *Journal of Marine System*, 1998, 5-23.
3. Gordon, A.L. & Huber, B.A., *J. Geophys. Res.*, 1984, **89**, 614-648.
4. Macdonalds, R.W., Carmack, E.C., McLaughlin, F.A., Falkner, K.K. & Swift, J.H., *Geophys. Res. Lett.*, 1999, **26(15)**, 2223-2226.
5. Meredith M.P., Heywood K.J., Frew R.D. & P. F. Dennis, *J. Marine Res.*, 1999, **57**, 449-470(22).

6. Jacobs, S.S., R.G.Fairbanks & Y.Horibe, *Oceanology of the Antarctic Continental Shelf, Antarctic Research Series*, edited by S.S. Jacobs, AGU, Washington, D.C, 1985, pp. 59-85.
7. Gat JR, *Ann. Rev. Earth Planet Sci.*, 1996, 24:225-262
8. Schotterer U., F. Oldfield & K. Frölich, *Global network for isotopes in precipitation. IAEA, Vienna*, 1996, pp 1-48.
9. Paul, A; Mulitza, S; Pätzold, J & Wolff, T, In: Fischer, G & Wefer, G (eds.), *Use of Proxies in Paleoceanography - Examples from the South Atlantic*. Springer-verlag Berlin Heidelberg, 1999, 655-686.
10. Delaygue, G., Bard E, Rollion C., Jouzel J., Stievenard M., Duplessy J.-C. & Ganssen G., *J. Geophys. Res.*, 2001, **106**, 4565.
11. Duplessy, J.-C., *C. R. Acad. Sc. Paris*, 1970, **271**, 1075-1078.
12. Kallel, N., Master's thesis. *Université de Paris Sud*, 1985.
13. Archambeau, A. S., Pierrie, C., Poisson, A. & Schauer, B. *Journal of Marine Systems*, 1998, **17**, 25-38.
14. Aoki S., M. Yoritaka & A. Masuyama, *J. Geophys. Res.*, 2003, **108**, NO. C4, 8081.
15. Aoki S., N. L. Bindoff & J. A. Church, *Gephys. Res. Lett.*, 2005, **32**, L07607.
16. Banks H. T. & N. L. Bindoff, *Journal of climate*, 2002, **16**.
17. Barnett T. P., D. W. Pierce, K. M. Achuta Rao, P. J. Gleckler, B. D. Santer, J. M. Gregory & W. M. Washington, *Science*, 2005, **309**, 284.

18. Gonfiantini R., In *Stable Isotope Hydrology: Deuterium and Oxygen-18 in the Water Cycle. Technical Report Series No.210* (eds. Gat J R and Gonfiantini R.), IAEA, Vienna 1981, 103-142.
19. Craig, H., *Geochimica et Cosmochimica Acta*, 1957, **12**, 133–149.
20. Craig, H. & L.I.Gordon, *V.Lischi e Figli, Pisa*, 1965, 122pp.
21. Craig H., *Science*, 1961, **133**, pp. 1702-03.
22. Carol K & McDonnell J (Eds.), *Isotope Tracers in catchment hydrology*. Elsevier Publisher, 1998, 839p.
23. Clark I D & Fritz P., *Environmental Isotopes in Hydrogeology*. Levis publisher, 1997, 328p.
24. Gat J. R., In *Stable Isotope Hydrology: Deuterium and Oxygen-18 in the Water Cycle*”, *Technical Report Series No.210* (eds. Gat J R and Gonfiantini R.), 1981, 21-33. IAEA, Vienna.
25. Mook W. G., *Introduction to Isotope Hydrology: Stable and Radioactive Isotopes of Hydrogen, Oxygen and Carbon*. Taylor & Francis, 2006.
26. Dansgaard W., *Tellus*, 1964, **16**, 436-468.

Table 1. Stable hydrogen isotopic composition (δD) and salinity of sea water

Station	Latitude(°)	Longitude(°E)	Salinity(PSU*)	δD (‰)
1	13.11	71.00	ND**	3.7
2	11.96	70.54	ND	4.2
3	11.00	70.02	ND	5.0
4	9.01	68.91	ND	3.5
5	8.03	68.38	ND	3.8
6	7.01	67.84	ND	4.3
7	5.97	67.25	ND	4.6
8	5.00	66.70	34.91	4.1
9	4.00	66.21	34.92	4.0
10	2.99	65.68	35.26	4.8
11	2.00	65.09	35.28	4.1
12	0.99	64.60	35.27	5.5
13	0.01	64.02	35.29	5.4
14	-0.72	63.67	35.35	6.5
15	-1.01	63.51	35.43	6.0
16	-1.37	63.30	ND	5.2
17	-2.00	62.94	35.45	7.0
18	-2.99	62.42	35.45	5.5
19	-3.48	62.19	ND	5.7
20	-4.00	61.92	34.90	5.4
21	-4.54	61.59	ND	5.5
22	-5.01	61.30	34.69	5.4
23	-6.01	60.75	34.62	4.3
24	-7.00	60.22	34.59	5.7
25	-7.50	59.96	34.75	6.0
26	-7.50	60.95	34.73	6.0
27	-20.17	57.35	35.06	6.3
29	-20.27	57.29	ND	4.8
30	-24.10	57.52	ND	4.9
31	-25.03	57.51	35.37	6.5
32	-26.04	57.50	35.39	5.8
33	-26.96	57.51	35.47	6.1
34	-27.98	57.50	35.63	6.4

35	-29.00	57.50	35.54	5.9
36	-29.98	57.49	35.52	5.1
37	-31.04	57.50	35.52	5.0
38	-32.01	57.51	35.46	3.9
39	-33.02	57.50	35.44	4.3
40	-33.99	57.50	35.13	6.2
41	-34.96	57.50	35.50	4.6
42	-36.03	57.51	35.49	5.6
43	-37.00	57.50	35.36	4.2
44	-38.02	57.50	35.25	6.3
45	-39.00	57.50	35.16	3.6
46	-40.04	57.50	35.37	5.1
47	-41.00	57.50	35.36	3.6
48	-42.00	57.50	34.67	1.6
49	-43.00	57.50	34.92	3.8
50	-43.99	57.50	34.61	1.4
51	-45.00	57.50	33.59	-4.3
52	-46.05	57.50	33.57	-3.8
53	-47.02	57.50	33.60	-2.5
54	-51.00	58.79	33.77	-2.6
55	-52.02	59.51	33.77	-3.6
56	-53.00	60.25	33.81	-3.4
57	-54.06	61.07	33.80	-2.3
58	-55.04	61.86	33.76	-1.6
59	-56.02	62.63	ND	-2.2
60	-56.99	63.44	33.8	-1.8
61	-58.00	64.30	33.68	-1.1
62	-59.01	65.18	33.75	-1.6
63	-60.05	66.11	33.69	-3.2
64	-60.98	66.97	33.57	-3.1
65	-62.02	67.96	33.82	-2.7
66	-63.01	68.99	33.51	-2.5
67	-64.04	70.03	33.81	-1.3
68	-65.00	71.03	33.97	-0.6
69	-66.00	72.16	33.88	-0.8
70	-66.99	73.95	33.75	-1.6
71	-68.01	77.54	33.40	-2.5

72	-67.01	71.12	33.34	-1.1
73	-66.34	69.06	ND	0.0
74	-65.79	64.96	ND	-0.7
75	-65.79	64.96	ND	-0.9
76	-65.66	64.00	ND	-1.3
77	-65.50	62.94	ND	-2.0
78	-65.39	62.00	ND	-2.7
79	-65.23	60.99	ND	-2.8
80	-65.10	59.97	ND	-1.2
81	-64.97	58.99	34.38	-2.3
82	-64.82	58.01	ND	-2.9
83	-64.56	56.09	ND	-2.0
84	-57.05	49.91	ND	-2.1
85	-56.00	50.01	ND	-1.9
86	-54.05	50.00	ND	-3.2
87	-43.82	49.20	ND	-2.6
88	-42.87	48.12	ND	-1.7
89	-42.01	48.01	ND	-2.3
90	-41.01	48.02	35.49	2.3
91	-39.00	48.00	35.51	5.1
92	-37.90	48.00	35.54	4.2
93	-37.00	48.00	35.51	2.8
94	-36.00	48.00	35.57	4.6
95	-35.02	48.00	35.53	3.6
96	-34.02	48.00	35.54	3.4
97	-32.99	48.00	ND	4.0

*PSU = Practical Salinity Units

** ND = not determined

Figure Captions:

Figure 1 Cruise Track shows locations of sample collection in the Indian Ocean, denoted by stars.

Figure 2 Variation of salinity (in psu i.e. Practical Salinity Units) of surface waters in the Indian Ocean.

Figure 3 Latitudinal variation of δD (not along a single longitude, involves samples from all locations shown in Fig. 1).

Figure 4 Schematic diagram showing different zones in the Southern Indian Ocean, where different hydrological processes dominate.

Figure 5 Plot of $\delta^{18}O$ vs. δD of surface sea water from the Indian Ocean (Best fit line with slope = 7.77 ± 0.06 , intercept = 0.22 ± 0.18 , $r^2 = 0.99$). Global Meteoric Water line is also shown for comparison.

Figure 1

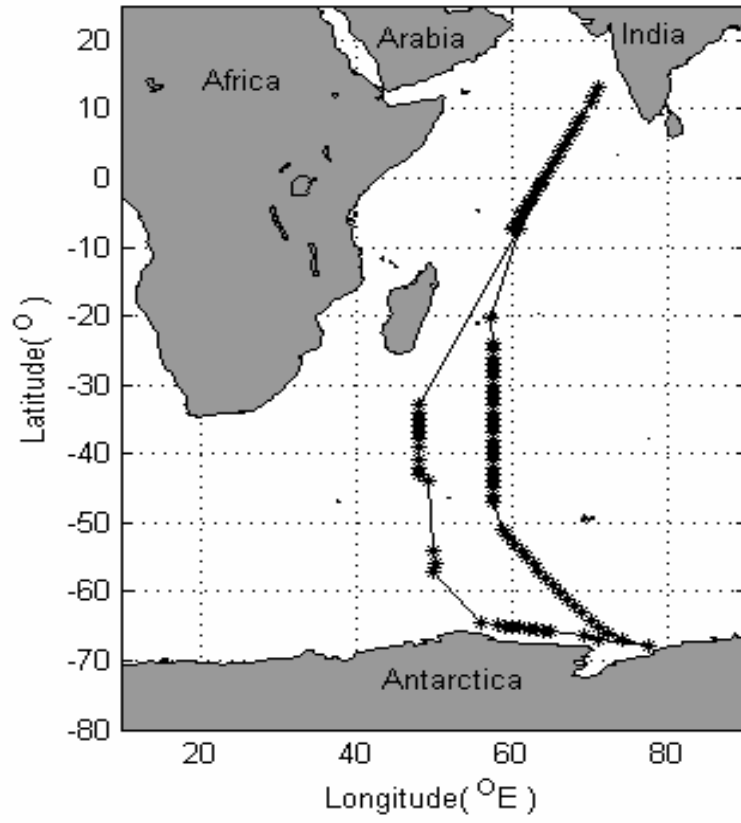


Figure 2

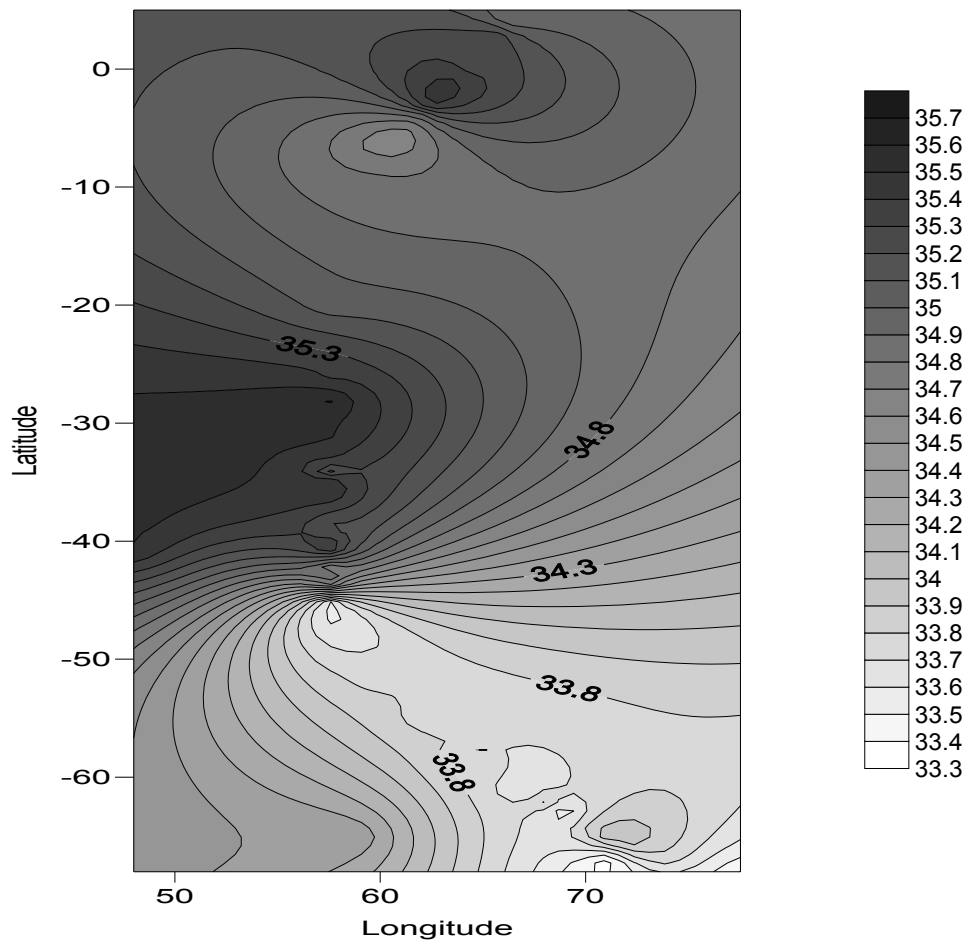


Figure 3

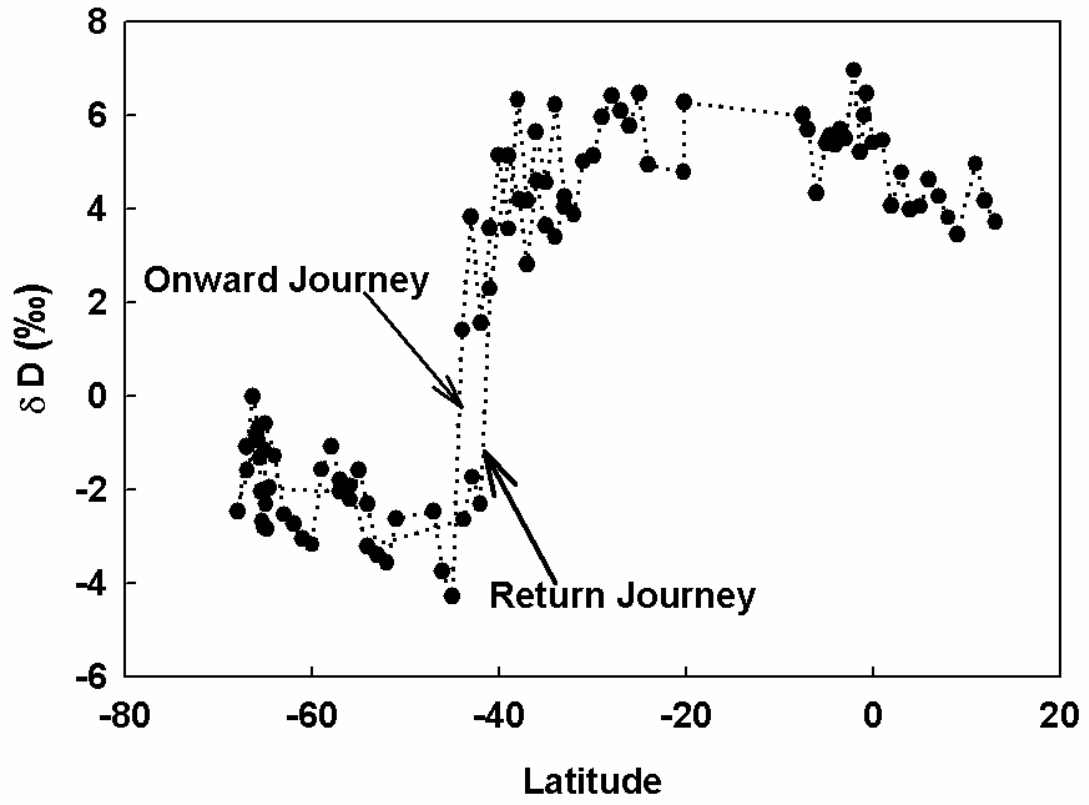


Figure 4

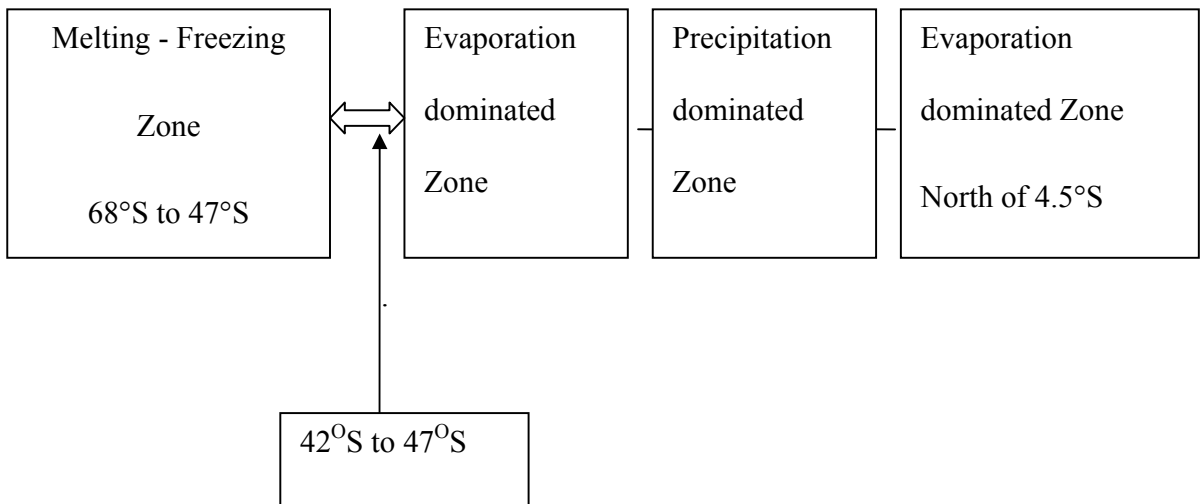


Figure 5

